USGS
science for a changing world

Postglacial Eruptive History, Geochemistry, and Recent Seismicity of Aniakchak Volcano, Alaska Peninsula

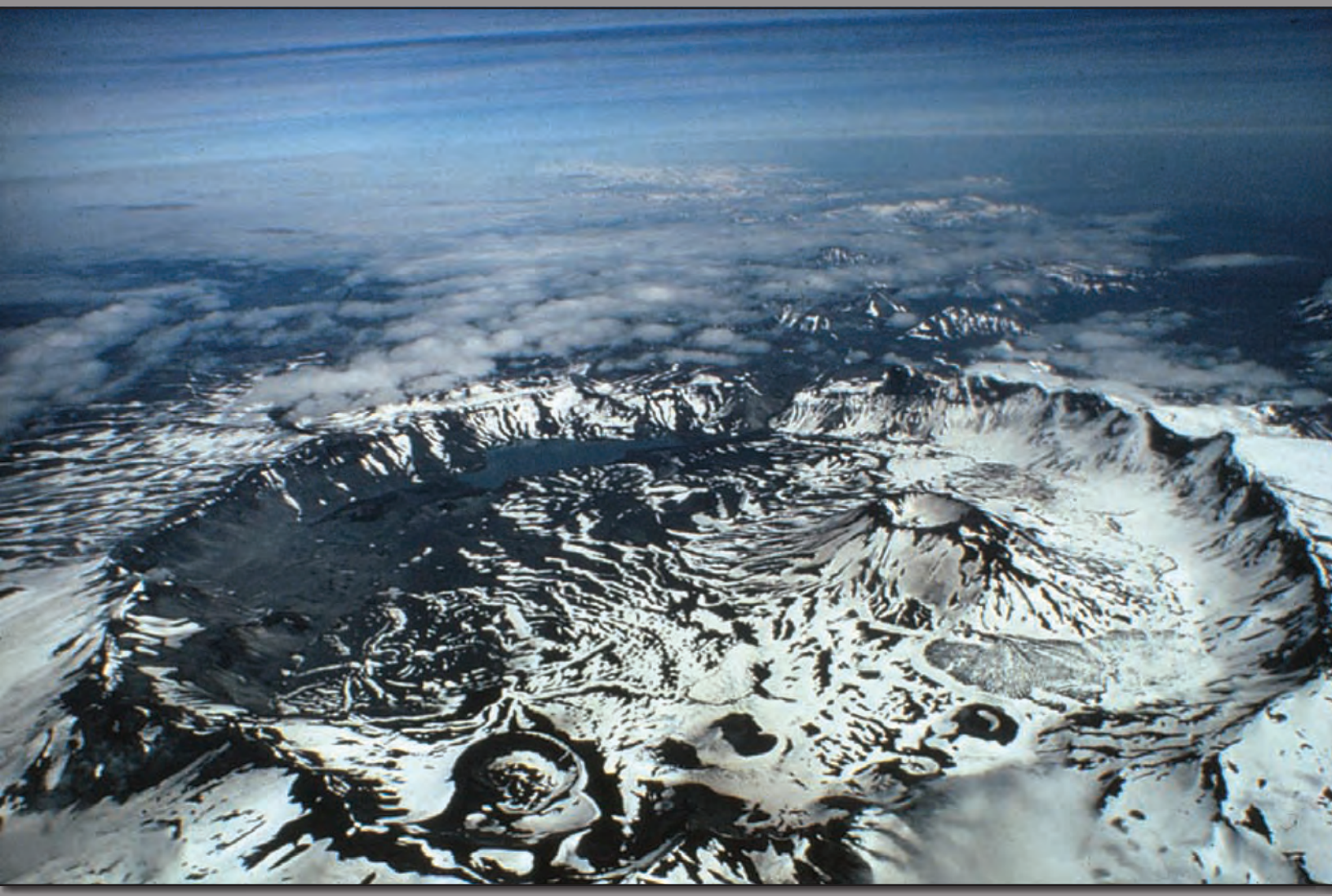

Professional Paper 1810

U.S. Department of the Interior
U.S. Geological Survey

Cover photograph. Oblique aerial photograph looking east over Aniakchak volcano and its caldera (National Park Service photo by M. Williams, 1977).

Postglacial Eruptive History, Geochemistry, and Recent Seismicity of Aniakchak Volcano, Alaska Peninsula

By Charles R. Bacon, Christina A. Neal, Thomas P. Miller, Robert G. McGimsey, and Christopher J. Nye

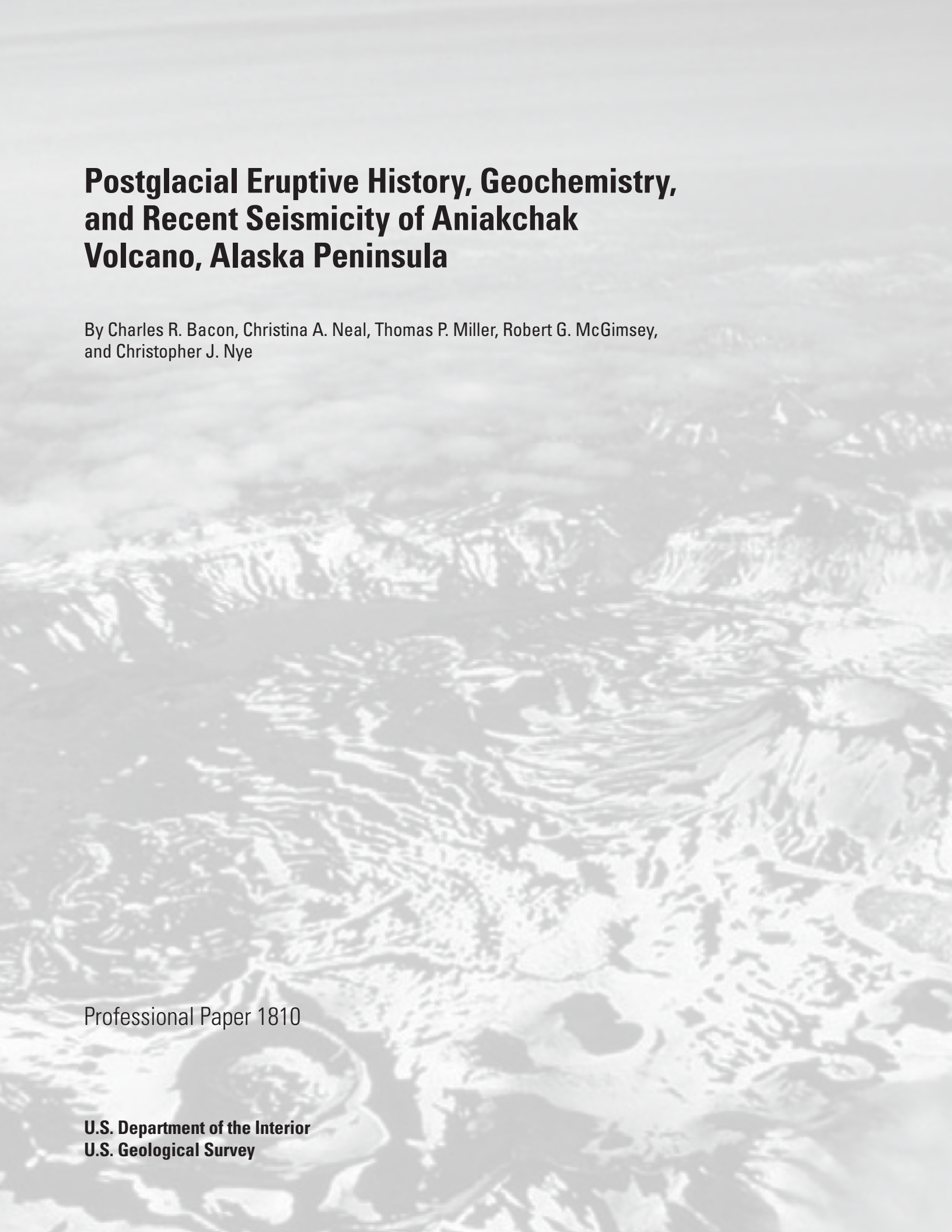

Professional Paper 1810

U.S. Department of the Interior
U.S. Geological Survey

U.S. Department of the Interior
SALLY JEWELL, Secretary

U.S. Geological Survey
Suzette M. Kimball, Acting Director

U.S. Geological Survey, Reston, Virginia: 2014

Suggested citation:
Bacon, C.R., Neal, C.A., Miller, T.P., McGimsey, R.G., and Nye, C.J., 2014, Postglacial eruptive history, geochemistry, and recent seismicity of Aniakchak volcano, Alaska Peninsula: U.S. Geological Survey Professional Paper 1810, 74 p., *http://dx.doi.org/10.3133/pp1810*.

ISSN 1044-9612 (print)
ISSN 2330-7102 (online)

Contents

Abstract 1
Introduction 2
Eruptive History Prior to 3,400 Years B.P. 4
    Pleistocene Aniakchak 4
    Products of the Aniakchak I Explosive Andesite Eruption 6
    Precaldera Dacites and Rhyodacites 11
        Dacite and Rhyodacite Lava Flows 11
        Dacite Pyroclastic Deposits Older Than Black Nose Pumice 12
        Black Nose Pumice 12
            Lower Black Nose Pumice Fall 13
            Intraplinian Ignimbrite 13
            Upper Black Nose Pumice Fall 13
        Post-Black Nose Pumice, Pre-Aniakchak II Interval 14
Products of the Aniakchak II Caldera-Forming Eruption 14
    Rhyodacite Pumice Fall 14
    Ignimbrite 14
        Rhyodacite Ignimbrite 14
        Mixed Ignimbrite 15
        Andesite Ignimbrite 16
        Lithic Breccia 16
Postcaldera Deposits and History 16
    Early Postcaldera Dacite Pumice Fall 16
    Subaqueous Domes 16
    Northwest Flank and Intracaldera Rhyodacite Lava Flows 22
    Ancestral Caldera Lake 22
    Tuff Cones 22
    Vent Mountain 24
    Half Cone 24
        Early Products of Half Cone and Nearby Vents 24
        Half Cone Pink and Brown Pumice Falls 27
        Proximal Late-Erupted Fall Layers 27
        Cobweb Lava Flow 27
    Blocky Cone 27
    1931 Eruption 28
        Historical Accounts 28
        Fall Deposit 28
        Spatter Agglutinate 30
        Main Crater Lava 30
        Late-Erupted Bombs 30
        Doublet and Slag Heap Lavas 30
Geochemistry 30
    Pleistocene Aniakchak Edifice 30

Aniakchak I Ignimbrite 34
Precaldera Dacites and Rhyodacites 34
Dacite–Rhyodacite Lava Flows 34
Black Nose Pumice 34
Other Pre-Aniakchak II Dacite Pumice Falls 35
Aniakchak II Products 35
Subaqueous Domes 35
Northwest Flank and Intracaldera Rhyodacite Lava Flows 43
Tuff Cones 43
Vent Mountain 43
Half Cone 43
Blocky Cone 44
Products of the 1931 Eruption 45
Radiogenic Isotopes 51
Recent Seismicity 52
Discussion 52
Eruptive Processes Through Time 52
Magma Evolution 58
Geochemical Features of Arc Magmas at Aniakchak 58
Precaldera Magma Geochemistry and Subsurface Processes 59
Geochemical Implications of Aniakchak II Magma Compositions 60
Rhyodacite Lava Flows and Subaqueous Domes 61
Basaltic Andesites of Breezy and Blocky Cones 61
Basaltic Andesites of Windy Cone 61
Andesite of Surprise Cone 61
Vent Mountain and Half Cone 61
Products of the 1931 Eruption 62
Aniakchak Magmatic System 63
Magma Transport and Storage Suggested by Earthquakes, Deformation, and Degassing 67
Hazards 68
Conclusions 68
Acknowledgments 70
References Cited 70
Appendix A. Electron Microprobe Analyses 74
Appendix B. Whole-Rock Chemical Analyses 74

Figures

1. Google Earth image of a portion of the Alaska Peninsula showing Aniakchak, Black Peak, and Veniaminof volcanoes 3
2. Aerial photographs of Aniakchak volcano and caldera 5
3. Photographs of Aniakchak caldera walls and edifice 7
4. Generalized geologic map of Aniakchak volcano and vicinity 9
5. Schematic composite stratigraphic sections 9
6. Photographs showing deposits of Aniakchak I 10

7. Oblique Google Earth view of Birthday Pass and upper Birthday Creek drainage showing deposits of Aniakchak I eruption and possible terminal moraine 11
8. Photographs showing precaldera dacites and rhyodacites north of The Gates 12
9. Photographs showing deposits of the Aniakchak II eruption 15
10. Maps of Aniakchak caldera 20
11. Photographs showing surface features of dacite domes inside Aniakchak caldera 23
12. Photographs of tuff cones and Vent Mountain 25
13. Photographs of Half Cone and its products 26
14. Photographs of Blocky Cone 28
15. Photographs showing products of the 1931 eruption 29
16. Silica variation diagrams for Pleistocene and pre-3,400-yr.-B.P. Aniakchak samples 31
17. Silica and P_2O_5 variation diagrams for Pleistocene and pre-3,400-yr.-B.P. Aniakchak samples 33
18. Chondrite-normalized rare-earth-element diagrams for pre-3,400-yr.-B.P. Aniakchak products 36
19. Primitive-mantle-normalized multielement diagrams for pre-3,400-yr-B.P. Aniakchak products 37
20. Silica variation diagrams for Aniakchak II and postcaldera, pre-1931 samples 38
21. Silica and P_2O_5 variation diagrams for Aniakchak II and postcaldera, pre-1931 samples 40
22. Chondrite-normalized rare-earth-element diagrams for Aniakchak II and postcaldera, pre-1931 samples 41
23. Primitive-mantle-normalized multielement diagrams for Aniakchak II and postcaldera, pre-1931 samples 42
24. Silica variation diagrams for Aniakchak II and postcaldera, pre-1931 samples with >56 weight percent SiO_2 44
25. Silica variation diagrams for products of 1931 eruption of Aniakchak volcano 46
26. Silica and P_2O_5 variation diagrams for products of 1931 eruption of Aniakchak volcano 48
27. Chondrite-normalized rare earth element diagrams for products of 1931 eruption of Aniakchak volcano 49
28. Primitive-mantle-normalized multielement diagrams for products of 1931 eruption of Aniakchak volcano 50
29. Isotopic data for postglacial products of Aniakchak volcano 55
30. Locations of 135 earthquake hypocenters located by the Alaskan Volcano Observatory for the period January 1, 2009, through January 3, 2013 55
31. Schematic west-southwest–east-northeast cross-sections of the Aniakchak magmatic system through time 65

Tables

1. Weighted mean and other radiocarbon dates for tephra and ignimbrite from Aniakchak volcano 17
2. Radiocarbon dates constraining post-caldera tephra fall deposits from Aniakchak 18

This page left intentionally blank.

Postglacial Eruptive History, Geochemistry, and Recent Seismicity of Aniakchak Volcano, Alaska Peninsula

By Charles R. Bacon, Christina A. Neal, Thomas P. Miller, Robert G. McGimsey, and Christopher J. Nye

Abstract

Aniakchak is a Pleistocene to Holocene composite volcano of the Alaska–Aleutian arc that suffered at least one caldera-forming eruption in postglacial time and last erupted in 1931. The glacially sculpted Pleistocene edifice lies atop gently folded Jurassic to Tertiary sedimentary rocks. Aniakchak products have geochemical characteristics typical of magmatic arcs. Parental basaltic magmas with a range of incompatible-element concentrations are derived from the mantle wedge above the Wadati–Benioff zone, drawn from a region broader than the edifice footprint, and focused in the crust into a conduit and storage system beneath the volcano. Over time, a column of crystal–liquid mush and solidified intrusions has developed to as shallow as a few kilometers below sea level (bsl), allowing differentiated melts to evolve, segregate, and accumulate in crystal-poor bodies as large as several tens of cubic kilometers in volume. The dominant process of magma evolution at Aniakchak is considered to be crystallization differentiation.

The oldest recognized postglacial explosive eruption, andesitic Aniakchak I, left nonwelded ignimbrite in valleys below the edifice and fines-poor welded ignimbrite or agglutinated fall deposits high on its flanks between ca. 9,500 and 7,000 years ago. A small caldera may have collapsed at the source of the ignimbrite, likely just west of the present Vent Mountain. Aniakchak I andesite is geochemically distinct among the postglacial Aniakchak suite for its high K_2O, Zr, and other incompatible-element contents. Subsequent to Aniakchak I, Plinian eruptions ca. 7,000 ^{14}C yr B.P. from a vent northeast of the edifice summit produced the Black Nose Pumice, consisting of a lower unit of rhyodacite lava, pumice fall, and intraplinian welded ignimbrite and an upper unit of dacite pumice fall and northeast flank lava flow. At least 20 additional Holocene eruptions are thought to have occurred before the Aniakchak II caldera-forming event.

The spectacular 10-km-diameter Aniakchak Crater is a caldera that collapsed during the voluminous Aniakchak II eruption ca. 3,590 cal yr B.P. (ca. 3,430 ^{14}C yr B.P.). This eruption produced rhyodacite Plinian pumice fall and ignimbrite, followed first by ignimbrite with both rhyodacite and andesite juvenile clasts, then by andesite ignimbrite. The mixed and andesite ignimbrite deposits commonly are partly welded. Ignimbrite is present in valleys surrounding the edifice and extends to the coast on both northwest and southeast. The crystal-poor rhyodacite is compositionally quite uniform (69.4–70.4 weight percent SiO_2) and is the most evolved and only hornblende-phyric magma erupted from Aniakchak. The andesite is unusual for Aniakchak in having low V and high Na_2O, Y, TiO_2, and, especially, P_2O_5 concentrations. Because both Aniakchak I and II andesites have close analogs at Veniaminof volcano ~100 km down the Alaska Peninsula, these comparatively unusual compositions reflect common processes and are unlikely to be due to local effects of crustal assimilation. With its top as shallow as 1.6–3.7 km bsl, a rhyodacite melt lens at least 400 m thick underlay the approximately 6 km by 8 km area described by the foundered cauldron block. The andesite reservoir apparently was similarly large but not contiguous with that of the rhyodacite, and the two magmas only mingled during transit to the surface during the eruption. The rhyodacite evidently was unrelated to precaldera dacite magmas. It and the andesite represent a new cycle of recharge, storage, and differentiation.

Products of the earliest recognized postcaldera volcanism are small dacite domes extruded from the ring-fracture system into a deep caldera lake and a dacite pumice fall dated at ca. 2,300 ^{14}C yr B.P. The lake probably filled to its maximum of ~620 m above sea level (asl) within a few hundred years of caldera collapse. Pumice Dome (~67.5 weight percent SiO_2) is compositionally similar to lava of the northwest flank flow and to lava exposed in the west wall of the 1931 Main Crater within the caldera, suggesting lateral transport of magma from a common source. Similarly, Vulcan and West Domes (~65.7 weight percent SiO_2) are geochemically indistinguishable yet were emplaced on opposite sides of the caldera floor. Adjacent to Vulcan, Bolshoi Dome is the least evolved (64.2 weight percent SiO_2). These postcaldera dacite–rhyodacites are not remnants of Aniakchak II magma but resulted from differentiation of recharge andesite or basaltic andesite magma.

The three tuff cones on the eastern caldera floor were constructed by alternating Surtseyan and hydrovolcanic explosions. Eruption of the basaltic andesite Windy and Breezy Cones on the ring-fracture system, and of andesitic Surprise

Cone inboard from them, may be related to unloading of the magmatic system by sudden lowering of the intracaldera lake by ~200 m ca. 1,860 ^{14}C yr B.P.

Vent Mountain cone was built by strombolian to violent-strombolian eruptions above the southern ring-fracture segment. Lava that issued from its base flowed as far as ~5 km. Alternating with activity of Vent Mountain, Half Cone produced vulcanian to Plinian explosive eruptions and effused lava above the northwestern ring-fracture segment. Plinian eruption at Half Cone ca. 400 ^{14}C yr B.P. was responsible for the widespread dacitic Pink Pumice and overlying andesitic Brown Pumice fall deposits, as well as intracaldera pyroclastic-flow and surge deposits. The most recent Half Cone activity ended with deposition of agglutinated spatter, edifice collapse, and effusion of the dacitic Cobweb lava flow. Although both vents erupted broadly similar andesite to dacite products, those of Vent Mountain commonly have slightly higher K_2O and lower Al_2O_3 and CaO than those of Half Cone. Melt inclusions in plagioclase from Pink Pumice record passive degassing prior to eruption from as shallow as ~2 km bsl.

Strombolian eruption of scoria and cinder constructed the small Blocky Cone after Half Cone and most Vent Mountain activity. Blocky Cone consists of basaltic andesite (~52.4 weight percent SiO_2) that is more primitive than any other postglacial Aniakchak ejecta save geochemically similar scoria of Breezy Cone. Melt inclusions in olivine phenocrysts indicate that this magma briefly stalled and partially degassed at ~2 km bsl. The relatively primitive magma avoided crystal–liquid mush by finding a path to the surface at the southwest edge of the ring-fracture system.

The only known historical eruption of Aniakchak took place along the outer western segment of the ring-fracture system in May and June 1931. In that eruption, nearly continuous explosive activity at Main Crater, as vigorous as subplinian, yielded dacite–rhyodacite followed by relatively voluminous andesite tephra, ending with minor basaltic andesite, in sum spanning the range ~67 to 56 weight percent SiO_2. Basaltic andesite lava eventually spread across much of the Main Crater floor, and small dacite–rhyodacite lava flows effused at Doublet Crater and Slag Heap (~66 and 69 weight percent SiO_2, respectively). Dissolved volatile contents of melt inclusions indicate that the main volume of dacite magma was stored at a minimum depth of ~4 km bsl.

Current indications of an active magmatic system at Aniakchak include high ^{3}He/^{4}He ratios of CO_2-rich gas escaping from a weakly thermal soda spring, a bull's-eye InSAR pattern of ongoing caldera floor subsidence, and episodic seismicity. Low-frequency (long period, LP) events, interpreted to reflect movement of magma or fluids in fractures, constitute the majority of located earthquakes. Epicenters for 135 events during 2009–2012 (maximum M_L 2.1) define a bow-tie pattern elongated approximately parallel to the Pacific–North America plate convergence azimuth, centered between Half Cone and Vent Mountain. Hypocenters define a laterally extensive region with events 14–25 km bsl that extends to 28 km bsl on the south, few events 7–14 km bsl beneath the caldera, and events <10 km bsl concentrated beneath Vent Mountain and the south caldera rim. Recent seismicity appears to be consistent with a long-lived mush that resides within a seismically quiet zone and from which magma escapes upward to be stored ephemerally as shallow as within ~2 km bsl.

Indications of ongoing activity of the Aniakchak magmatic system suggest that eruptions could be expected following seismic unrest, which potentially could be of as short duration as hours to days. The most likely locations of new vents would appear to be ring-fracture-influenced and west of a north-northwest—south-southeast line through the caldera center. Eruptive scenarios, as described in the preliminary hazard assessment, would include hydromagmatic explosions, possibly followed by effusion or strombolian eruption of basaltic andesite to Plinian eruption of dacite. Lava and pyroclastic flows or surges probably would be limited to within the caldera, but ash fall could affect extensive regions downwind. Another voluminous eruption, such as Aniakchak II, is considered unlikely in the near future. Although the InSAR study indicates subsidence, the possibility that evolved magma may be accumulating beneath the central part of the caldera is worthy of consideration when interpreting future monitoring data.

Introduction

Aniakchak is a historically active caldera volcano of the Alaska–Aleutian arc. Located on the Alaska Peninsula 670 km southwest of Anchorage (fig. 1), the volcano and its pyroclastic apron are mainly within Aniakchak National Monument and Preserve. Ancestral Aniakchak is a glacially sculpted Pleistocene composite volcano that consists of basaltic andesite to dacite lava flows and fragmental rocks. Early in postglacial (Holocene) time, a voluminous eruption (Aniakchak I; Miller and Smith, 1987) left geochemically distinctive andesite pyroclastic-flow deposits (ignimbrite) in valleys and on the flanks of the edifice. This event was followed by dacite eruptions, at least one of which produced a widespread pumice fall deposit ca. 7,000 yr B.P. (VanderHoek, 2009). Unless otherwise noted, ages reported here are given in radiocarbon years before present (yr B.P., "present" being 1950 C.E.).

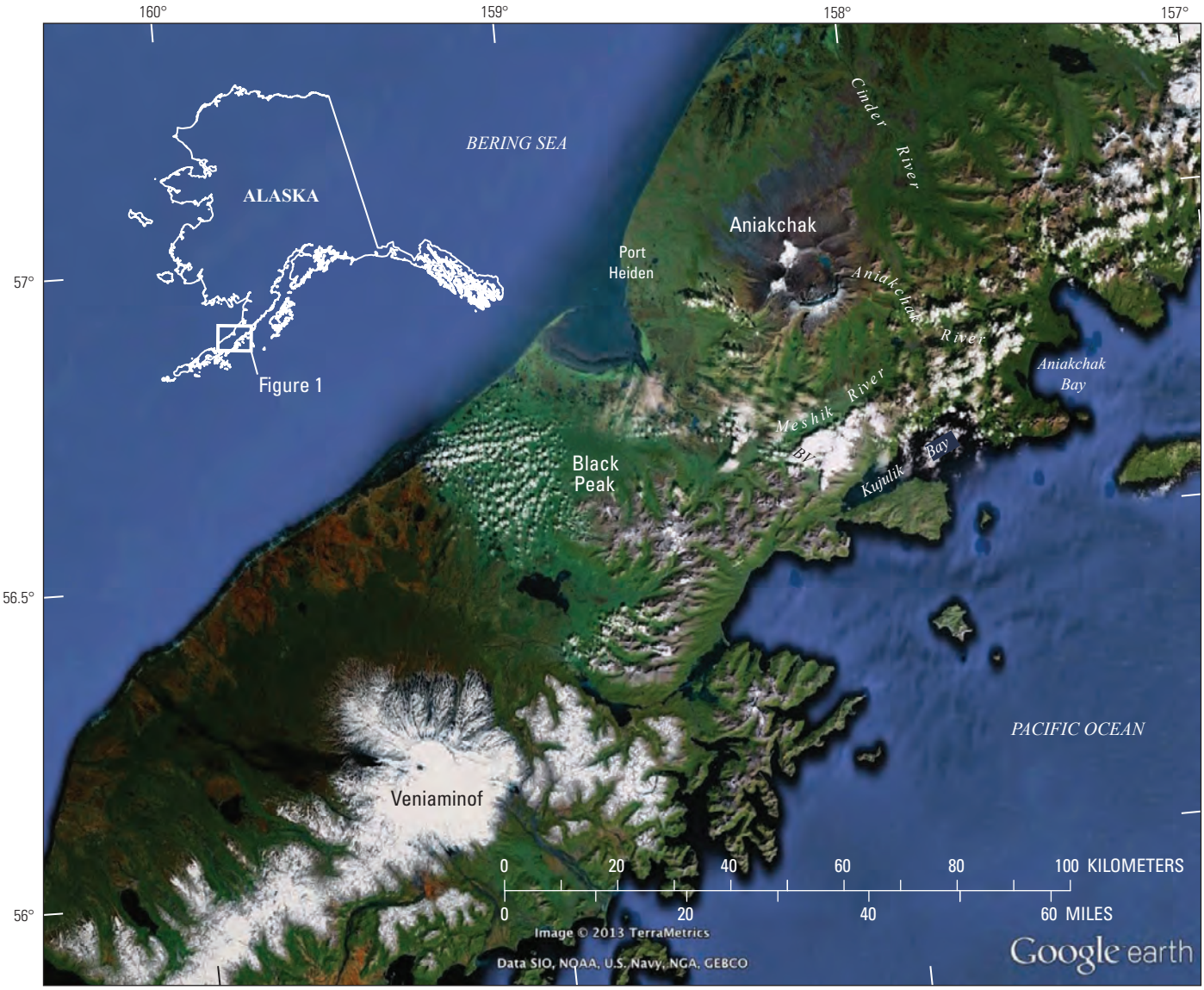

Figure 1. Google Earth image of a portion of the Alaska Peninsula showing Aniakchak, Black Peak, and Veniaminof volcanoes. Blue Violet Creek (BV), mentioned in the section on "Products of the Aniakchak II caldera-forming eruption," drains into Meshik River.

The striking 10-km-diameter caldera known as Aniakchak Crater formed by collapse of the ancestral Aniakchak volcano (fig. 2) during a major explosive eruption ca. 3,430 yr B.P. (Miller and Smith, 1987) that is notable for highly mobile pyroclastic flows (Miller and Smith, 1977). Those flows deposited voluminous compositionally zoned ignimbrite composed of buff-colored rhyodacite (~68–70 weight percent SiO_2) mingled with and overlain by dark gray andesite (~57–60 weight percent SiO_2) (Dreher and others, 2005). The precaldera edifice of Aniakchak volcano is unusual among eastern Aleutian arc volcanoes with ~10 km diameter calderas in being far less voluminous than Veniaminof, Okmok, Fisher, or Emmons Lake volcanoes (Miller and Smith, 1987). In fact, the Aniakchak caldera walls expose Jurassic and Cretaceous sedimentary rocks beneath edifice lavas. Prehistoric postcaldera volcanism has formed four lava domes, a flank lava flow, three tuff cones, and a small scoria cone that we refer to with informal names (capitalized only for clarity), and the larger edifices of Half Cone and Vent Mountain within the caldera (Neal and others, 2001). The domes were emplaced within a caldera lake that catastrophically drained ca. 1,860 B.P. (VanderHoek and Myron, 2004) and thereby rapidly cut The Gates notch in the caldera wall (McGimsey and others, 1994; Waythomas and others, 1996). The caldera-forming eruption, and subsequent eruptive activity, profoundly disrupted human occupation of the area for an extended period (VanderHoek and Myron, 2004).

The most recent eruption of Aniakchak took place during May and June 1931. The 6-week-long eruption, strongest during May 1-11, rained "egg-size" scoria 30 km to the west in Port Heiden (then Meshik), spread millimeters of ash fall as far as Kodiak Island, and repeatedly interfered with radio communications in the area. New lava flows were emplaced in the Main (1931) Crater and as small flows at Doublet Crater and Slag Heap toward the end of the activity (see figure 10 for locations of named features within the caldera). Within and near the caldera, the 1931 deposit consists of white pumice lapilli near the bottom and grades upward through a main unit dominated by tan to brown pumice to an upper unit of black pumice. Like an eruption of Half Cone ca. 400 yr B.P. and eruptions at many other Alaskan volcanoes, the 1931 Aniakchak eruption began with relatively silica-rich dacite magma (as much as 69 weight percent SiO_2 in 1931) and ended with relatively silica-poor (basaltic) andesite magma (as little as 56 weight percent SiO_2) (Nicholson and others, 2011). Potential volcanic hazards at Aniakchak were assessed by Neal and others (2001). Ongoing seismicity, escape of magmatic gas, and subsidence of the caldera floor indicate that the magmatic system is active. The Alaska Volcano Observatory (AVO), a consortium of the U.S. Geological Survey (USGS), University of Alaska Fairbanks (UAF), and Alaska Division of Geological and Geophysical Surveys (ADGGS), monitors Aniakchak for any signs of reawakening.

Postglacial Aniakchak is of notable significance to volcanology for its compositionally zoned and highly mobile pyroclastic flows of the caldera-forming eruption, subaqueous domes and catastrophic draining of the caldera lake, and the well documented 1931 eruption. Aniakchak is of petrologic and geochemical interest because of the compositional diversity of its magmas and the common occurrence of zoned eruptions. In this paper we compile geologic information from field studies to document the stratigraphic record of eruptive history. That record is incomplete and still relatively little studied for deposits older than the Aniakchak II caldera-forming event. Here, we document what is known about the products of the largest eruptions. Because systematic petrographic descriptions are not available, we note phenocryst mineralogy only for certain distinctive units. We draw upon the AVO database of chemical analyses of whole-rock specimens from the authors' collections and those made during University of Alaska Fairbanks (UAF) student research projects. The geochemical data characterize products of specific eruptions or volcanic vents, and thereby allow discontinuously exposed deposits to be categorized. Although it is beyond the scope of this report to quantitatively model the magmatic evolution of Aniakchak, processes responsible for the compositions of erupted magmas may be inferred from the systematics of geochemical variations. We plot locations (epicenters) and hypocenters of earthquakes located by AVO for 2009–2012 and suggest how they may be related to magmatic plumbing. The stratigraphic and geochemical data we present will serve as a framework for future topical studies and refinement of the eruptive history of Aniakchak volcano.

Eruptive History Prior to 3,400 Years B.P.

This chronicle begins with a brief overview of Pleistocene ancestral Aniakchak and an account of the state of knowledge of postglacial, precaldera volcanism.

Pleistocene Aniakchak

The lava flows that make up the ancestral Aniakchak volcano are well exposed in the caldera walls and on the south flank of the edifice (fig. 3). Subjacent Mesozoic and Tertiary rocks were mapped and described by Detterman and others (1981a). Aniakchak volcano is located on the north limb and crest of a regional antiform than plunges to the southwest beneath Quaternary alluvial fan and swamp deposits (Detterman and others, 1981b) in the Meshik River drainage (fig. 1). Eccentric collapse of the caldera has revealed outcrops of lava above talus in the north caldera wall and atop Upper Jurassic Naknek Formation and Upper Jurassic and Lower

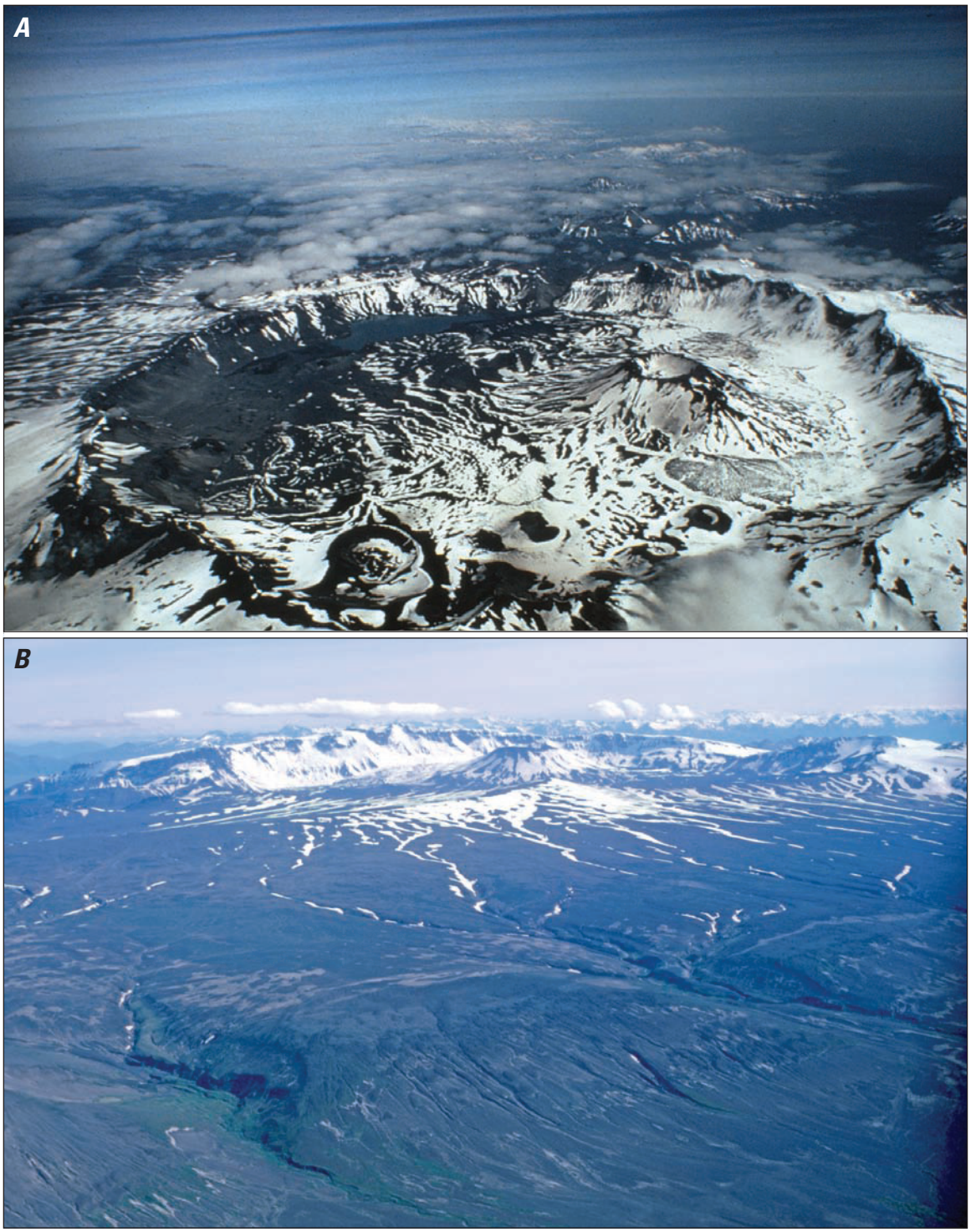

Figure 2. Aerial photographs of Aniakchak volcano and caldera. *A*, View looking east over caldera (National Park Service photo by M. Williams, 1977). *B*, View south-southwest over flank to caldera. Prominent cone within caldera is Vent Mountain.

Cretaceous Staniukovich Formation marine sedimentary rocks in the south wall from The Gates to Birthday Pass. Deep erosion of the south flank of Aniakchak volcano on the Pacific side of the Aleutian Range exposes the base of an embayed cap of Aniakchak lavas on Upper Cretaceous Chignik Formation nearshore and nonmarine sedimentary rocks and Naknek and Staniukovich strata. By contrast, the north, west, and northeast flanks are almost completely hidden beneath unconsolidated pyroclastic debris (fig. 4). Typical minimum elevation of lava exposure on the north flank and in the north caldera wall is ~1,500 ft (~460 m) above sea level (asl), though locally lava crops out as low as 700 ft (~210 m) asl on the northwest. A high ridge that radiates northwest from the north rim suggests a flank vent system, while a north-northeast ridge appears to be a divide between glacial valleys. Gentle slopes below 1,500 ft (460 m) asl on the north may be underlain by lava flows and (or) fragmental debris from Aniakchak or by Eocene and Paleocene Tolstoi Formation sedimentary rocks and volcanics in the Eocene and Oligocene Meshik Formation, which are well exposed in bluffs and slopes south of Barabara Creek west of the edifice and in Birthday Creek valley (fig. 4). North-northeast of the caldera, Aniakchak fragmental debris onlaps and obscures bedrock, presumably the Tertiary formations, that underlies a ~4 km x 8 km west-southwest–east-northeast elongated ~1,200 ft (~370 m) asl mesa. In the south caldera wall, the base of the Aniakchak lava pile is as high as ~3,000 ft (~910 m) asl below Aniakchak Peak, which rises to >4,400 ft (>1,340 m) asl. The lowest mapped remnants of Aniakchak lava on the south flank are at ~1,000 ft (~300 m) asl.

The concept of late Pleistocene Aniakchak that emerges is of a composite volcano of moderate size whose glacially sculpted summit would have been south of the center of the present caldera. Bedrock morphology of glacial valleys heading in Aniakchak lavas would have been essentially as now, with the exception of that of The Gates and Aniakchak River that was extensively modified by draining of the intracaldera lake. Birthday Creek glacial valley cut deeply into the southwest flank of the edifice and extended as a significant declivity well into the area above the present southwest caldera floor. The width and east–west trend of Birthday Creek valley near the modern caldera rim suggest that ice of sufficient volume to carve this large valley may have been sourced in a small late Pleistocene caldera.

The Pleistocene eruptive history preserved by the edifice lavas has yet to be studied in detail. Reconnaissance sampling and geochemical analysis of about 30 specimens provides a general compositional range for Aniakchak erupted magmas over the probable several hundred thousand years during which the edifice was constructed (Nye and others, 1993). There doubtless exist materials emplaced during glacial conditions, so that a record of volcanism during different climatic conditions could be obtained through additional field study and argon geochronology. For the present report, we are limited to employing the geochemistry of edifice lavas as context for compositional diversity among products of postglacial Aniakchak.

Products of the Aniakchak I Explosive Andesite Eruption

Miller and Smith (1987) recognized ignimbrites from two major eruptions, Aniakchak I and Aniakchak II. Aniakchak I nonwelded andesite ignimbrite is overlain by a sequence of tephras that includes ca. 4,600 yr B.P. ash from Black Peak (Miller and Smith, 1987; McGimsey and others, 2003) and therefore is significantly older than the ca. 3,400 yr B.P. Aniakchak II caldera-forming eruption (figs. 5*A* and 6*A*). Both Aniakchak I and the andesite portion of compositionally zoned Aniakchak II occur as dark-gray nonwelded, poorly sorted ignimbrite and also as partly welded fines-poor agglutinated bomb deposits. The latter material is locally exposed in gullies on the north flank (fig. 4, unit Qag). Aniakchak I and andesitic Aniakchak II exposures can be indistinguishable in the field. Where stratigraphic evidence for a pre-3,400-yr B.P. age is lacking, however, these units can be readily identified by their chemical compositions. Even though their silica concentrations and crystal contents are similar, Aniakchak I andesite has uniquely high K_2O, Zr, and many other incompatible-element concentrations (see "Geochemistry" section). Systematic search for Aniakchak I using geochemical fingerprinting has not been done, so the true maximum extent of pyroclastic flows from that eruption remains to be determined.

Deposits of unconsolidated and partly welded andesite bombs and ash found low in north-northwest flank gully exposures, in Birthday Creek drainage and Birthday Pass, and below the caldera rim north of The Gates have distinctive Aniakchak I chemistry. These are considered to have been emplaced by pyroclastic flows during one or a few closely spaced eruptions that constitute the Aniakchak I event. The deposits in valleys clearly postdate the last major glacial advance. Large patches of Aniakchak I partly welded ignimbrite, consisting of flattened bombs as large as ~1 m and lithic fragments in an indurated matrix, are present on north and south sides of the floor of the Birthday Pass beheaded glacial valley at elevations between ~2,100 ft (640 m) and ~2,450 ft (750 m) asl (fig. 6*B*; see also fig. 10*A*). Vertical cooling joints cut the entire ~30-m-thick exposure on the north side of the valley, where differences in induration suggest three or more flow units within a single cooling unit. Possibly, cliff exposures of these remnants of partly welded Aniakchak I ignimbrite were quarried by an early Holocene glacier that originated higher on ancestral Aniakchak, before formation of the caldera that we associate with Aniakchak II. The implication is that the Aniakchak I eruption was not accompanied by caldera collapse or, if a caldera formed, it either was too small to engulf the high-edifice source of the Birthday Creek glacier or it rapidly filled with ice that then spilled out Birthday Pass. Alternatively, presence of partly welded Aniakchak I ignimbrite on either side of Birthday Pass but not in the center of the valley could reflect deposition of ignimbrite along the margins of a glacier that occupied the upper valley at the time of the eruption. In that scenario, nonwelded ignimbrite lower in Birthday Creek valley was deposited in the valley floor below

the terminus of the glacier, now marked by a low north-northwest-trending ridge that may be the glacier's terminal moraine 1.8 km west of the pass at ~1,850 ft (560 m) elevation (fig. 7). In that case, the glacier could have been beheaded by caldera collapse associated with the Aniakchak I eruption.

The unique chemical composition of Aniakchak I andesite allows the stratigraphy on the volcano's flanks to be tied to deposits on the caldera rim. Stratigraphic relations are well displayed north of The Gates (fig. 5*B*). Here, Aniakchak I nonwelded ash, bombs, and ash-coated lithic fragments (as large as at least 30 cm), interpreted to be proximal ignimbrite or possibly a lahar, make up the lowest exposed postglacial deposit (fig. 6*C*). A minimum of 3 m thick (the base is not exposed), this unit is overlain by poorly sorted probable fall deposits that contain Aniakchak I bombs to 60-cm diameter. A few tens of meters to the east, separated from the nonwelded deposit by a covered interval, is a 2m-thick outcrop of Aniakchak I agglutinated black vitric cauliform (cauliflower-shaped) bombs (fig. 6*D*). The moderately flattened bombs are as large as 70 cm across. The virtually clast-supported agglutinated bomb deposit, interpreted as proximal Aniakchak I ignimbrite, rests on gravel or colluvium and is overlain by Black Nose Pumice (described below). Correlation of Black Nose Pumice with a fall deposit described and dated at ca. 7,000 yr B.P. by VanderHoek (VanderHoek, 2009; VanderHoek and Myron, 2004) constrains the date of the Aniakchak I eruption to between ca. 9,500 deglaciation and ca. 7,000 yr B.P.

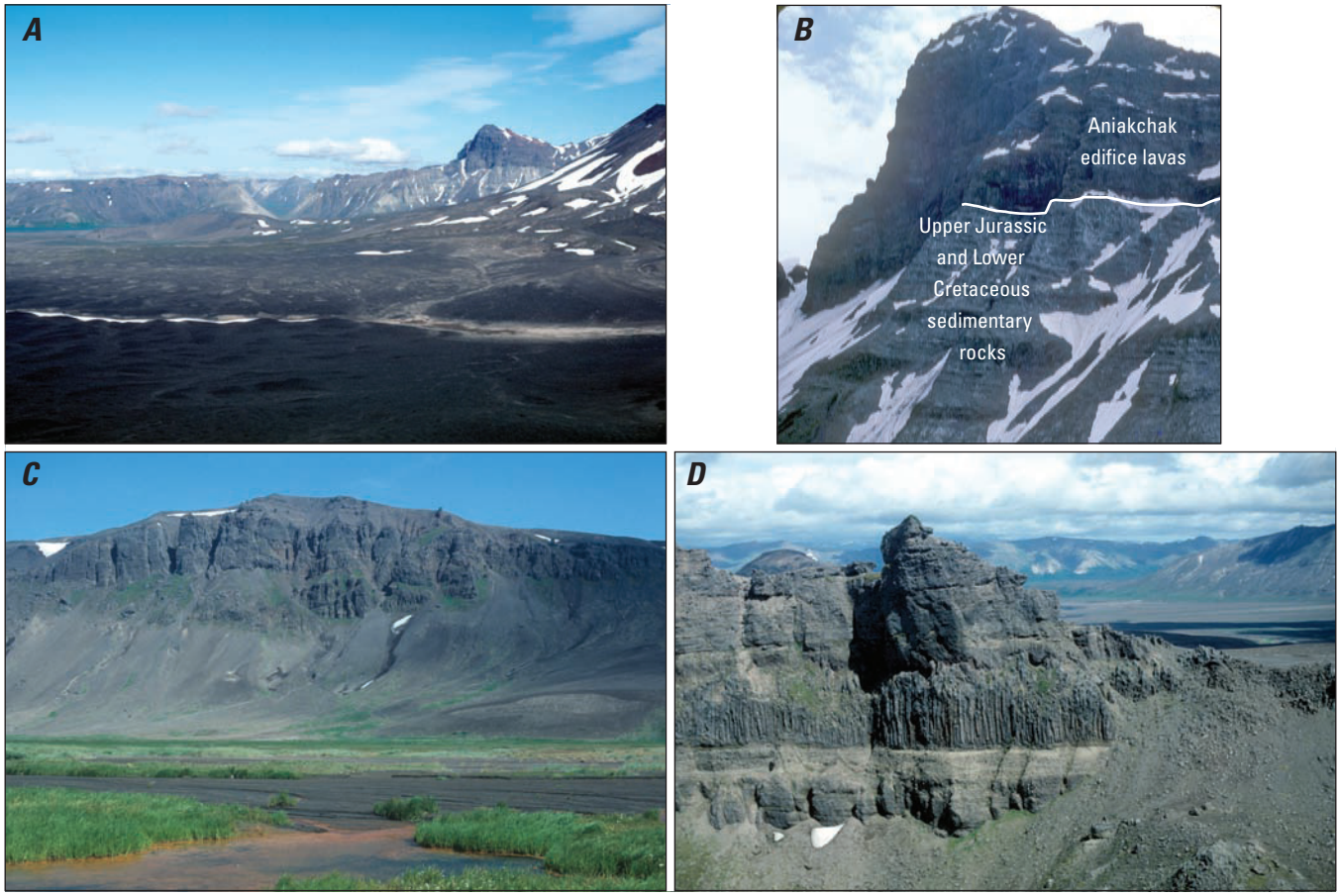

Figure 3. Photographs of Aniakchak caldera walls and edifice. Features shown are labeled in figure 4. *A*, View over Vent Mountain lava east across caldera to The Gates and Black Nose; shoulder of Vent Mountain on right. *B*, Caldera wall below Black Nose. Dark edifice lavas rest on lighter-colored Upper Jurassic Naknek Formation and Upper Jurassic and Lower Cretaceous Staniukovich Formation marine sedimentary rocks. *C*, Edifice lavas in north caldera wall viewed from west end of Surprise Lake. *D*, Aerial view eastward of southeast-flank edifice lavas and breccias of The Garden Wall.

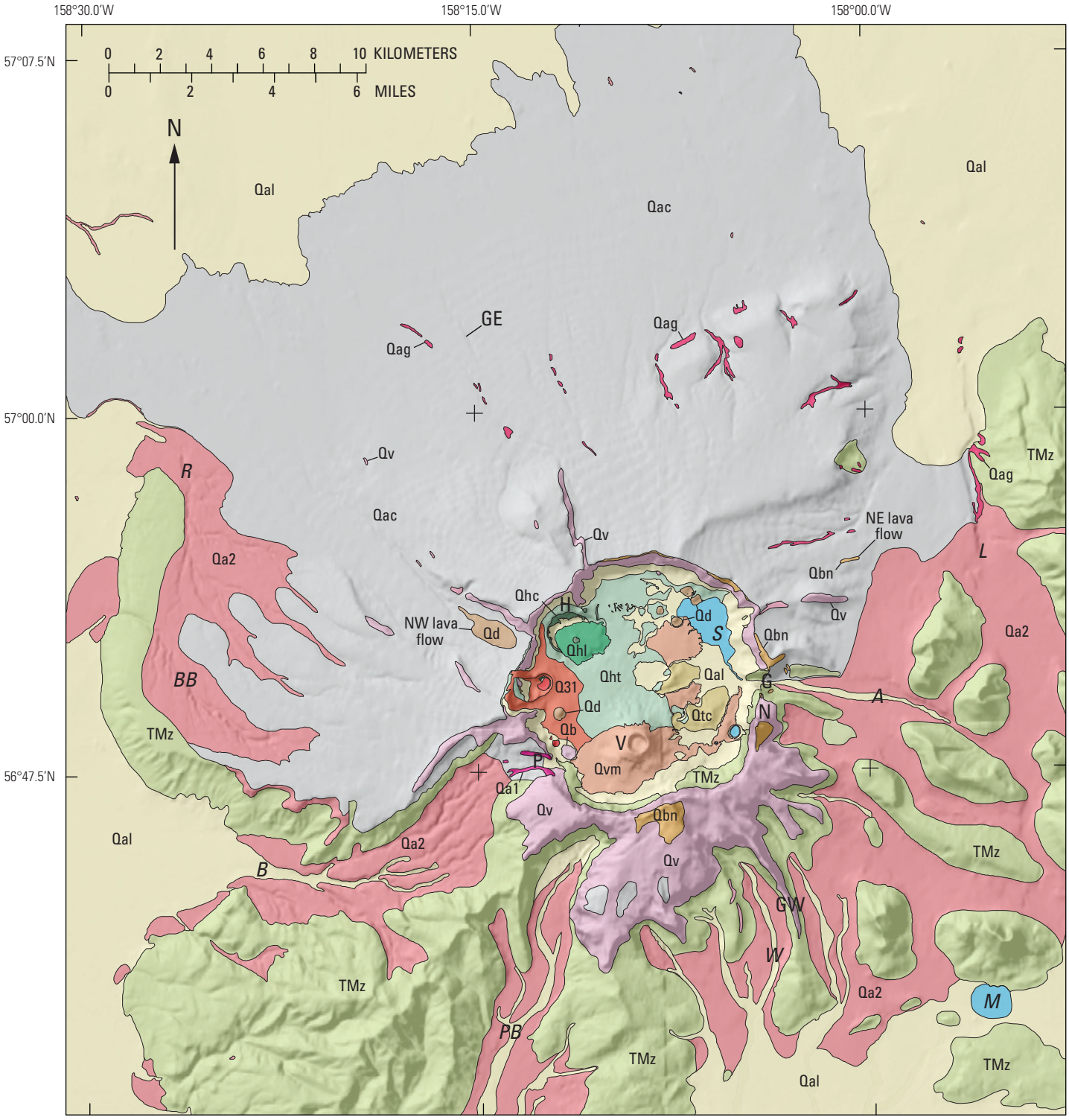

EXPLANATION

QUARTERNARY

Surficial units

- Qal — Undivided surficial deposits
- Qac — Ash and colluvium

Volcanic rocks

- Q 31 — 1931 lava and tephra
- Qb — Blocky cone scoria
- Qhl — Half Cone cow flop lava flow
- Qht — Half Cone tephra
- Qhc — Half Cone lava and deposits
- Qvm — Vent Mountain lava and scoria
- Qtc — Tuff cone
- Qd — Subaqueous domes and related lava
- Qa2 — Aniakchak II ignimbrite
- Qag — Agglutinate-like ignimbrite
- Qbn — Black Nose Pumice and related lava
- Qa1 — Aniakchak I ignimbrite
- Qv — Aniakchak edifice volcanic rocks

TERTIARY AND MESOZOIC

- TMz — Sedimentary rocks

Figure 4. (facing page) Generalized geologic map of Aniakchak volcano and vicinity (modified after unpublished compilation by T.P. Miller, D.H. Richter, R.L. Smith, and C.A. Neal). See figure 10A for more detailed map of caldera geology. Unit Qag consists of fines-poor welded andesite ignimbrite that is dominantly Aniakchak II but may include outcrops of Aniakchak I. Unit Qhc consists of pyroclastic deposits and lava flows from Half Cone. Unit Qa2 consists of nonwelded to welded ignimbrite that is dominantly Aniakchak II but may include outcrops of Aniakchak I; ignimbrite from both eruptions is present in some localities (see text). Tephra from 1931 eruption shown only within caldera. Geographic names: A, Aniakchak River; B, Birthday Creek; BB, Barabara Creek; G, The Gates; GW, The Garden Wall; H, Half Cone; L, Lava Creek; M, Meshik Lake; N, Black Nose; P, Birthday Pass; PB, Plenty Bear Creek; R, Reindeer Creek; S, Surprise Lake; V, Vent Mountain; W, Wind Creek. Locality GE on north flank is gully exposure in figure 6A. Hillshade base from U.S. Geological Survey 30-m digital elevation data.

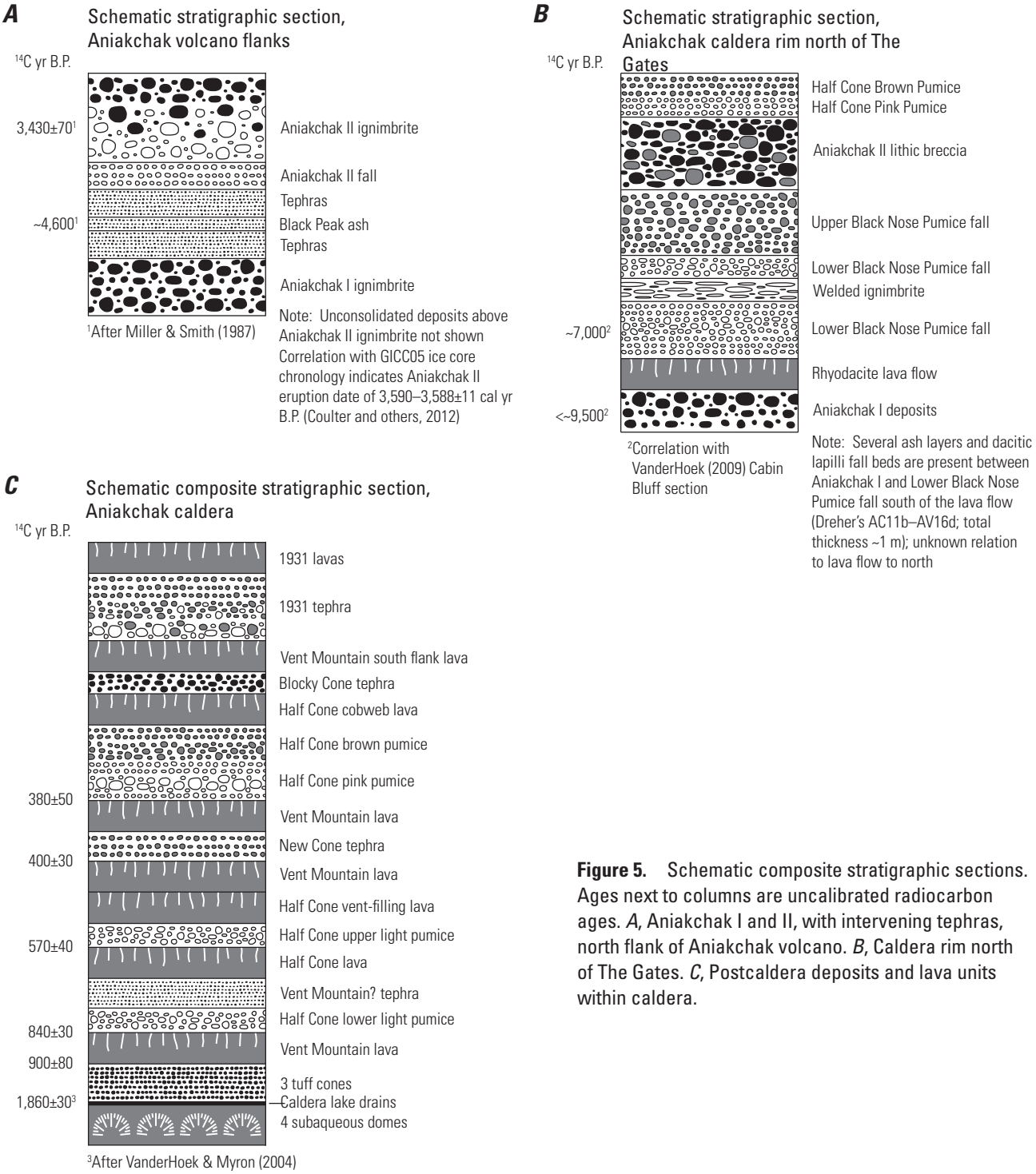

Figure 5. Schematic composite stratigraphic sections. Ages next to columns are uncalibrated radiocarbon ages. *A*, Aniakchak I and II, with intervening tephras, north flank of Aniakchak volcano. *B*, Caldera rim north of The Gates. *C*, Postcaldera deposits and lava units within caldera.

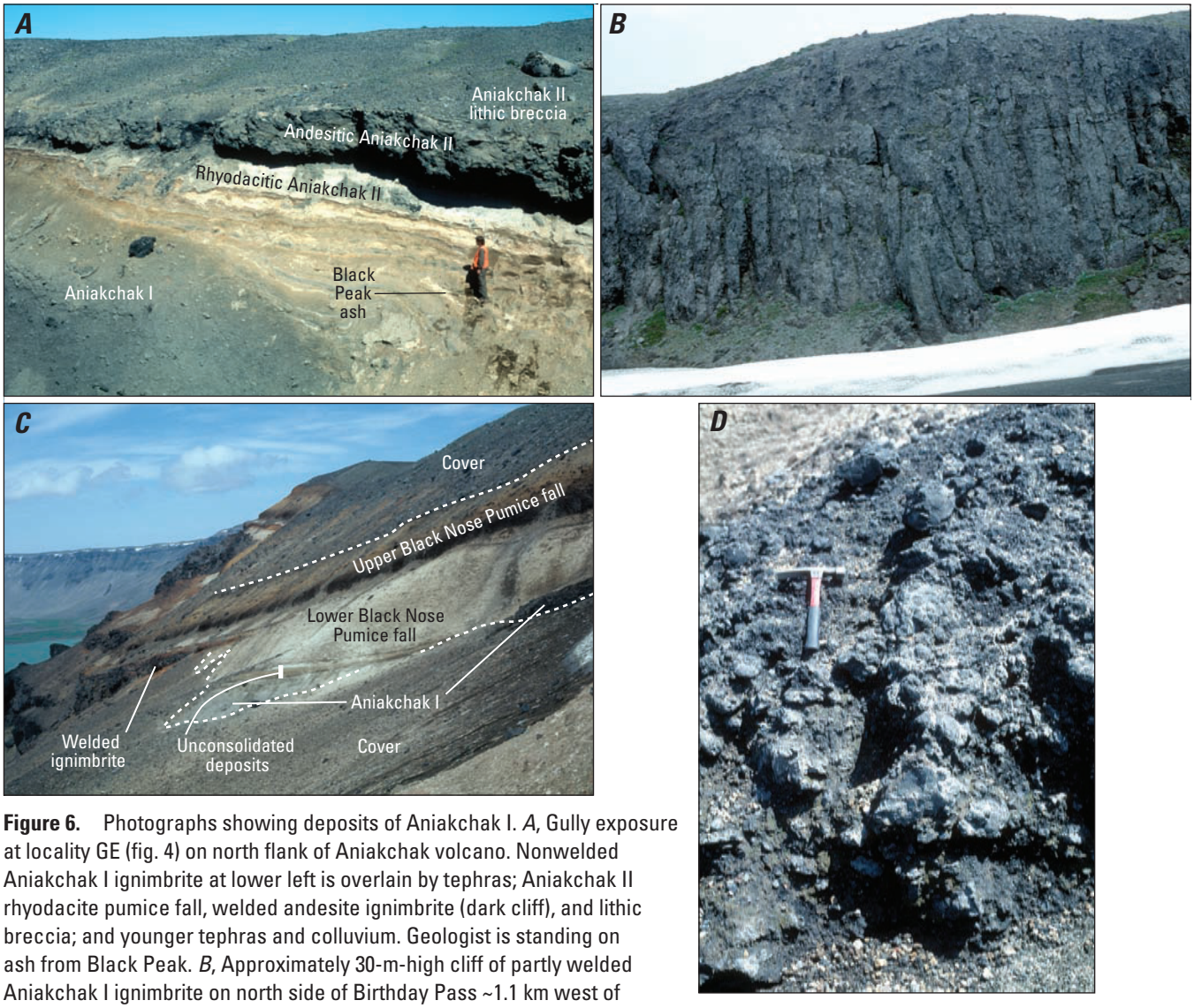

Figure 6. Photographs showing deposits of Aniakchak I. *A*, Gully exposure at locality GE (fig. 4) on north flank of Aniakchak volcano. Nonwelded Aniakchak I ignimbrite at lower left is overlain by tephras; Aniakchak II rhyodacite pumice fall, welded andesite ignimbrite (dark cliff), and lithic breccia; and younger tephras and colluvium. Geologist is standing on ash from Black Peak. *B*, Approximately 30-m-high cliff of partly welded Aniakchak I ignimbrite on north side of Birthday Pass ~1.1 km west of caldera rim (fig. 7). *C*, Postglacial pyroclastic section north of The Gates. Andesite bombs seen in the lowest part of the exposure are Aniakchak I composition. *D*, Agglutinated Aniakchak I cauliform (cauliflower-shaped) bombs underlie Black Nose Pumice a few tens of meters east of the exposure in *C*.

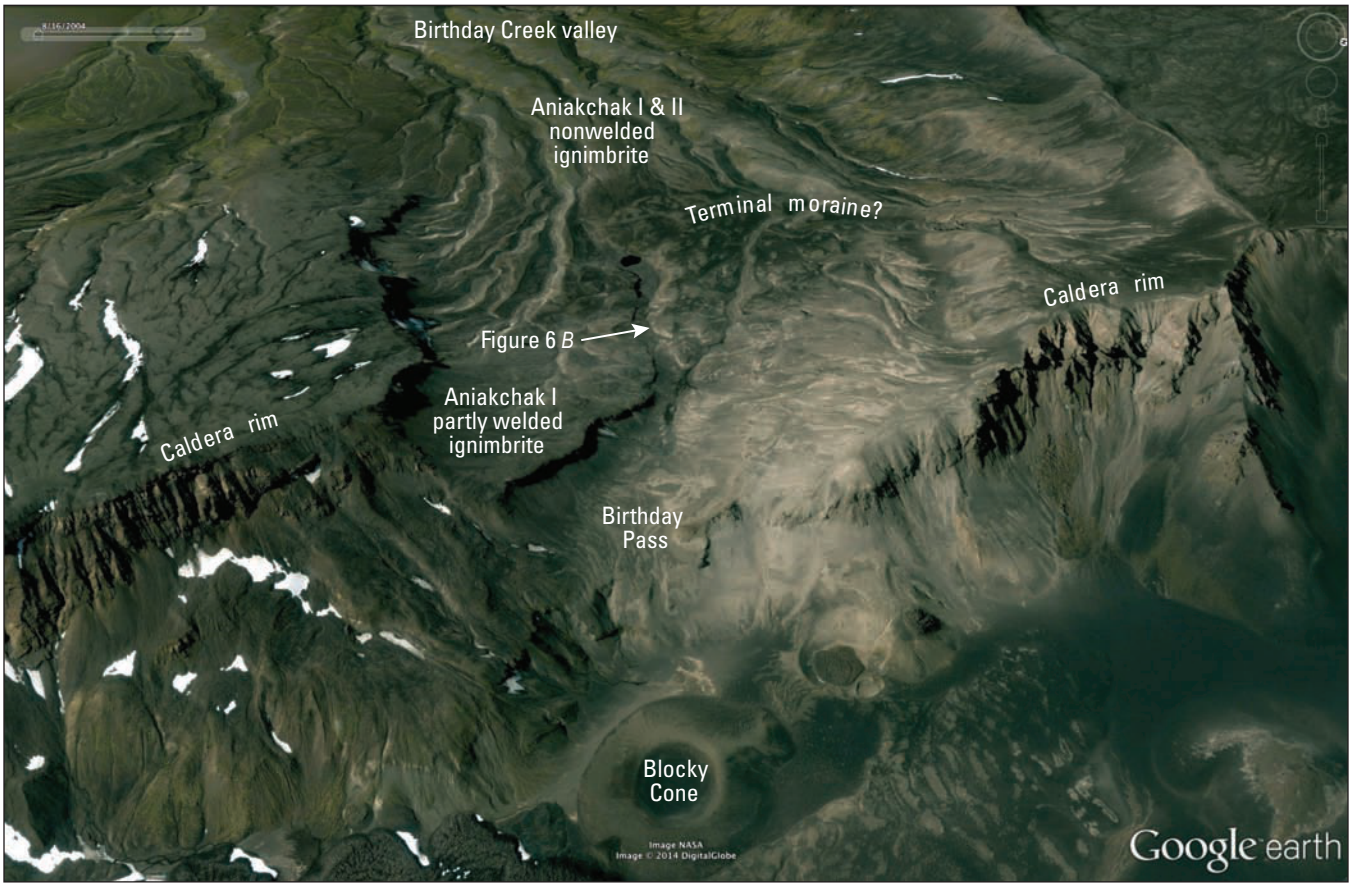

Figure 7. Oblique Google Earth view of Birthday Pass and upper Birthday Creek drainage showing deposits of Aniakchak I eruption and possible terminal moraine. Arrow indicates location of photograph in figure 6*B*.

Precaldera Dacites and Rhyodacites

Two lava flows and several pyroclastic deposits are younger than the last major glacial advance but preceded the Aniakchak II caldera-forming eruption. For convenience, these are referred to as precaldera dacites and rhyodacites.

Dacite and Rhyodacite Lava Flows

A blocky flow of dacite lava is present on the northeast flank of Aniakchak volcano (fig. 4, included in unit Qbn). Compositional affinity of the lava with deposits on the caldera rim indicates that the flow likely postdates Aniakchak I. Dreher (2002, p. 17) reported Aniakchak II lithic breccia resting on the lava.

A second precaldera silicic lava flow or dome is exposed in the cliff at the caldera rim north of The Gates (figs. 5*B* and 8*A*; also included in unit Qbn in map figures). The rhyodacite composition of the lava is more differentiated than that of the northeast flank lava but is virtually identical to that of the overlying lower Black Nose Pumice, which suggests that the lava represents an early phase of the Black Nose Pumice eruption sequence. The lava appears to overlie Aniakchak I deposits.

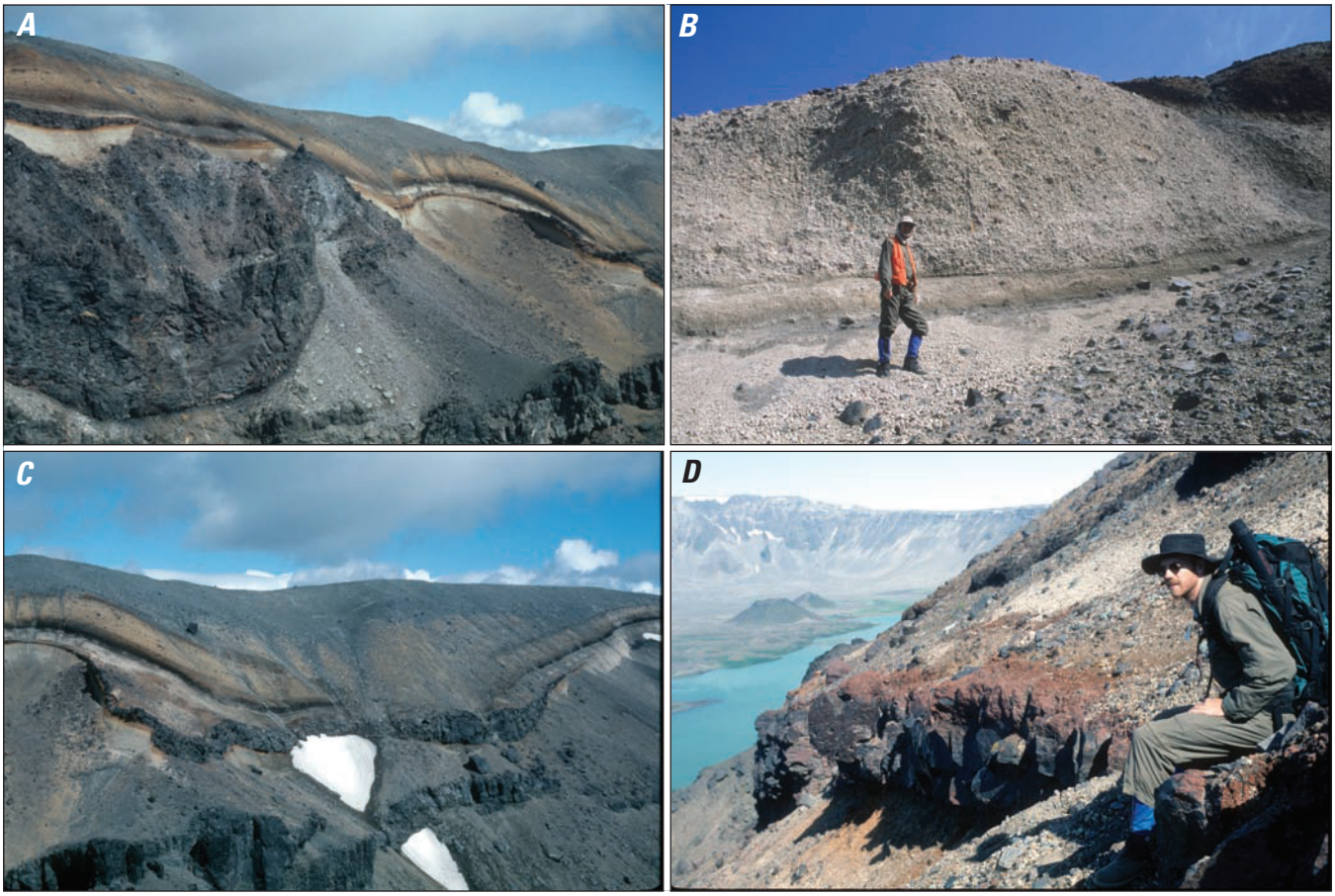

Figure 8. Photographs showing precaldera dacites and rhyodacites north of The Gates. *A*, Aerial view of rhyodacite lava flow forming dark cliff at left, overlain by Black Nose Pumice. Buff colored layers are lower Black Nose Pumice fall with intraplinian welded ignimbrite showing as dark layer of irregular thickness; overlying dark and orange layers are upper Black Nose Pumice fall. Total height of view ~100 m (330 ft). Lowest cliff exposures at lower right are edifice lava. *B*, Lower Black Nose Pumice fall; upper Black Nose Pumice fall at upper right. *C*, Aerial view of Black Nose Pumice deposits immediately south of and continuous with *A*; intraplinian welded ignimbrite thickens in topographic depressions on underlying lower Black Nose Pumice. Height from top of edifice lava to top of view ~75 m (245 ft). *D*, Detail of intraplinian welded ignimbrite near south end of exposures north of The Gates.

Dacite Pyroclastic Deposits Older Than Black Nose Pumice

A meter or more thickness of unconsolidated deposits overlie Aniakchak I material and underlie the Black Nose Pumice in the exposure north of The Gates shown in figure 6*C* ("unconsolidated deposits"). The juvenile clasts in these deposits are dacite pumice. The sequence consists of ≤1 cm of buff ash, 1 cm of gray ash, 15 cm of pumice fall with obsidian chips, 5 cm of dark gray ash, 1 m of pumice fall with ≤0.5 cm obsidian chips and rare bombs as large as 30 cm, and 1 m of ashy probable surge deposit. The two uppermost beds are erosionally truncated. Additional work on tephras, below ash from Black Peak in flank exposures such as shown in figure 6*A* and in distal exposures studied by VanderHoek (2009), may establish correlations with the caldera rim deposits.

Black Nose Pumice

Following Dreher's (2002, p. 17) description of the Black Nose Pumice and prior informal usage of this term, we apply the name to dacite and rhyodacite Plinian pumice fall deposits and intercalated (intraplinian) welded rhyodacite ignimbrite north of The Gates and to correlative deposits elsewhere near the caldera rim. The unit is named for exposures 2.5 km south of The Gates at Black Nose, although a more accessible and probably more complete section is present north of The Gates. An ~2,000-m^2 patch of apparent fall deposit is preserved on a northeast-trending spur at ~1,800 ft (550 m) asl south of the Aniakchak River immediately east of The Gates, which indicates that a deeply incised valley headed just east of the present caldera rim at the time of the Black Nose eruptions. Similarly, a prominent 1,500 ft (460 m) asl bench ~1–2 km east-northeast of The Gates appears to be capped by Black

Nose Pumice. Other remnants of Black Nose Pumice may be present on the ~400 x 700 m bench at ~2,300-ft (700 m) elevation south of The Gates. Black Nose Pumice also may be present below younger deposits on the north and west caldera rim. North of The Gates, Black Nose Pumice dips gently towards the caldera and conformably overlies 1 cm of gray ash and 1 cm of brown ash that rest upon the eroded surface of the previously described unconsolidated dacite pyroclastic deposits. The Black Nose Pumice is overlain by Aniakchak II lithic breccia. The Black Nose Pumice is subdivided into lower and upper subunits (figs. 5*B* and 8).

Lower Black Nose Pumice Fall

The well-sorted beds of the lower Black Nose Pumice consist of highly inflated crystal-poor buff-colored pumice that is rhyodacite in composition. The pumice is chemically less evolved and lacks the hornblende phenocrysts that are present in Aniakchak II rhyodacite pumice (Dreher, 2002). Maximum pumice clast size is ~30 cm. Many clasts have pink interiors and are fractured so that they fall apart when removed from the outcrop. The unit is ~8–10 m thick north of The Gates.

The age of the lower Black Nose Pumice is constrained by tephrochronology. A 45-cm-thick bed of relatively coarse silicic pumice ~40 km southeast of the caldera near Aniakchak Bay (fig. 1) was described by VanderHoek and Myron (2004, their figures 7, 8; Cabin Bluff section, ANI 99–K) and tentatively correlated by them with Aniakchak I. However, on the basis of our electron microprobe analyses of glass, magnetite, and ilmenite from sample ANI 99–K and from Black Nose Pumice on the caldera rim (appendix A, tables A1 and A2), we find that this bed correlates instead with lower Black Nose Pumice. A bulk chemical analysis of lapilli from sample ANI 99–K (appendix B, table B1) bears a resemblance to lower Black Nose Pumice but does not exactly match any Aniakchak pumice, presumably owing to postdepositional modification or another artifact that has resulted in increased MnO and P_2O_5 and decreased SiO_2 concentrations. Fe-Ti oxide thermometry and oxygen barometry for lower Black Nose Pumice and sample ANI 99–K yields preeruption temperatures of ~940–950 °C and oxygen fugacity near that of the Ni-NiO buffer (appendix A, table A2), similar to conditions calculated in the same way for lower Black Nose Pumice oxide analyses in Dreher (2002). Peat from beneath the Cabin Bluff pumice bed yielded a radiocarbon age of 7,350±70 yr B.P., whereas soil beneath the same bed 600 m distant gave 6,760±60 yr B.P. (table 1; VanderHoek and Myron, 2004; VanderHoek, 2009), leading us to suggest an age of ca. 7,000 yr B.P. for the lower Black Nose Pumice. A comparatively thin tephra bed (VanderHoek and Myron, 2004, sample ANI 99–L) beneath the principal fall deposit at Cabin Bluff (ANI 99–K) contains glass and Fe-Ti oxides compositionally similar to those of the principal deposit as well as another population of glass that is more evolved and oxides that have somewhat different compositions (appendix A, tables A1 and A2). We tentatively interpret the lower bed as representing one or more eruptions of Aniakchak volcano precursory to the Black Nose Pumice eruptions.

Intraplinian Ignimbrite

Welded ignimbrite occurs within the lower Black Nose Pumice north of The Gates ~2 m below the top of the lower Black Nose Pumice fall (figs. 5*B*, 8*A*, 8*C*, and 8*D*). About 1–2 m thick at the locality shown in figure 8*D*, the ignimbrite pinches out south towards The Gates and thickens to the north to at least 10 m in topographic lows. The pumice fall deposit immediately beneath the ignimbrite is oxidized brick red by air trapped and heated by the ignimbrite. Fiamme in the welded ignimbrite, which are as large as 30 cm in length, are identical in composition to lower Black Nose Pumice clasts. Where examined, the ignimbrite consists of a principal thick flow unit with reversely graded base, overlain by a possible second flow unit ~1 m thick, the entire deposit forming a single cooling unit. Although lithic fragments are present, no lithic concentration zones were observed. The ignimbrite likely represents collapse of the Plinian eruption column, probably owing to vent widening and increase in eruption rate as deduced for the similar Wineglass Welded Tuff at Crater Lake, Oregon (Kamata and others, 1993).

The ignimbrite is partly to densely welded. Where it is relatively thick, welding and crystallization range, from bottom to top, through (1) black vitrophyric fiamme in a brick-red oxidized vitric matrix; (2) a zone in which the larger fiamme have devitrified cores; (3) devitrified fiamme in black vitric matrix; (4) black vitrophyric fiamme in brick-red vitric matrix; and (5) partly welded tuff with rusty tan matrix. The thickest sections of ignimbrite, which were not visited, probably are devitrified in their interior portions. Thick ignimbrite has gas pockets as large as 50 cm by 25 cm high.

Upper Black Nose Pumice Fall

The upper Black Nose Pumice is a Plinian fall deposit that conformably overlies the lower Black Nose Pumice. As large as 40 cm, clasts of brown pumice are silicic dacite, slightly less evolved than the underlying ignimbrite and lower Black Nose Pumice. This pumice has greater phenocryst content than the lower unit (Dreher, 2002). The well-sorted beds are variably oxidized and incipiently welded. Basal upper Black Nose Pumice fall is partly welded and forms a dark-gray band in caldera rim exposures. This nearly uniform-thickness band and the underlying variable-thickness ignimbrite, separated by ~2 m of buff-colored pumice fall, make a distinctive pair of dark-gray stripes across exposures near the rim of the northeast quadrant of the caldera (figs. 8*A* and 8*C*). The preserved thickness of upper Black Nose Pumice north of The Gates is as much as ~15 m but varies considerably, implying modification during a significant period of erosion. The deposit is overlain by Aniakchak II lithic breccia.

The distribution of upper Black Nose Pumice and any distal correlations have yet to be established, though the thickness, composition, and coarseness of the deposit at the caldera rim imply wide dispersal downwind. Analyzed dacite pumice from a fall deposit beneath Aniakchak II ignimbrite in lower Reindeer Creek (fig. 4, near west edge), sampled by Dreher (2002; sample 98AC70D), has unique composition but is closest to basal upper Black Nose Pumice.

Post-Black Nose Pumice, Pre-Aniakchak II Interval

The geologic record of Aniakchak eruptive activity in this time interval has only begun to be studied. The tephra record is complicated by the possible presence of material from Black Peak and Veniaminof volcanoes. Some of the deposits described by VanderHoek (2009), VanderHoek and Myron (2004), and Riehle and others (1999) are thought to represent eruptions of Aniakchak. However, few radiocarbon ages are associated with these tephras. Neal and others (2001, p. 4), referring to Riehle and others (1999), suggest that at least 20 explosive eruptions occurred at Aniakchak in postglacial time before the Aniakchak II eruption. It is not surprising that deposits from this time interval have not been reported from caldera rim exposures, because the irregular thickness of upper Black Nose Pumice fall at the caldera rim indicates that that unit was eroded before (or possibly by) the Aniakchak II eruption. Gully exposures lower on the edifice and in the pyroclastic apron beyond (such as in fig. 5*A*) are likely to be fruitful places for future study of Aniakchak tephras that may be correlated with distal ash beds.

Products of the Aniakchak II Caldera-Forming Eruption

Modern Aniakchak caldera formed during a large explosive eruption that produced widespread pumice fall and an extensive ignimbrite sheet. The ignimbrite is significant for the high mobility of the pyroclastic flows that deposited it (Miller and Smith, 1977) and for dramatic compositional zonation of rhyodacite followed by andesite (Miller and Smith, 1977; Dreher, 2002; Dreher and others, 2005). Ash from this eruption has been identified over a large part of the Alaska Peninsula and on the Alaska mainland as far north as the Seward Peninsula (Riehle and others, 1987; Begét and others, 1992). Miller and Smith (1987) reported a weighted mean age of 3,430±10 B.P. for three charcoal samples from the ignimbrite at widely separated localities. Recalculation of the weighted mean age and uncertainty yields 3,430±70 yr B.P. with a mean square of weighted deviates (MSWD) of 0.31 (table 1). Begét and others (1992) reported a similar weighted mean age of 3,435±40 yr B.P. (MSWD 1.02) for the three charcoal dates plus two on peat beneath ash (from Miller and Smith, 1987) and one from beneath distal ash on the Seward Peninsula (from Kaufmann and Hopkins, 1985). The calendrical age of the eruption is suggested to be 3,590–3,588±11 cal yr B.P. (Coulter and others, 2012) by correlation with chemically analyzed glass shards associated with an acid spike in Greenland ice cores (Pearce and others, 2004; Denton and Pearce, 2006), which compares favorably with the calibrated ±2σ age range of 3550–3870 cal yr B.P. and preferred ±1σ age of 3,660±70 cal yr B.P. for 3,430±70 ^{14}C yr B.P. (table 1).

Rhyodacite Pumice Fall

A buff-colored pumice fall deposit found north and northwest of the caldera marks the first phase of the Aniakchak II eruption. In all known exposures it is overlain by ignimbrite. The pumice fall is well exposed in sea cliff exposures along the Bering Sea coast 28 km northwest of the caldera near the mouth of Reindeer Creek (fig. 9*A*), where an ~20-cm-thick bed mantles underlying topography and contains angular pumice clasts as large as 5 cm (Dreher, 2002). The deposit is ~50 cm thick at a locality 10 km north-northwest and ~75 cm thick 5 km north of the caldera (Dreher, 2002). Pumice composition is identical to the most evolved rhyodacite pumice in the ignimbrite. Begét and others (1992) indicate a northward dispersal axis for Aniakchak II tephra, but the total volume of the fall deposit is not well constrained.

Ignimbrite

The ignimbrite of the Aniakchak II caldera-forming eruption, exposed in glacial valleys around the Aniakchak edifice, on the Pacific coast, and in Bering Sea cliffs as far as 50 km from the caldera (fig. 4), originally covered an area ≥2,500 km^2 (Miller and Smith, 1977). Ignimbrite in valleys is as much as 70–100 m thick. The eruption produced a minimum of 14 km^3 dense rock equivalent (DRE) of rhyodacite and 13 km^3 DRE of andesite, most apparently deposited as ignimbrite (Dreher and others, 2005). This total of 27 km^3 does not include the likely substantial volume of ejecta that must have accumulated within the caldera (see, for example, Lipman, 1997). The following descriptions summarize information presented by Dreher (2002), who subdivided the ignimbrite deposits into rhyodacite, mixed, and andesite units, supplemented by the authors' field observations.

Rhyodacite Ignimbrite

The first ignimbrite emplaced, the rhyodacite unit is largely obscured by overlying mixed and andesite ignimbrite. Maximum pumice size in the poorly sorted and seemingly structureless deposit typically is ~20 cm. Rhyodacite ignimbrite may have only rhyodacite clasts or may contain several percent of andesite clasts, up to a maximum of 25 percent. The deposit is as much as 30–40 m thick near the heads of Plenty Bear, Wind, and Birthday Creeks (fig. 4). Rhyodacite ignimbrite is exposed in Reindeer Creek (fig. 4) all the way to the Bering Sea cliffs. Ignimbrite in most exposures is nonwelded. In Reindeer Creek, the deposit is incipiently welded 12 km

from the caldera, where it is at least 23 m thick and overlain by andesite ignimbrite; at 16 km, the base is exposed, the interior of the deposit is partly welded and forms cliffs as high as 3 m, and pumice clast size increases upward. Rhyodacite ignimbrite is revealed in gullies 10 km northeast of the caldera, where it is overlain by fines-poor welded andesite ignimbrite (fig. 9*B*). Nonwelded rhyodacite ignimbrite 2.5 m thick, with maximum pumice size 6 cm, overlies the fall deposit in a depression in beach deposits visible in the Bering Sea cliffs near the mouth of Reindeer Creek (fig. 9*A*). A small exposure 26 km south of the caldera in Blue Violet Creek (fig. 1) probably is Aniakchak II rhyodacite ignimbrite or a related surge or remobilized deposit.

Mixed Ignimbrite

Dreher (2002) stated that most ignimbrite that contains both andesite and rhyodacite juvenile clasts at the same stratigraphic level has at least 25 weight percent andesite, and he therefore defined mixed ignimbrite as having 25–75 weight percent andesite. The cutoff between mixed and other ignimbrite is arbitrary and, for practical purposes, mixed ignimbrite has abundant clasts of both rhyodacite and andesite. Mixed ignimbrite is found at ≥10 km from the caldera. The deposit occurs between rhyodacite and andesite ignimbrite 15 km southwest of the caldera in Barabara Creek (fig. 4). More commonly, rhyodacite ignimbrite, if present, is not exposed and

Figure 9. Photographs showing deposits of the Aniakchak II eruption. *A*, Rhyodacite ignimbrite overlying ~20 cm of rhyodacite pumice fall southwest of Reindeer Creek, Bering Sea coast. *B*, Rhyodacite ignimbrite overlain by thin andesite ignimbrite ~13 km west of caldera, Reindeer Creek (photograph by W. Hildreth). *C*, Mixed ignimbrite overlain by andesite ignimbrite 10 km east of the caldera, Lava Creek. *D*, Conglomerate clast in lithic breccia north of The Gates.

mixed ignimbrite may be overlain by andesite ignimbrite, as in Lava Creek 10 km east of the caldera (fig. 9C). There, Lava Creek has cut down to resistant, partly welded mixed ignimbrite, which suggests that mixed ignimbrite may be partly welded in other drainages at or below present creek-bed levels. In exposures on the Bering Sea coast and in a gravel pit in Port Heiden, the mixed deposit is tens of meters thick and comprises three flow units. Mixed ignimbrite occurs on the Pacific side of the peninsula, beyond passes as high as 260 m in the rugged Aleutian Range and as much as 50 airline km from the caldera; total thickness of mixed and andesite ignimbrite at Kujulik Bay is 10 m (fig. 1; Miller and Smith, 1977).

Andesite Ignimbrite

Agglutinated cauliform (cauliflower-shaped) andesite bombs with little interstitial fine-grained matrix constitute partly welded andesite ignimbrite or proximal fall on the flanks of the edifice in exposures 2–11 km from the caldera on northwest to east-northeast azimuths (figs. 6*A* and 9*C*). Comparison with spatter-rich andesitic pyroclastic-flow deposits at Santorini, Greece, described by Mellors and Sparks (1991), suggests that the Aniakchak II partly welded material probably had a similar flow origin, possibly involving access of water to the vent(s). At greater distances, the deposit is matrix-supported nonwelded ignimbrite that commonly is lithic-rich near its base, such as in Reindeer and Birthday Creeks. Banded rhyodacite–andesite pumice clasts are common in mixed and andesite ignimbrite.

Lithic Breccia

Clast-supported lithic breccia, comprising volcanic clasts from the edifice and cobbles and boulders, including granitic rocks, from conglomerates in the underlying Mesozoic sedimentary section, is present on the upper flanks of Aniakchak volcano (fig. 9*D*). Lithic clasts commonly are several tens of cm across and may exceed 2 m in maximum dimension (figure 8 of Druitt and Bacon, 1986). Juvenile clasts, at least as large as 50 cm, are of Aniakchak II andesite. The bulk, if not all, of the lithic breccia is considered to be the proximal facies of the andesite ignimbrite unit (fig. 6*A*).

Postcaldera Deposits and History

As at most volcanoes, the more recent events are represented by deposits accessible in greater detail than earlier ones because of burial of the older units. Our understanding of postcaldera geologic history is based on unpublished geologic mapping summarized in figure 10*A*. The topographic map in figure 10*B* gives elevations and names of features. The sequence of products as presently understood is depicted in the composite stratigraphic section in figure 5*C*. The postcaldera record at Aniakchak is complicated by a caldera lake having been present for part of the post-Aniakchak II period. Lacking detailed chronological information on early post-Aniakchak II tephras save one, we have no concrete information about the postcaldera eruptive history before extrusion of dactic domes on the lake floor. We describe here an early dacite explosive eruption, subaqueous lava effusions, catastrophic draining of the lake, subsequent hydromagmatic eruptions, later effusive and explosive eruptions, and, finally, the 1931 C.E. events and products.

Early Postcaldera Dacite Pumice Fall

Cream-colored dacite pumice fall is exposed locally in cutbanks beyond the north flank of Aniakchak volcano. Soil from beneath this deposit 18 km north-northwest of the caldera at ~200 ft (60 m) elevation yields an age of 2,130±40 yr B.P., whereas organic sediment from beneath the deposit 14 km north of the caldera at ~300 ft (30 m) elevation gives an age of 2,300±80 yr B.P. (table 2). The weighted mean of these ages is 2,160±40 yr B.P. (table 1), but the large MSWD leads us to prefer the older of the two for a provisional age of ca. 2,300 yr B.P. The composition of a sample of pumice clasts (NA9413) does not exactly match that of any potentially correlative unit within the caldera but nevertheless is rather similar to that of West Dome. We tentatively consider the ca. 2,300 yr B.P. pumice fall to be the product of an explosive eruption within the caldera that preceded or possibly was contemporaneous with emplacement of the subaqueous domes that are described next.

Subaqueous Domes

Within Aniakchak caldera, the oldest known products of postcaldera volcanism are four lava domes that were effused in a caldera lake. Relative ages of informally named Pumice, West, Vulcan, and Bolshoi Domes (fig. 10*A*) are unknown. Pumice Dome is the most chemically evolved, two analyzed samples having 67.2 and 67.7 weight percent SiO_2. Single samples from Vulcan and West Domes are compositionally similar at 65.6 and 65.8 weight percent SiO_2, respectively, while a sample from Bolshoi Dome has 64.2 weight percent SiO_2. The virtually identical compositions of the samples from Vulcan and West Domes suggest that they were emplaced at about the same time.

Table 1. Weighted mean and other radiocarbon dates for tephra and ignimbrite from Aniakchak volcano.

[Dates calibrated using method of Stuiver and Reimer (1993), Calib 7.0 software, and the calibration of Reimer and others (2013); B.P. (before present) ages are reported with respect to 1950 C.E.; age results rounded to the nearest 10 years. S.E., standard error; MSWD, mean square of weighted deviates; n.a., not applicable]

Unit	Reported or weighted mean ^{14}C age ±1 S.E. yr B.P.	MSWD	Calibrated 2σ age range cal yr B.P.	Preferred ±1σ age cal yr B.P.	Notes
Pink Pumice fall	380±50	0.09	310–510	350±20 470±40	Weighted mean of 2 dates
New Cone tephra	400±30	1.45	430–510	480±20	Weighted mean of 3 dates
Half Cone upper light pumice	570±40	0.07	520–650	550±10 620±20	Weighted mean of 2 dates
Half Cone lower light pumice	840±30	0.03	690–800	760±30	Weighted mean of 3 dates
Soil above Surprise Cone (?) tephra	900±80	0.01	680–940	830±80	Weighted mean of 2 dates
Above pebbly sediment, Aniakchak River mouth; flood?	1,860±30	0.16	1,720–1,870	1,780±50	Weighted mean of 2 dates (VanderHoek and Myron, 2004)
Early postcaldera pumice fall	2,160±40	3.61	2,040–2,310	2,140±30 2,270±30	Weighted mean of 2 dates
Aniakchak II ignimbrite	3,430±70	0.31	3,550–3,870	3,660±70	Weighted mean of 3 charcoal dates (Miller and Smith, 1987)
Lower Black Nose Pumice?	6,760±60	n.a.	7,510–7,700	7,620±40	Soil below tephra (VanderHoek, 2009)
Lower Black Nose Pumice?	7,350±70	n.a.	8,020–8,330	8,130±80	Peat below tephra (VanderHoek, 2009)

Table 2. Radiocarbon dates constraining postcaldera tephra fall deposits from Aniakchak.

[Units dated are preliminary based on field correlations and, where possible, bulk chemistry of juvenile clasts; locations in decimal degrees, NAD83 datum; dates calibrated using method of Stuiver and Reimer (1993), Calib 7.0 software, and the calibration of Reimer and others (2013); B.P. (before present) ages are reported with respect to 1950 C.E.; age results rounded to the nearest 10 years]

Field number	Laboratory number	Locality	Latitude (North)	Longitude (West)	Material dated	Unit	Reported ^{14}C age ±1σ yr B.P.	$\delta^{13}C$	Calibrated 2σ age range cal yr B.P.	Preferred calibrated ±1σ age cal yr B.P.	Notes[1]
NA02-6C	GX-29531	14 km N of caldera	57.0670	158.0900	Wood	Half Cone Pink Pumice	360±80	-26.7	280–530	410±90	G(STD) full pretreatment
NA94-24A	B-76809	Pumice Dome gully	56.9348	158.1104	Wood	Half Cone Pink Pumice	390±60	-28.8	310–520	470±40	B(AMS)
85AMm28	I-14, 222	Uncertain	Uncertain	Uncertain	Wood	Half Cone Pink Pumice	500±80	Not determined	430–660	560±80	T
85AMm14	2358	13 km NNE of caldera	57.0583	158.0833	Organic sediment	Half Cone Pink Pumice	590±90	Not determined	480–700	590±60	U
85AMm20	2358	11 km N of caldera	57.0500	158.1250	Organic sediment	Half Cone Pink Pumice	590±160	Not determined	300–800	600±130	U
NA92-68	WW212 CAMS9851	3 km NE of Vent Mtn	56.9018	158.1114	Uncertain	New Cone	390±60	Not determined	310–520	470±40	L(AMS)
94-CW104-C14-1	B-77038	4 km NE of caldera	56.9556	158.0278	Wood	New Cone?	340±50	-28.8	310–500	390±70	B(STD) full pretreatment
94-CW105-C14-1	B-77039	14 km N of caldera	57.0670	158.0901	Organic sediment	New Cone?	460±50	-25.1	430–560	510±30	B(AMS) acid wash; low C sediment
NA93-104A	W-6540	Pumice Dome gully	56.9348	158.1104	Wood	Half Cone upper light pumice	560±60	Not determined	510–660	540±20 620±20	U(STD) full pretreatment
NA97-12I	GX23441	6 km ESE of caldera	56.8698	157.9769	Soil; humic fraction	Half Cone upper light pumice	580±50	-25.8	520–660	550±10 620±30	G(AMS) full pretreatment
NA97-6C	GX23439	Pumice Dome gully	56.9348	158.1104	Soil; humic fraction	Half Cone lower light pumice	300±115	-26.5	240–520	390±110	G(STD) full pretreatment
94-CW110-C14-1	B-77041	NE caldera rim	56.9387	158.0899	Plant	Half Cone lower light pumice	830±60	-28.3	670–910	740±50	B(AMS) full pretreatment
NA97-12A	GX23440	6 km ESE of caldera	56.8698	157.9769	Soil; humic fraction	Half Cone lower light pumice	840±60	-26.6	680–910	740±60	G(AMS) full pretreatment
NA97-13B	GX23442	12 km SE of caldera	56.7878	157.9566	Soil; humic fraction	Half Cone lower light pumice	850±55	-26.4	680–910	740±50	G(STD) full pretreatment
NA97-6B	GX23438	Pumice Dome gully	56.9348	158.1104	Soil; humic fraction	Above Surprise Cone?	890±150	-26.5	620–1090	810±120	G(STD) full pretreatment

Table 2. Radiocarbon dates constraining postcaldera tephra fall deposits from Aniakchak.—Continued

[Units dated are preliminary based on field correlations and, where possible, bulk chemistry of juvenile clasts; locations in decimal degrees, NAD83 datum; dates calibrated using method of Stuiver and Reimer (1993), Calib 7.0 software, and the calibration of Reimer and others (2013); B.P. (before present) ages are reported with respect to 1950 C.E.; age results rounded to the nearest 10 years]

Field number	Laboratory number	Locality	Latitude (North)	Longitude (West)	Material dated	Unit	Reported ^{14}C age ±1σ yr B.P.	$\delta^{13}C$	Calibrated 2σ age range cal yr B.P.	Preferred calibrated ±1σ age cal yr B.P.	Notes[1]
NA94-24D	B-76810	Pumice Dome gully	56.9348	158.1104	Organic sediment	Above Surprise Cone?	910±90	-26.2	680–970	840±80	B(STD) acid wash; low C sediment
NA02-6B	GX29530	14 km N of caldera	57.0670	158.0901	Soil; humic fraction	Dacitic pumice; source uncertain	2,130±40	-25.1	2,000–2,180 2,240–2,300	2,100±60	G(AMS) full pretreatment
94-CW106-C14-1	B-77040	18 km NNW of caldera	57.0943	158.2740	Organic sediment	Dacitic pumice; source uncertain	2,300±80	-25.8	2,110–2,520	2,320±210	B(STD) acid wash; low C sediment

[1]B, Beta Analytic; U, U.S. Geological Survey Laboratory, Reston (M. Rubin, analyst) and Menlo Park (S. Robinson, analyst); G, Geochron Laboratory; L, Lawrence Livermore, Mass Accelerator date, T, Teledyne; STD, Standard ^{14}C processing; AMS, Accelerator mass spectrometry.

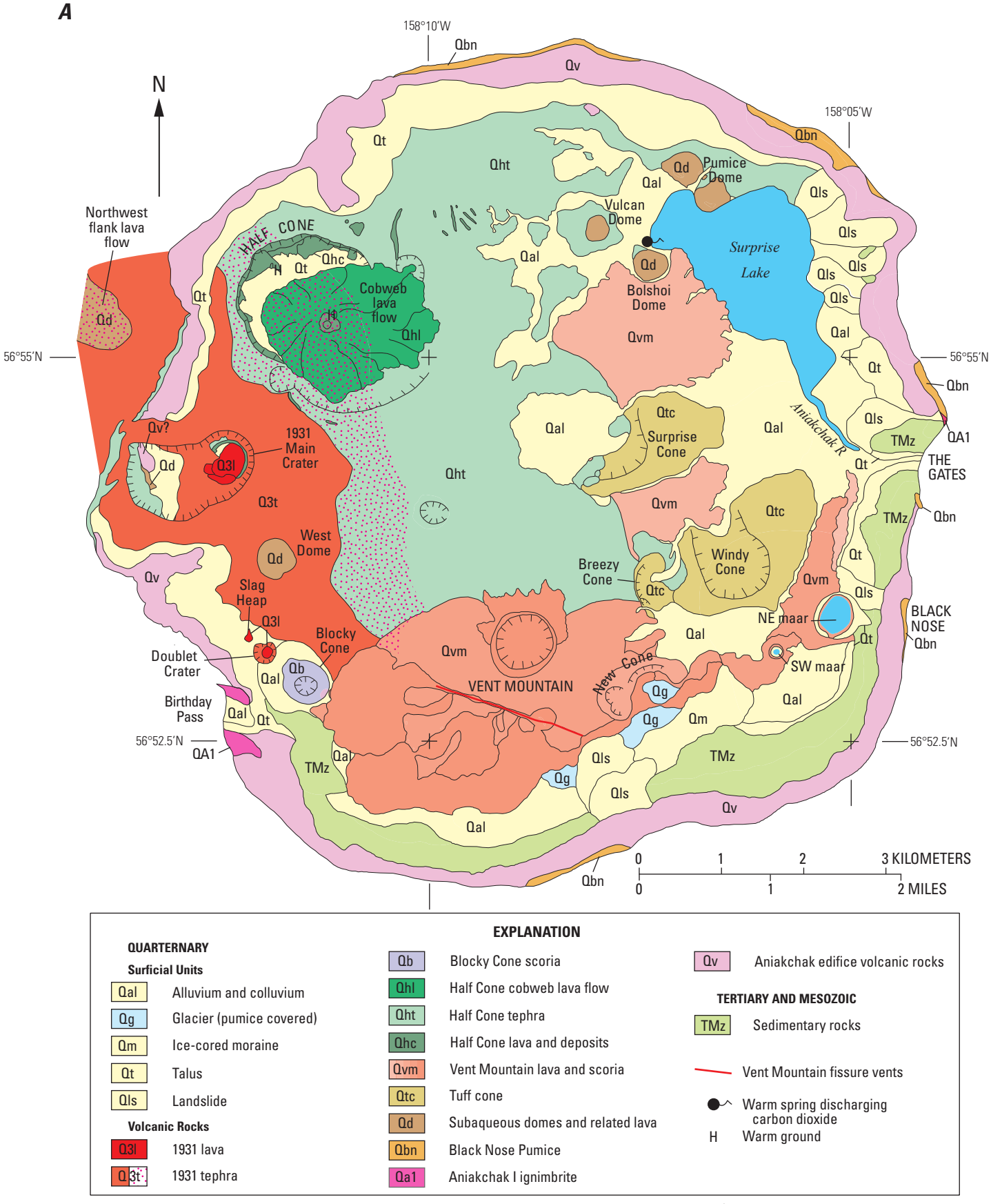

Figure 10. Maps of Aniakchak caldera. *A*, Simplified geologic map of Aniakchak caldera (modified after figure 5 of Neal and others, 2001, and unpublished geologic mapping by C.A. Neal, R.G. McGimsey, and T.P. Miller). Tephra of 1931 eruption (unit Q3t) shown by solid color where thick (visible in aerial photographs) and by stipple pattern where thinner or mantling northwest flank lava flow. *B*, Portion of the Chignik D–1 quadrangle 1:63,360-scale topographic map (U.S. Geological Survey, 1963) with corrected location of Half Cone and addition of informal names.

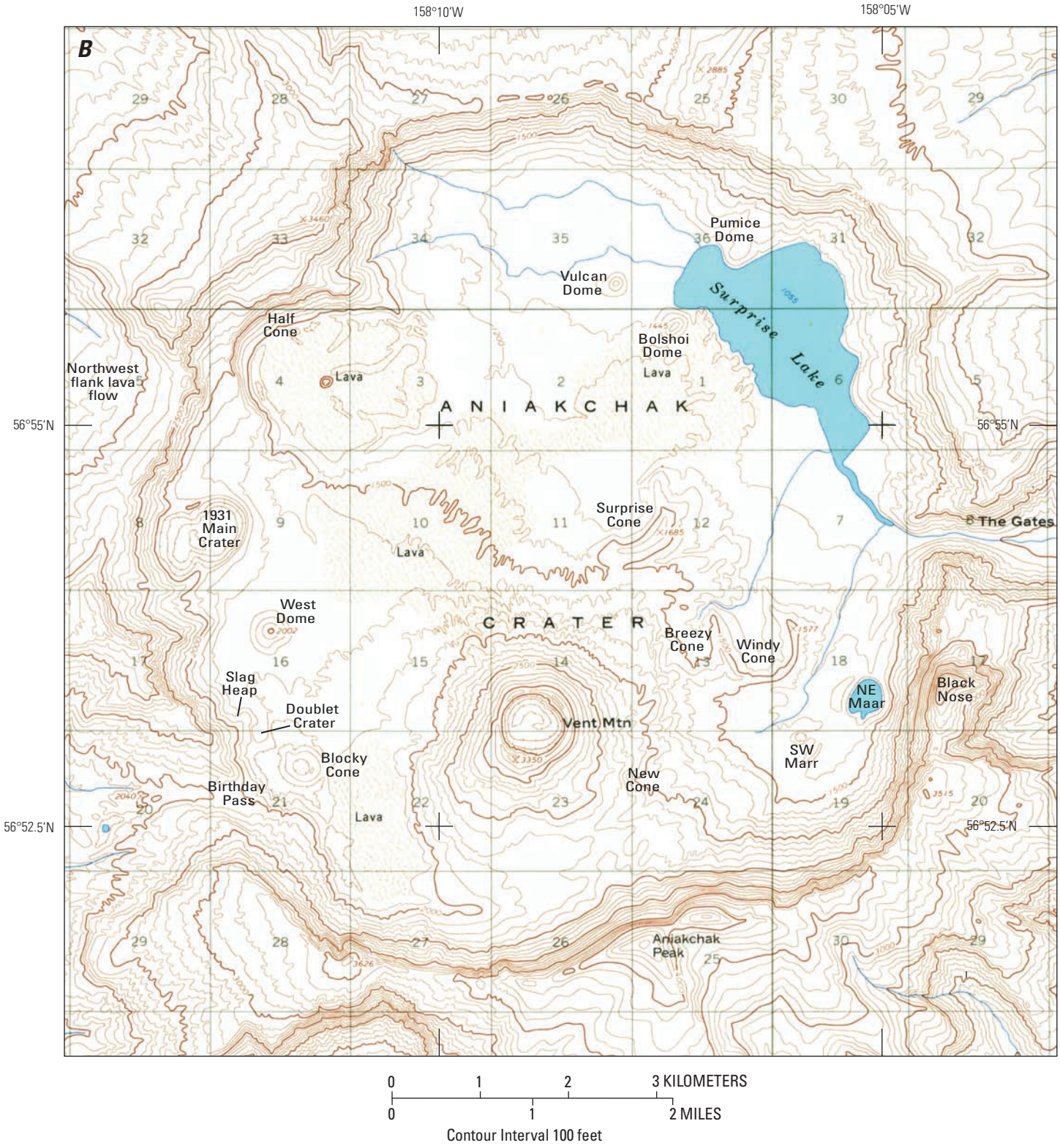

Figure 10.—Continued.

Morphologies and surface features of the domes and the glassy character of the dacite lavas indicate that they were emplaced in water. The surface of Pumice Dome, poorly exposed other than in gullies and facing Surprise Lake, consists of pumiceous dacite in pillow-like forms ~0.3–2 m across (fig. 11*A*) that are atypical of subaerial silicic lava but are consistent with extrusion into standing water. The surfaces consist of frothy, friable, light gray to white pumice characterized by cm-scale radial fracturing and irregular jointing (Allen and McPhie, 2000). Vugs as large as 20 cm across occur within pillows. Interstitial material is also pumiceous, banded, and radially fractured. West, Vulcan, and Bolshoi Domes are conical mounds of dacite vitrophyre whose flanks are coated by talus composed of finely vesicular to dense, polygonal joint blocks shed from outcrops on their upper portions. Outcrops on these three domes have fracture patterns (figs. 11*B–F*) that are characteristic of chilling of degassed lava effused in water (see, for example, Goto and McPhie, 1998). Many structures and fracture patterns in lava flows and domes emplaced in contact with melt water within glaciers or adjacent to glacial ice (Lescinsky and Fink, 2000; Spörli and Rowland, 2006) closely resemble those in the domes at Aniakchak. Although hyaloclastite or breccia carapaces are not evident, 2–3-cm-thick patches of gray, sandy, and partially indurated tuffaceous sediment are found in pockets on the summit of Vulcan Dome. Thick glacial ice probably was not present at any time in the post-Aniakchak II caldera, whereas a deep intracaldera lake must have existed when the dacite domes were emplaced.

Northwest Flank and Intracaldera Rhyodacite Lava Flows

Rhyodacite lava high on the northwest flank of Aniakchak volcano (fig. 4; labeled NW lava flow) is compositionally identical to a thin lava flow exposed within the caldera at ~2,500 ft (760 m) asl 1.5 km to the south, high in the west wall of the 1931 Main Crater (fig. 10; see also "Geochemistry" section), above the level of any possible caldera lake. Little tephra is present and no Aniakchak I or II bombs have been reported on the blocky surface of the northwest lava flow where it has been examined, consistent with the flow being younger and similar in age to the lava in the caldera. The source of the intracaldera lava flow is unknown but appears to have been high on the caldera wall just inside the rim. The vent for the northwest flank flow must have been at ~2,400 ft (730 m) asl, 600 m west-northwest of the caldera rim. On the basis of their composition and apparent post-Aniakchak II age, these two flows are thought to have been approximately contemporary with Pumice Dome.

Ancestral Caldera Lake

Surprise Lake (1,055 ft, 322 m asl) is a remnant of a larger caldera lake evidenced by wave-cut benches on the northeast caldera walls and patches of lake sediment at several locations within the caldera (McGimsey and others, 1994). The lake filled until it overtopped a low point on the east rim of the caldera and then rapidly drained, possibly aided by eruptive activity (McGimsey and others, 1994) or by headward erosion of the canyon of the Aniakchak River. The draining produced a catastrophic flood as the ensuing torrent cut the gorge called The Gates in altered and fractured sedimentary rock (Waythomas and others, 1996). At the time of these publications, the ~1,610 ft (490 m) asl wave-cut terrace recognized by McGimsey and others (1994) was thought to represent the high stand of the caldera lake. Subsequent fieldwork indicated that all four dacite domes were emplaced subaqueously. Because West Dome has a summit elevation of 2,002 ft (610 m), the lake must have reached at least that height, although uplift or tilting of the southwestern caldera floor since the lake drained cannot be ruled out. McGimsey and others (1994) noted that Birthday Pass, elevation ~2,030 ft (620 m), evidently was not overtopped by the lake. Two additional low points in the caldera rim, northeast and east of Surprise Lake, are at ~2,130 ft (650 m) elevation. Both are underlain by Aniakchak volcanic rocks. Before downcutting, the minimum elevation of the caldera wall at The Gates implied by the topographic map (U.S. Geological Survey, 1963; fig. 10*B*) could have been between ~1,900 ft (580 m) and ~2,100 ft (640 m). Because West Dome was emplaced beneath water, its summit elevation and the elevations of Birthday Pass and other low points on the caldera rim together suggest that the surface of the caldera lake probably reached close to 2,030 ft (620 m) asl before it overtopped the wall and cut The Gates. When the lake drained is constrained by radiocarbon ages of 1,850±40 yr B.P. on soil (silt) and 1,870±30 yr B.P. on wood from above pebbly sediment near the Aniakchak River mouth (VanderHoek and Myron (2004, their table 8.1, appendix C, and p. 161–162). The weighted mean of these ages is 1,860±30 yr B.P. (table 1), which apparently dates a change from a pebbly beach to a depositional environment. The suggested date for the flood falls within an ~200 yr gap in human habitation near the mouth of the Aniakchak River (VanderHoek and Myron, 2004, p. 190–191). Evidence for lake sediments on apparently younger tuff cones within the caldera presented in the next section suggests that the catastrophic draining that produced the flood did not cut The Gates to their entire depth but left a residual lake that was larger and higher than present Surprise Lake.

Tuff Cones

Three breached tuff cones form subdued arcuate ridges of bedded phreatomagmatic tephra on the eastern part of the caldera floor (fig. 10*A*, unit Qtc). Embraced and nearly surrounded by younger Vent Mountain lava flows, Surprise, Windy, and Breezy Cones rise ~120 m above the surrounding terrain to define 500–1,000-m-diameter explosion craters (figs. 12*A* and *B*). Two samples of juvenile scoria from

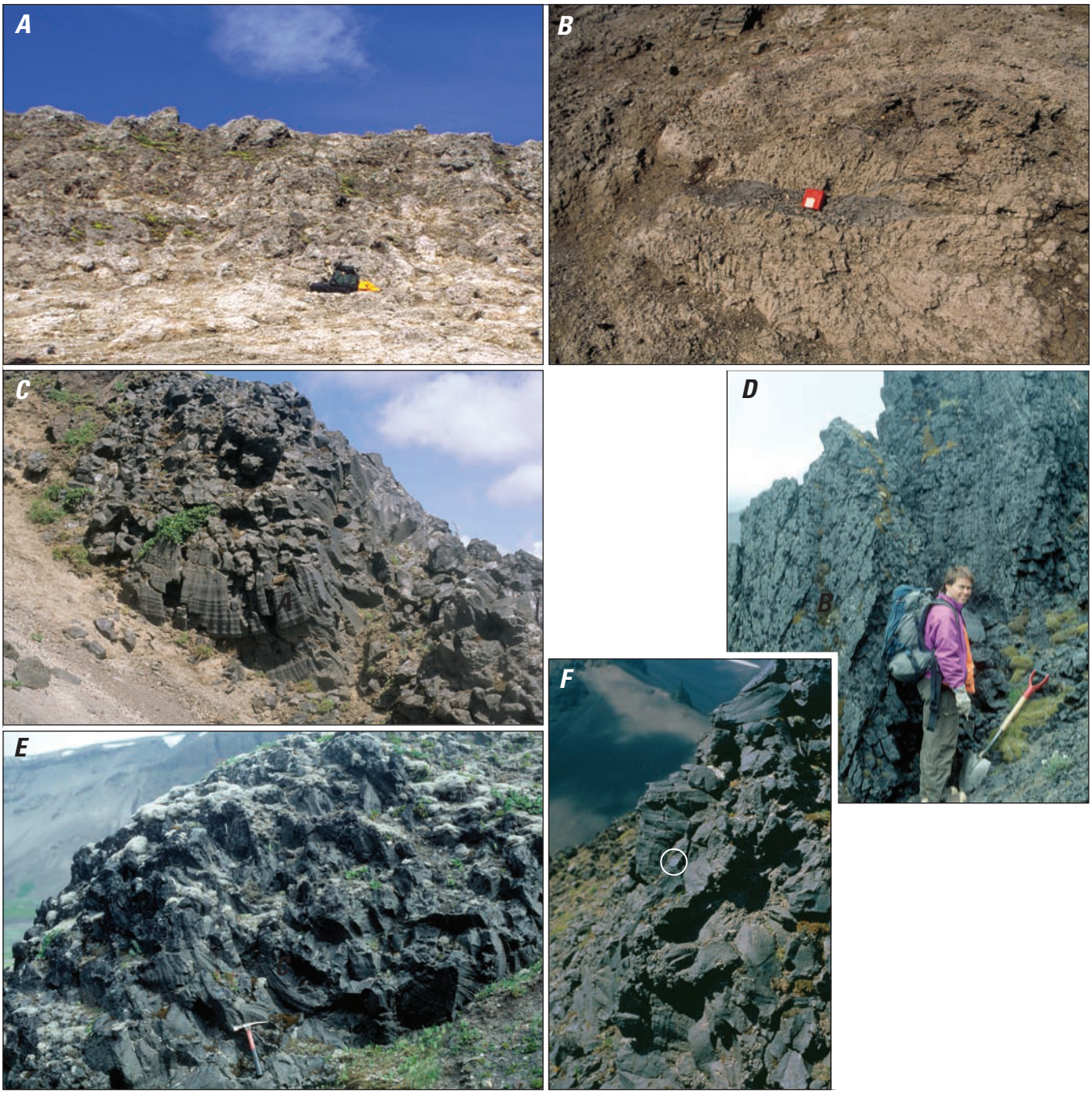

Figure 11. Photographs showing surface features of dacite domes inside Aniakchak caldera. *A*, Pillow-like forms of fractured pumiceous dacite of Pumice Dome. *B*, Detail of pillow in Pumice Dome. *C*, Columns and semi-arcuate structure in vitrophyre of West Dome. Note parallel bands made by steps on joint surface that formed by incremental fracture growth. *D*, Sheet-like sets of columns in vitrophyre, surface of Vulcan Dome. *E*, Poorly developed columns composed of intersecting semiarcuate fractures displaying incremental fracture growth in vitrophyre of Bolshoi Dome. *F*, Pillow forms on West Dome. Note void in center of pillow and radiating, curvilinear columns, lens cap (circled) in center of image for scale. (Photos in *A*, *B*, and *F* by C.A. Neal.)

Surprise Cone have 57.9 and 58.4 weight percent SiO_2, while single analyses of scoria from Windy and Breezy Cones yield 55.3 and 52.3 weight percent SiO_2, respectively. Based on the similar appearances of the tuff cones, we infer that they all are roughly similar in age. Radiocarbon dating of a soil above lapilli tephra of Surprise Cone-like chemistry (NA97-6A) returned a weighted mean age of 900±80 yr B.P. (tables 1 and 2), giving a minimum age for Surprise Cone. Superposition relationships are unclear, although Windy Cone tephra appear to overlap Breezy Cone. The tuff cones have not been dated directly but are thought to postdate catastrophic draining of the caldera lake to approximately their elevation. Lacustrine clayey silt and sand are present in the breach of Surprise Cone and on a wave-cut terrace north of Surprise Lake at 1,226 ft (374 m) asl (McGimsey and others, 1994). Eruptions responsible for the tuff cones likely took place in shallow water, as suggested by the sediments within Surprise Cone. The basaltic andesite to andesite eruptions may well have been facilitated by unloading that resulted from rapid draining of the ancestral caldera lake to about the ~1,400-ft (430 m) elevation of Surprise and Windy Cone craters, although we cannot rule out the possibility that the tuff cone eruptions occurred earlier, during filling of the lake. Two well-preserved maar craters southeast of Windy cone demonstrate that phreatic or phreatomagmatic explosions occurred in the recent past, presumably under hydrologic conditions similar to present time. A third explosion crater, which also evidently did not produce juvenile ejecta and probably is unrelated to ascent of mafic magma, is approximately midway between Vent Mountain and Half Cone (fig. 10*A*).

Vent Mountain

Vent Mountain scoria and spatter cone is the most prominent topographic feature within the caldera (figs. 10, 12*C* and 12*D*). The cone rises 440–530 m above the caldera floor to an elevation of 3,350 ft (1,021 m). The 210-m-deep summit crater has a diameter of ~800 m. Numerous blocky lava flows emanate from the cone's lower flanks and from a prominent fissure vent that cuts the southwest flank. Although some outcrops of basaltic andesite and mafic andesite lava west of The Gates and in the larger maar crater possibly had source vents now hidden beneath Vent Mountain, the majority of products attributed to that volcano are silicic andesite and dacite.

We describe the eruptive history of Vent Mountain beginning with lava flows inferred to be some of the earliest. Thickly tephra-mantled lava that flowed between Bolshoi Dome and Surprise Cone and now fronts onto Surprise Lake apparently came from Vent Mountain, as did lava that flowed between Surprise and Windy Cones. Early lava flows that originated at the west-northwest–east-southeast-trending fissure that cuts the south flank of Vent Mountain and from the summit crater are exposed in the walls of the fissure, as scattered outcrops on the south flank, overlying the east edge of New Cone, and in the walls of the two maar craters. The most far travelled of these flows terminates ~1 km southwest of The Gates (fig. 10*A*). Tephra compositionally similar to Vent Mountain lava is stratigraphically above Half Cone lower light pumice (weighted mean age 840±30 yr B.P., table 1) and below Half Cone upper light pumice (weighted mean age 570±40 yr B.P., table 1) in a section 6 km east-southeast of the caldera (table 2). On the east-southeast flank of Vent Mountain, New Cone was the source of lava that preceded much of that from Vent Mountain itself. Three radiocarbon dates on material associated with tephra thought to have a New Cone source (table 2) have a weighted mean age of 400±30 yr B.P. (table 1), though only the 390±60 yr B.P. date is from within the caldera. Tephra considered to predate New Cone is as young as Half Cone upper light pumice.

The youngest Vent Mountain lavas emanate from the south fissure vents, draping the south flank between lobes of earlier lava and spreading out from the southwest and south bases of the Vent Mountain edifice to pond against the caldera wall. One of these flows incised a channel into a small glacier and descended to the northeast through New Cone crater to overlap earlier Vent Mountain lava. Tephra from multiple eruptions at the summit, the south fissure, and New Cone blankets the west, south, and east flanks of the Vent Mountain edifice. The youngest products of Vent Mountain are agglutinated spatter plastered on the north side of the cone and a small lava dome in the summit crater. The total volume of Vent Mountain lava and tephra probably exceeds 1.5 km^3. If the radiocarbon constraint on New Cone is correct, much of Vent Mountain lava was erupted since ca. 400 yr B.P. The youngest flows and agglutinate predate only the 1931 eruption.

Half Cone

Half Cone is the crescentic remnant of an andesite–dacite composite edifice that abuts the northwest caldera wall, its unsupported southeast half having been destroyed during explosive eruptions late in this volcano's life (fig. 13*A*). The most recently active feeding conduit of Half Cone is marked by the center of the radially symmetrical Cobweb dacite flow (fig. 13*B*).

Early Products of Half Cone and Nearby Vents

In the north wall of Half Cone, coarse poorly sorted pumice fall layers form wedges tapering away from both sides of the truncated, crater-filling dome (fig. 13*C*). Beds of the lowest approximately one-third of the western wedge, which are rich in coarse, relatively dark dense clasts, are crosscut by lighter colored pumiceous beds of the middle third. A small remnant of a lava dome rests on the latter beds and is overlain by the uppermost third of the wedge beds, which are intermediate in color. These deposits are overlain by the ca. 400 yr B.P. Pink Pumice fall sequence (see next section). Thick exposures of lava in the west wall are compositionally identical to the crater-filling dome and may be equivalent. Xenoliths of

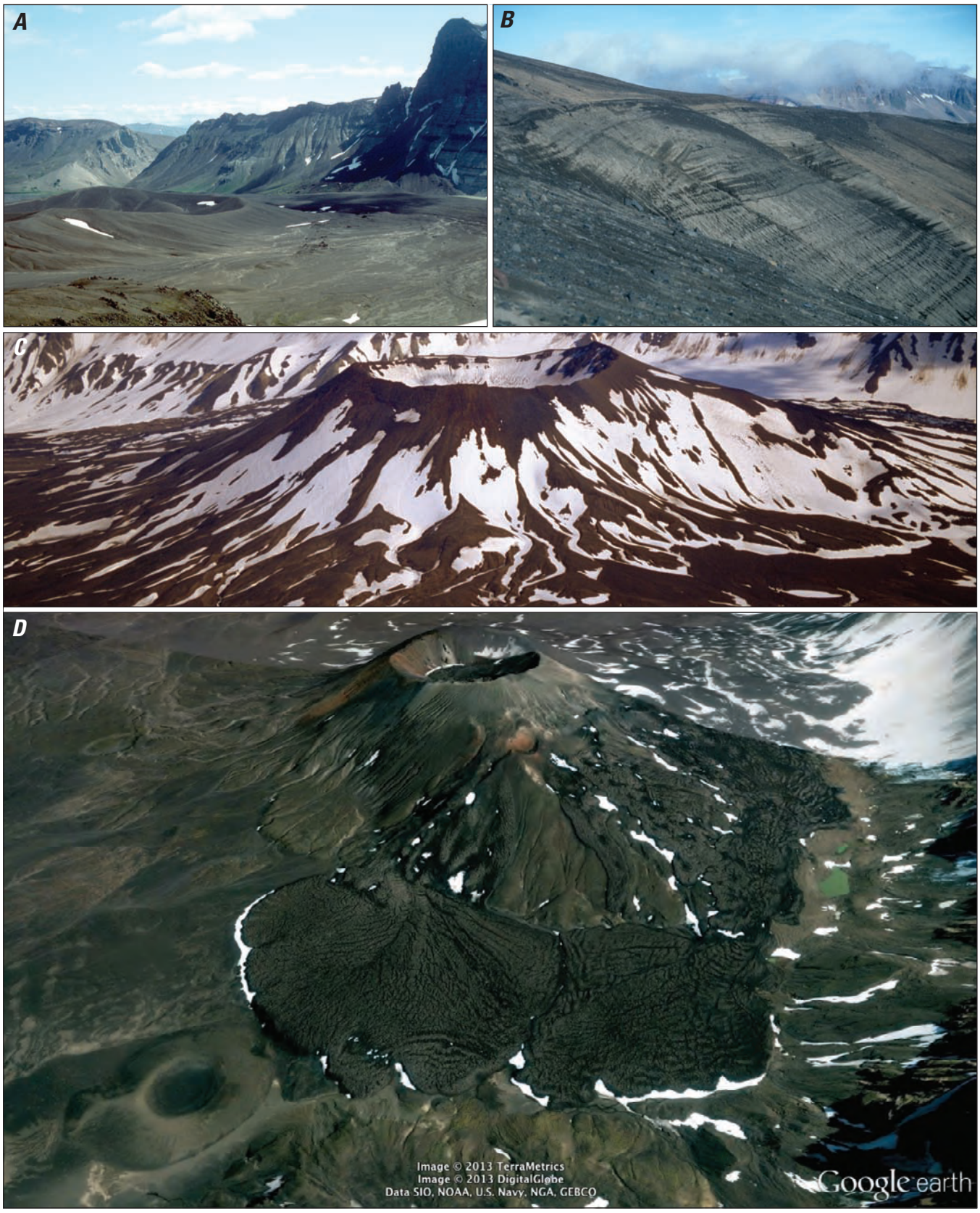

Figure 12. Photographs of tuff cones and Vent Mountain. *A*, Windy Cone in left center, The Gates in distance, and Black Nose on right. *B*, View looking northwest of tephra section on Breezy Cone. Visible tephra section is on the order of 10 m thick. *C*, Aerial view of north flank of Vent Mountain (photograph by R.G. McGimsey). *D*, Google Earth view of southwest flank of Vent Mountain (summit crater diameter ~800 m), showing young lava flows and fissure vent system; Blocky Cone (crater diameter ~300 m) is in lower left corner.

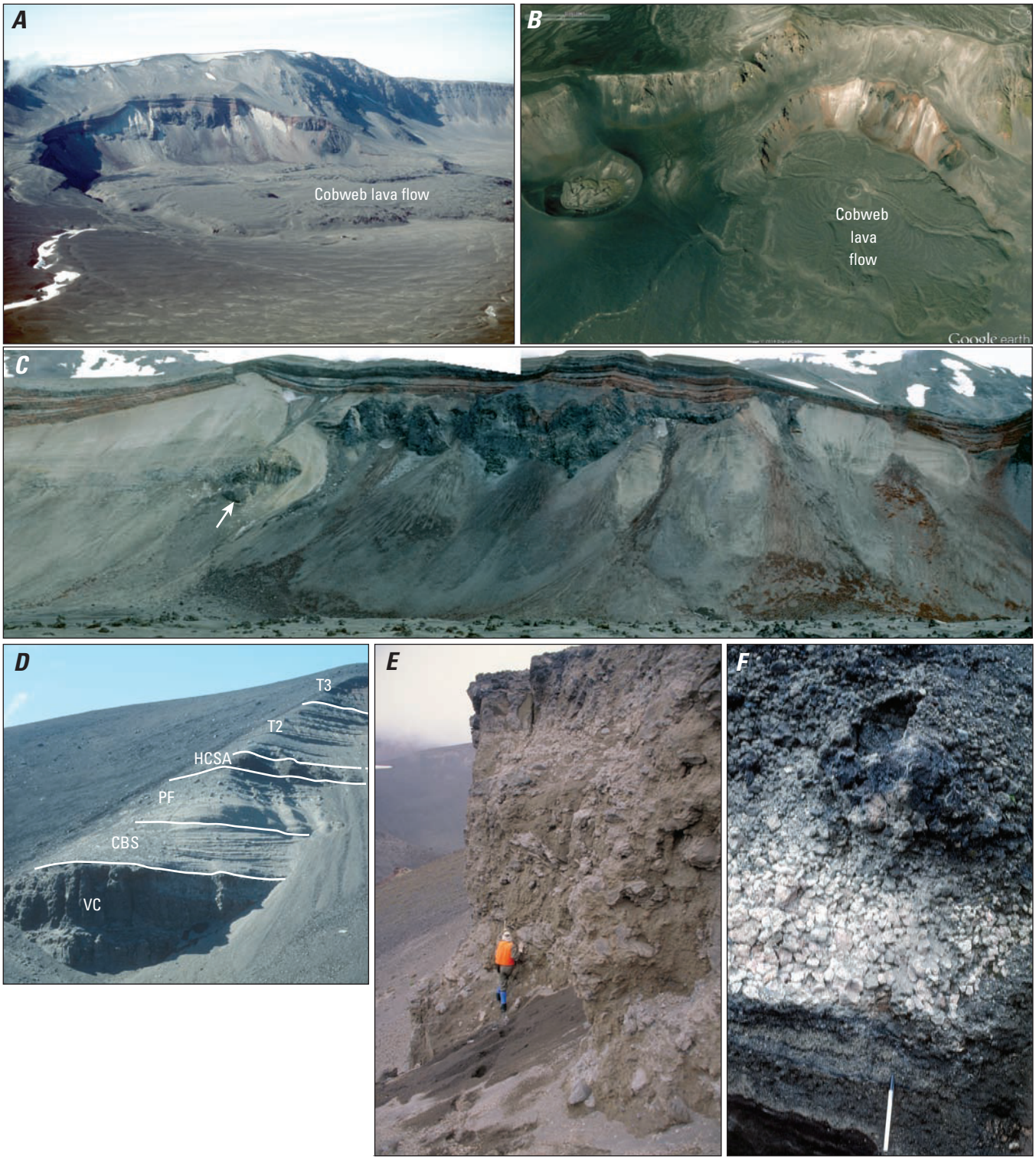

Figure 13. Photographs of Half Cone and its products. *A*, Aerial view of Half Cone and Cobweb lava flow; flow field is about 2 km across and as much as 50 m thick. *B*, Google Earth view of Half Cone, Cobweb lava flow (right), and 1931 Main Crater (left). *C*, Steep, ~300-m-high exposure through Half Cone vent-filling lava (dark cliff) and overlying Half Cone pyroclastic deposits. Cobweb lava flow, mantled by 1931 tephra, in foreground. Arrow points to compositionally unique andesite lava. *D*, Half Cone pyroclastic deposits form the lower half of the north wall of the 1931 Main Crater; overlying bedded deposits are from the 1931 eruption (see also fig. 15*C* and Nicholson and others, 2011, their figure 3*F*). Unit labels and thicknesses after Nicholson and others (2011): VC, 22 m exposed of partly welded deposit; CBS, 13 m of cross-bedded surge deposits; PF, 31 m of pumice fall deposits; HCSA, 5 m of spatter agglutinate; T2, 40 m of 1931 tephra T2; T3, 41 m of 1931 tephra T3. *E*, Partly welded deposit at base of exposure in *D*. Photograph by R.G. McGimsey. *F*, Compositionally zoned Pink Pumice fall deposit in gully on Pumice Dome. Pencil for scale.

distinctive white felsite are common in these dacite lavas. The northeasternmost lava in the Half Cone wall, thick dacite that has prominent vitrophyre columns above its base, is likely correlative with the crater-filling dome judging from its proximity and similar appearance.

The western near-vent fall-deposit wedge of Half Cone lies on silicic andesite (63 weight percent SiO_2) lava of unique composition known only from that locality. Subhorizontal vitrophyre columns ~6–10 cm across, perpendicular to a caldera-facing vertical joint surface that strikes east-northeast, suggest that this lava may have effused from a buried vent near the northwest caldera wall and encountered ice or deep snow in the caldera before the eruption of Half Cone.

Pumice-fall and pyroclastic-flow deposits from Half Cone are exposed in the north wall of the 1931 Main Crater 2 km to the south (fig. 13*D*). Here, the cliff at the base of the section (fig. 13*E*) is composed of >22 m of partly welded or indurated coarse pyroclastic-flow material, much like spatter-rich pyroclastic-flow deposits at Santorini (Mellors and Sparks, 1991), containing andesite bombs as large as 0.6 m × 2 m and similar in composition to Half Cone pyroclasts (59 weight percent SiO_2). This unit is overlain by 13 m of pumiceous cross-bedded surge layers, 31 m of pumice-fall deposits, 5 m of Half Cone ca. 400 yr B.P. spatter agglutinate, and an 81-m-thick section of 1931 materials (Nicholson and others, 2011, their figure 3F). Dacite tephra older than the Pink Pumice and considered to have a Half Cone source, and which therefore may be correlative with proximal deposits at Half Cone and with the section exposed in the 1931 Main Crater, have weighted mean radiocarbon ages of 840±40 and 570±40 yr B.P. (tables 1 and 2, lower and upper light pumice, respectively).

Half Cone Pink and Brown Pumice Falls

A series of Plinian eruptions ca. 400 yr B.P. produced widespread pumice falls and destroyed much of the original Half Cone edifice (Neal and others, 2001; Browne, 2006). Pyroclastic flows and surges affected much of the caldera floor. Canyons to the east of Half Cone expose more than 40 m of pyroclastic-flow deposits related to this event. Outside the caldera, the pumice fall is 10 cm thick at least 50 km to the north. Fine ash may extend as far as 330 km (Riehle and others, 1999). Total erupted volume is estimated at 0.75 to 1.0 km^3 (Neal and others, 2001). The areally extensive units are two volumetrically subequal, successive Plinian fall deposits known by the informal unit names of the Pink Pumice (fig. 13*F*) and the overlying Brown Pumice; the contact between Pink and Brown Pumice falls is gradational through a modest thickness. The dacitic Pink Pumice (63–67 weight percent SiO_2) is highly vesicular and carries few phenocrysts. Two horizons within the Pink Pumice deposit have relatively coarse pumice and lithic clasts. The normally graded Brown Pumice layer consists of relatively crystal-rich andesite pumice (58–62 weight percent SiO_2). White felsite (77 weight percent SiO_2), granitic, and crystal tuff xenoliths are common in the fall deposits. Five radiocarbon dates are for materials associated with the Pink Pumice (table 2). We consider the weighted mean of 380±50 yr B.P. (table 1) for the two youngest dates, which are for wood and for which stratigraphic context is clear, to provide the most accurate constraint on the Pink Pumice eruption.

Proximal Late-Erupted Fall Layers

Atop the Pink and Brown Pumice layers on Half Cone itself are several more light and dark colored fall beds that have a total thickness of ~60 m. These vary from nonwelded pink-to-buff pumice fall to brick-red oxidized lithic-rich fall breccia and dark gray welded agglutinate. The variations in lithic content and welding are due to changes in eruption intensity at the vent. Although these layers have not been studied in detail, their thicknesses decrease substantially over short distances from Half Cone. Outcrops of this agglutinate are found as short, low ridge segments near the surface on the caldera floor northeast of Half Cone, as patches on Vent Mountain and West Dome, and in the wall of the 1931 Main carter. They are cut by the cliff face of Half Cone and are overlain by deposits of the 1931 eruption.

Cobweb Lava Flow

The final product of the Half Cone vent was crystal-rich dacite (~65–66 weight percent SiO_2) that spread radially to form the Cobweb lava flow (figs. 13*A* and *B*), now heavily mantled with tephra of the 1931 eruption. The flow has arcuate pressure ridges that are approximately concentric about a low central cratered cone above the vent, which is located somewhat west of center of the 1.5 km (north–south) by 2 km (east–west) lava field (fig. 10*A*). At least six rifts traverse the flow surface from the center to the edges like spokes of a wheel. The longest of these appears to have channeled late-erupted lava northeast all the way to the margin of the flow field. Late-moving lava also emerges as short toes from the north and south margins of the field. The lava terminates on the northwest near the base of the Half Cone cliff. We adopt the name Cobweb for this lava flow after B.R. Hubbard (1932), who called it the “Avernian Cobweb.” “The poisonous vapors of Avernus, Italy, killed many birds, and Hubbard witnessed the same at Aniakchak, which seems why he adopted this name” (W. Hildreth, written commun., 2014).

Blocky Cone

The well-preserved, 60-m-high cinder cone with ~20-m-deep crater near the southwest caldera wall opposite Birthday Pass is informally known as Blocky Cone (figs. 12*D* and 14). Although Blocky Cone is mantled by lithic debris from the nearby 1931 vent, fresh basaltic andesite scoria is exposed on the southeast flank of the cone. This is some of the most mafic postcaldera magma (52.2–52.5 weight percent SiO_2), comparable only to products of Breezy Cone. Blocky

Cone appears to be younger than the Half Cone Pink and Brown Pumice (fig. 5*C*) and to overlie older lava of Vent Mountain. Blocky Cone tephra has not been reported to be on the surface of the youngest Vent Mountain lava that nearly reaches the cone's eastern base, which suggests that this late-erupted Vent Mountain lava is younger than Blocky Cone.

1931 Eruption

The most recent eruption of Aniakchak took place during May and June 1931. The following description of the events and deposits is drawn from Neal and others (2001) and Nicholson and others (2011). The total volume of erupted material was about 0.9 km^3 (or 0.3 km^3 of dense phenocryst-poor magma; Nicholson and others, 2011), less than 1 percent of which was lava. Like the ca. 400 yr B.P. eruption of Half Cone and eruptions at many other Alaskan volcanoes, the 1931 Aniakchak eruption began with relatively silica-rich dacite–rhyodacite magma (as much as 69 weight percent SiO_2 in 1931) and ended with relatively silica-poor basaltic andesite magma (as little as 56 weight percent SiO_2) (Nicholson and others, 2011). Although Nicholson and others (2011) termed the more silicic products trachydacite, the Aniakchak analyses straddle the dacite/trachydacite boundary (their figure 7) and we choose to refer to these samples as dacite for simplicity.

Historical Accounts

The 6-week-long eruption, strongest during May 1–11, rained "egg-size" scoria 30 km to the west in Port Heiden (then called Meshik), spread millimeters of ash fall as far as Kodiak Island, and repeatedly interfered with radio communications in the area. The principal record of the events of 1931 comes from the writings of B.R. Hubbard, the "Glacier Priest" of the University of Santa Clara, California (Hubbard, 1932, and references in Neal and others, 2001, and Nicholson and others, 2011; see the latters' figure 4 for summary). The first reported activity was a column of white steam seen May 1 at 10 a.m. local time from Meshik, which was followed at 12 p.m. by an explosion that sent a black mushroom-shaped incandescent plume to an estimated 6 km height. On May 11, after nearly continuous explosive activity since May 1, a large explosion produced heavy ashfall that resulted in total darkness for several hours within 100 km of the volcano. Activity then reduced until, on May 20, large explosions again occurred. Ash fell through at least May 28, and explosive eruption was still in progress on June 10 and 13. New lava was emplaced as small flows at Doublet Crater and Slag Heap and, towards the end of the activity, in the Main (1931) Crater. The Main and Doublet Crater lava flows were moving at least as late as July 1 and 3, respectively.

Fall Deposit

Within and near the caldera, the 1931 deposit consists of white pumice lapilli near the bottom and grades upward through a main unit dominated by tan to brown pumice to an upper unit of black pumice (fig. 15*A*). Nicholson and others (2011) divided the fall deposit into corresponding mappable tephra units T1, T2, and T3. White to light gray unit T1 (0.02 km^3 DRE) is present to the north of the Main Crater as far as 15 km from vent but is not present in the Main Crater wall section. Juvenile clasts are dominantly dacite. Unit T1 may be noticeably darker at its base than its top owing to a greater proportion of lithic fragments near the base. Most

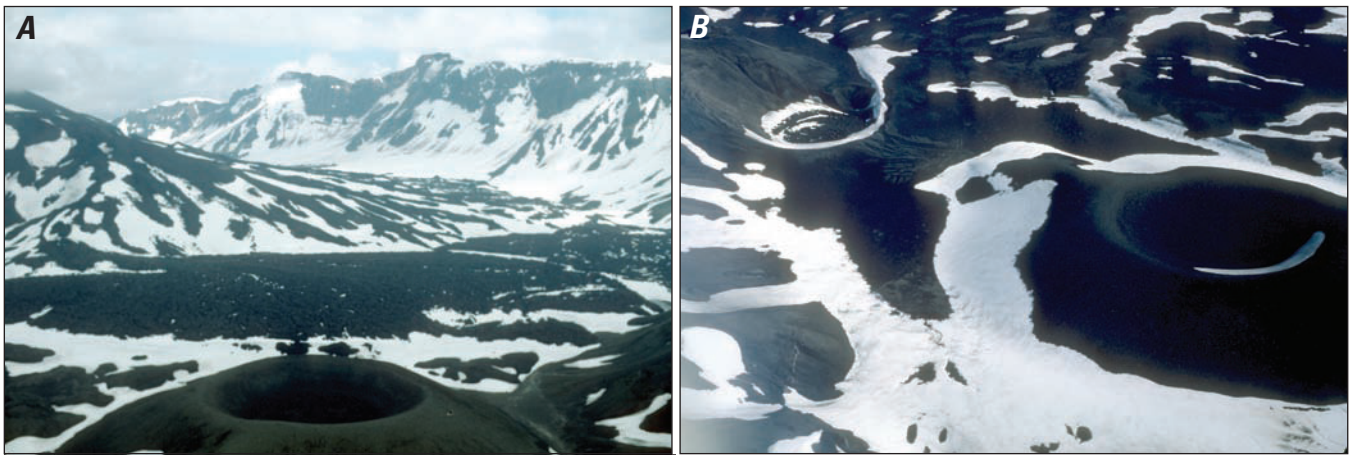

Figure 14. Photographs of Blocky Cone. *A*, Aerial view southeast over Blocky Cone to southwest flank of Vent Mountain. *B*, Oblique aerial view to north; Blocky Cone on right, Doublet Crater in upper left.

voluminous and lithic-rich of the three units is T2 (0.24 km^3 DRE), which consists of alternating beds of fine ash and coarser tan, brown, or black andesite lapilli; white pumice is rare. Eyewitness accounts of distal ashfall are thought to be exclusively unit T2 because reports of white pumice characteristic of T1 are lacking and T2 is the most voluminous tephra unit. Unit T3 (0.009 km^3 DRE) is seen only in the Main Crater wall (fig. 15*B*), where it consists of lithic-poor alternating beds of coarse- and fine-grained relatively dense black andesite and basaltic-andesite scoria. Ash grains in unit T3 are dense and blocky in comparison to grains in T1 and T2.

Figure 15. Photographs showing products of the 1931 eruption. *A*, Basal fall deposit in pit dug above Half Cone. Yellow tape is ~35 cm long. Total thickness of fall deposit is ~200 cm here. *B*, North wall of 1931 Main Crater showing tephra section. Tephra units T2 (40 m thick) and T3 (41 m thick) of the 1931 eruption overlie an exposed thickness of 71 m of Half Cone units. Slope is partly mantled by spatter agglutinate. (Photograph by C.A. Neal; compare with figure 13D and Nicholson and others, 2011, figure 3F). *C*, Main Crater with lava on crater floor, Half Cone in left distance (photograph by T. Plucinski). *D*, Aerial view to southeast of Slag Heap and, beyond, Doublet Crater lava flows near southwest caldera wall.

Spatter Agglutinate

A 50–100-cm-thick stratified deposit of agglutinated frothy brown and dense black basaltic-andesite lapilli and minor scoria bombs partly mantles the north and east wall of the Main Crater (fig. 15*B*). Lapilli and bombs are similar to those of unit T3.

Main Crater Lava

Vesicular basaltic andesite lava covers much of the floor of the Main Crater (fig. 15C). The flow surface is mantled by spatter agglutinate. The likely vent is marked by a depression near the center of the flow, while a distinct tongue of lava flowed west adjacent to the south base of the crater wall.

Late-Erupted Bombs

Lithic blocks and juvenile bombs fell in two areas at the end of the 1931 eruption, a larger bomb field east of the Main Crater and a smaller one north of a small phreatic explosion pit at the north rim of Doublet Crater. Black to brown highly vesicular bombs similar to those of the spatter agglutinate are present as much as 500 m east of the Main Crater rim.

Doublet and Slag Heap Lavas

Dacite lava covers the floor of Doublet Crater as a flat ~100-m-diameter circular flow 2.2 km south of the Main Crater (Figures 10*A* and 15*D*). Descending from a bench 50 m above the caldera floor 2.2 km south of the Main Crater, the rhyodacitic Slag Heap flow (fig. 15*D*) is broken by deep transverse and longitudinal fractures that give its surface a scored appearance. The two flows are blanketed with T2 tephra and scattered lithic fragments, coarser on the Doublet Crater flow.

Geochemistry

The geochemical database for Aniakchak consists of 374 analyses of rock samples collected by Alaska Volcano Observatory (AVO) geologists and University of Alaska Fairbanks graduate students (appendix B, table B1). The 346 of these analyses that can be assigned unambiguously to eruptive units form the basis for figures, descriptions, and interpretations in this paper; remaining uncertain samples are indicated by "?" in appendix B, table B1. All of the chemical analyses were performed by the GeoAnalytical Laboratory at Washington State University in Pullman, Washington, by wavelength-dispersive X-ray fluorescence (XRF) and inductively coupled plasma mass spectrometry (ICP-MS). Strict quality control over many years ensures that the database is internally consistent and accurate. See http://soe.wsu.edu/facilities/geolab/technotes for analytical procedures and precision.

The compositions of Aniakchak geologic units are described here in order of eruption with reference to silica and other variation diagrams and chondrite-normalized rare earth element (REE) and primitive-mantle-normalized multielement ("spider") plots. Implicit in using the geochemical data to help establish stratigraphic relationships is the concept that samples from outcrops that are not contiguous but are analytically indistinguishable are likely to represent approximately contemporaneous eruption of a single magma or closely related magmas.

Isotopic data for 15 samples from Aniakchak, all postglacial in age, were presented by George and others (2004). These results are described at the end of the "Geochemistry" section.

Pleistocene Aniakchak Edifice

Lava samples from Pleistocene Aniakchak volcano were mainly obtained from caldera wall exposures. The 29 analyses in the database are presented here without designation of relative or absolute age because knowledge of edifice geologic relations is insufficient. Nevertheless, these data give a measure of the range of compositions erupted at Aniakchak over a likely span of several hundred thousand years (Nye and others, 1993) and thus provide context for the chemistry of postglacial magmas.

Pleistocene lavas range from basalt to dacite (fig. 16). Compatible element concentrations at the mafic end of the spectrum are relatively low (for example, MgO<6 weight percent) and indicate that none of the samples represents primary magma from the mantle; all have undergone processing and chemical fractionation at crustal depths. At any given silica content there are wide variations in incompatible element concentrations. For example, medium-K and high-K magmas (Gill, 1981) are represented, and K_2O, TiO_2, Zr, and Y vary by factors of 2–3 in andesites (fig. 16). Some of the Pleistocene lavas have high Al_2O_3 contents (>18 weight percent), and these also have high values of Eu/Eu* (europium anomaly), which suggests that they have accumulated plagioclase.

Figure 17 presents diagrams that help to classify the Aniakchak rocks and that will be useful for later discussion of processes. The Pleistocene lavas fall into two series on the plot of silica versus chondrite-normalized La/Yb ratio, a measure of the slope of the REE pattern. The high La/Yb series is not represented among postglacial products of Aniakchak. Most of the Pleistocene lavas plot in the tholeiitic field on the silica versus FeO*/MgO diagram (Miyashiro, 1974), though some with >59 weight percent SiO_2 are calc-alkalic. Nye and others (1993) pointed out that early and mid-precaldera basaltic andesites are tholeiitic whereas late-precaldera lavas are calc-alkalic.

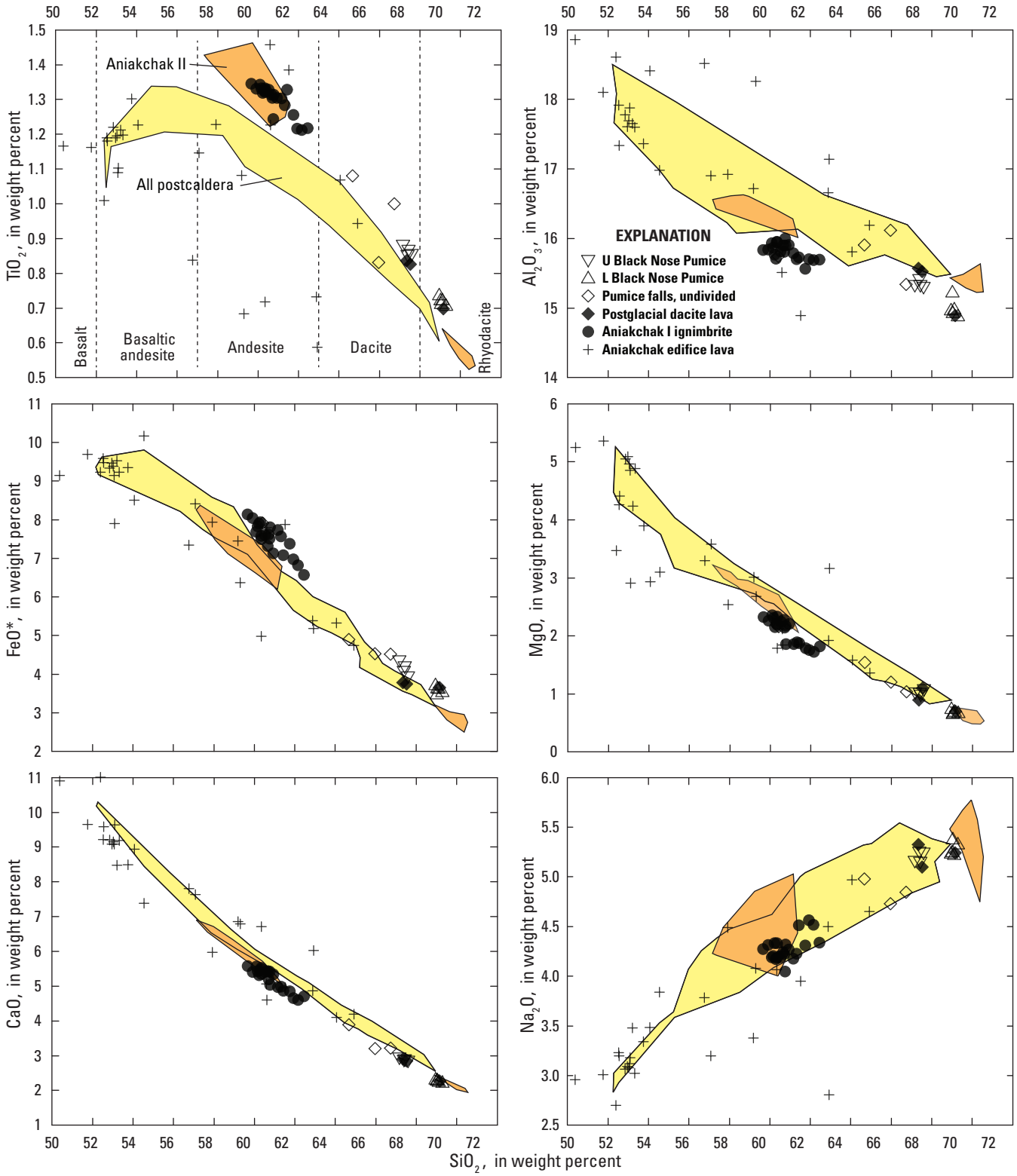

Figure 16. Silica variation diagrams for Pleistocene and pre-3,400-yr.-B.P. Aniakchak samples. Major element oxides recalculated to sum to 100 weight percent volatile-free. Fields indicate compositional ranges of postcaldera units (yellow) and bimodal Aniakchak II products (orange).

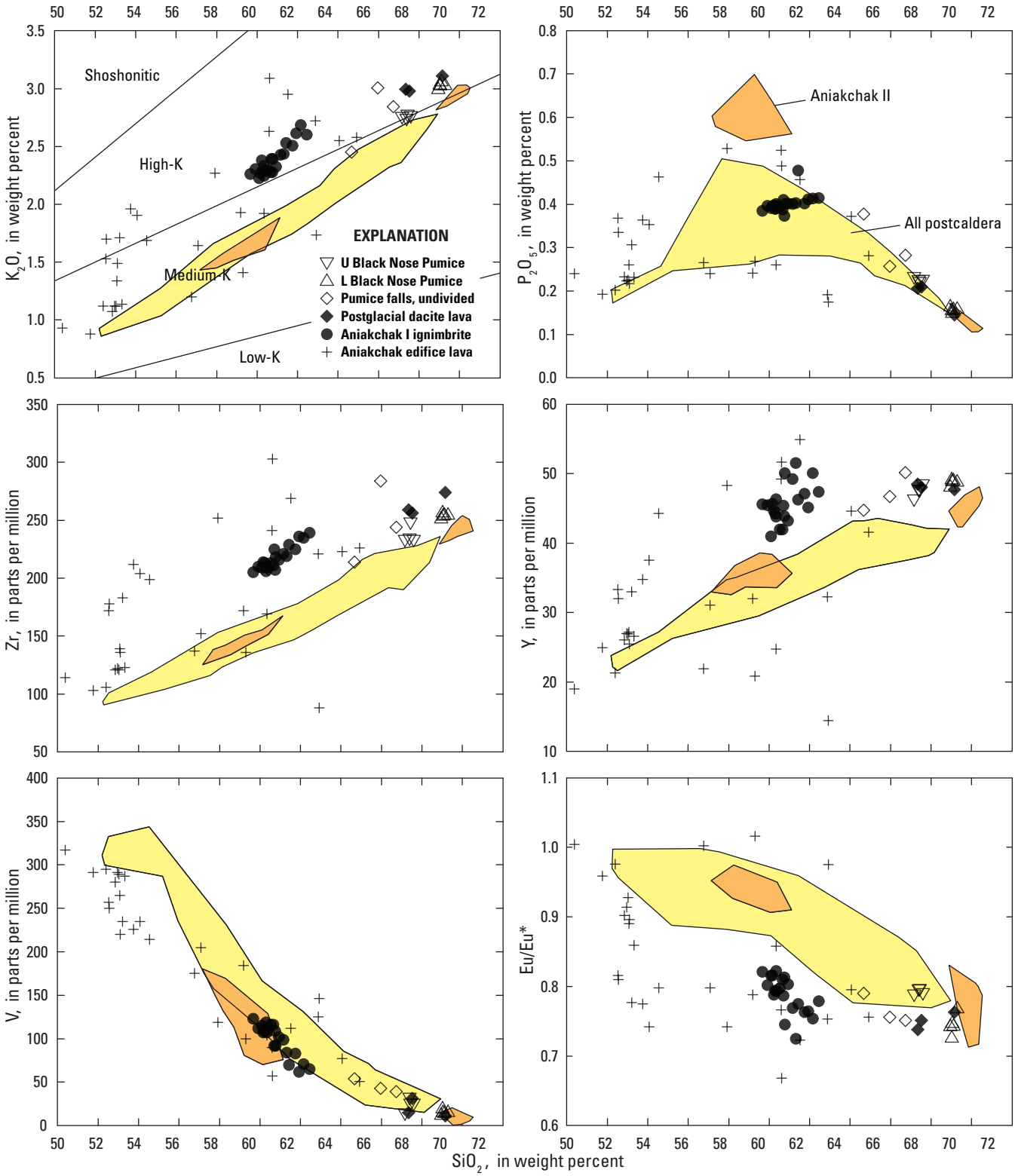

Figure 16.—Continued.

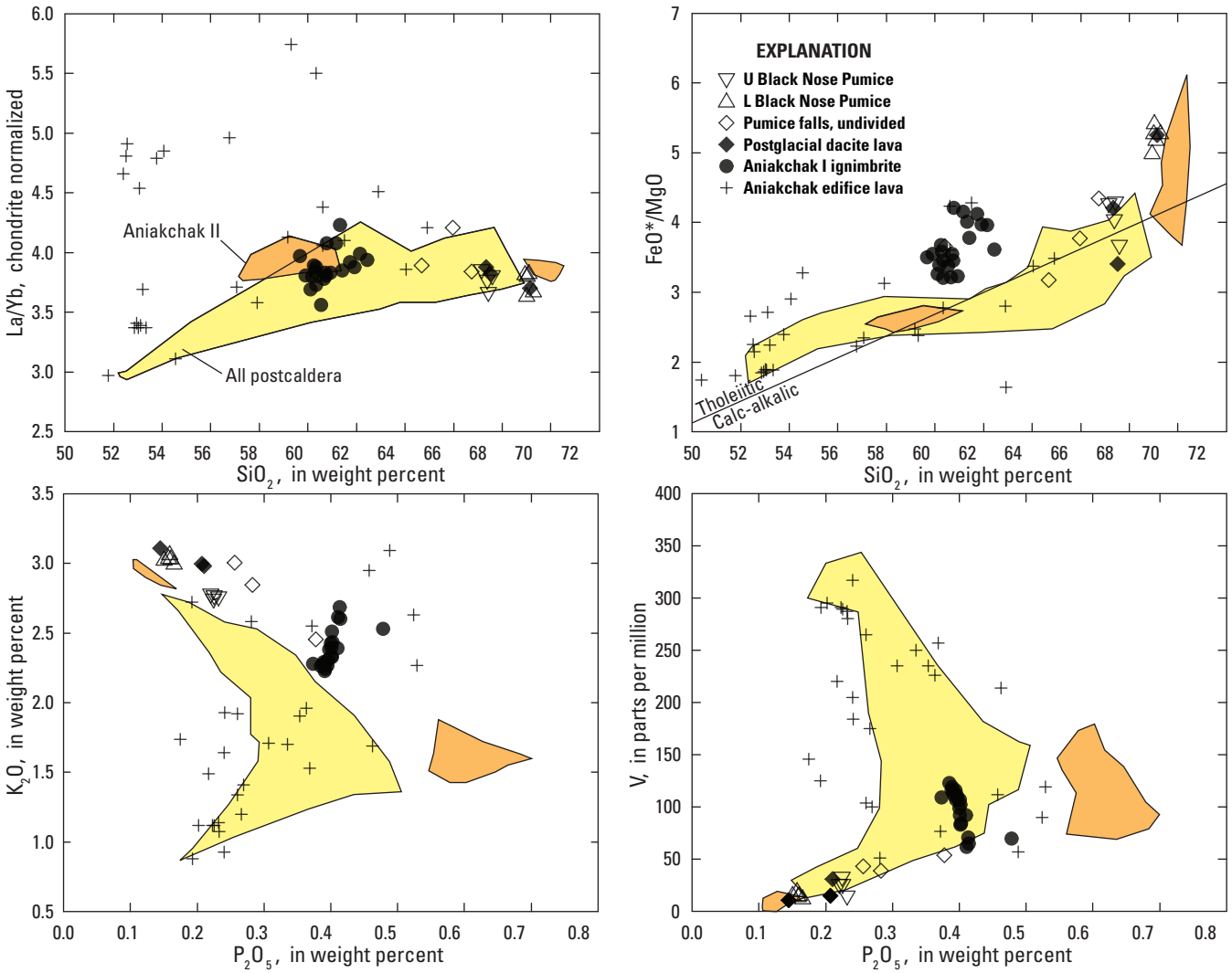

Figure 17. Silica and P_2O_5 variation diagrams for Pleistocene and pre-3,400-yr.-B.P. Aniakchak samples. Major element oxides recalculated to sum to 100 weight percent volatile-free. La/Yb ratios normalized to values for CI chondritic meteorites (McDonough and Sun, 1995). FeO* is total Fe calculated as FeO. Fields indicate compositional ranges of Aniakchak II (orange) and younger units (yellow).

Chondrite-normalized REE patterns for edifice lavas (fig. 18*A*) cover ranges of concentrations and slopes that encompass those for all other samples and, in fact, are considerably greater. The highest light REE (LREE) values for edifice lavas exceed, and the lowest heavy REE (HREE) values are lower than, those of postglacial samples. Some REE pattern slopes are steeper as well, as evident also in figure 17. Most edifice lavas have prominent negative Eu anomalies (Eu/Eu*<1; fig. 16), which also are common among the majority of postglacial samples.

Multielement diagrams in which values for each sample are normalized to elemental concentrations deduced for Earth's primitive mantle (McDonough and Sun, 1995), arranged in order of increasing incompatibility in mantle minerals from right to left, are useful geochemical fingerprints of magmas and highlight differences between eruptive units at a glance. Data for edifice lavas plotted in figure 19*A* delimit the range at Aniakchak. The patterns have common features that also are characteristic of magmas at convergent plate (subduction) environments such as the Alaska–Aleutian arc: overall negative slope, high fluid-mobile U and Pb, and low high-field-strength-elements (HFSE) Nb and Ta. Depressed values for Sr, P, and Ti result from sequestration in plagioclase, apatite, and titanomagnetite, respectively. These minerals were removed from magmas during subsurface crystallization differentiation, or retained in crystal residues of partial melting, causing erupted magmas to be depleted in elements compatible in them. The few samples with anomalously high Sr contents probably have accumulated plagioclase. Scatter in Cs relative abundances likely results from minor alteration of the affected samples. Although in detail there are real differences in relative abundances of the elements illustrated in figure 19*A* for the edifice samples, the overall similarity of the majority of the patterns implies histories involving common processes that operated on subduction-related parent magmas.

Aniakchak I Ignimbrite

The distinctive chemical composition of andesite of the Aniakchak I ignimbrite allows the deposit to be readily distinguished from the commonly similar appearing Aniakchak II andesite ignimbrite simply on the basis of K_2O, P_2O_5, or Zr content (fig. 16). Characteristic features that set Aniakchak I apart from other postglacial Aniakchak andesites are high FeO*, K_2O, and incompatible trace elements such as Zr and Y coupled with low MgO and Eu/Eu*. The range in SiO_2 content for 21 clasts is a narrow 59.7–62.4 weight percent. Concentrations of compatible elements decrease, and those of incompatible elements increase, with increasing SiO_2 in a manner consistent with crystallization differentiation that involves plagioclase, pyroxene, and titanomagnetite. Increases in P_2O_5 with increasing SiO_2 (fig. 16), and with increasing K_2O and decreasing V (fig. 17), indicate lack of apatite saturation during differentiation. We show the narrow field of Aniakchak I andesite compositions on all REE and multielement diagrams as an index for illustrating differences among compositions of eruptive units.

Rare-earth-element patterns for Aniakchak I andesite samples (fig. 18*B*) are approximately parallel and show greater negative Eu anomalies (decreasing Eu/Eu*) with increasing overall REE concentrations. These features result from concentration of elements incompatible in the plagioclase-dominated crystallizing assemblage and preferential incorporation of Eu^{2+} into plagioclase. Multielement diagrams (fig. 19*B*) also indicate a narrow compositional range for Aniakchak I andesite. These patterns for Aniakchak I ignimbrite are similar to patterns for many other postglacial Aniakchak products, although they do feature high relative P contents in comparison to postglacial andesites other than Aniakchak II.

Precaldera Dacites and Rhyodacites

Dacite–Rhyodacite Lava Flows

The dacite lava flow on the northeast flank of the Aniakchak volcano is the less evolved of the two units considered here. At ~67.4 weight percent SiO_2, many features of its chemistry are closely similar to those of upper Black Nose Pumice (figs. 16 and 17). However, though SiO_2 contents are similar, the lava flow has slightly higher levels of incompatible, and lower levels of compatible, elements than the pumice (figs. 16 and 17). The composition of the rhyodacite lava flow or dome in the caldera wall north of The Gates (69.2 weight percent SiO_2) is identical to that of the lower Black Nose Pumice that rests upon it. As would be expected from the above observations, these dacite–rhyodacite lavas have REE and multielement patterns that are virtually indistinguishable from those of Black Nose Pumice (figs. 18*C* and 19*C*). These lavas logically are effusive equivalents of the Black Nose Pumice deposits. The rhyodacite lava was extruded before the compositionally similar lower Black Nose Pumice and the dacite lava possibly after the upper Black Nose Pumice, though that relationship has not been investigated specifically by searching for the relevant pumice fall deposits on the lava flow.

Black Nose Pumice

The geochemistry of the lower and upper Black Nose Pumice fall deposits, each of distinct composition, is described and contrasted in this section. A sample of fiamme (AC-09) from the intra-Plinian ignimbrite is compositionally indistinguishable from pumice of the enclosing lower Black Nose Pumice fall and therefore is not described separately.

Lower Black Nose Pumice is rhyodacite, five samples having 69.1–69.3 weight percent SiO_2. As noted above, the composition of a lava flow in the caldera wall north of The Gates is identical to that of the overlying lower Black Nose Pumice. Incompatible elements, TiO_2, and FeO* are present at slightly higher concentrations, and Al_2O_3 lower, in the lower

Black Nose Pumice than in postcaldera dacites and rhyodacites (fig. 16). Similarly, FeO*/MgO is near the maximum value for Aniakchak magmas (fig. 17) and Eu/Eu* is low (fig. 16).

Less evolved than the lower, the upper Black Nose Pumice has 67.2–67.6 weight percent SiO_2 (four samples) and other oxide and elemental concentrations broadly consistent with being genetically related to the lower Black Nose Pumice. This also is evident in REE and multielement diagrams (figs. 18 and 19), in which lower Black Nose Pumice samples have slightly lower compatible element contents, deeper Eu anomalies, and higher LREE and HREE contents (compare figs. 18*E* and 18*F*, 19*E* and 19*F*). Patterns for HREE are concave upward for both units. The two units should be readily distinguishable (for example, see appendix A) in distal tephra sequences and, if both are present, would provide strong evidence of their Aniakchak source; chemical analyses of glass in representative pumice clasts from the caldera rim section will be necessary for direct comparison with distal tephras. Both lower and upper units are measurably less evolved than Aniakchak II rhyodacite, which also is distinctive in carrying hornblende phenocrysts. The northeast flank dacite lava flow, as previously mentioned, is quite similar in composition to upper Black Nose Pumice.

Other Pre-Aniakchak II Dacite Pumice Falls

Three analyses of dacite pumice are not assigned to stratigraphic units. These are shown in figures 16, 17, 18*D*, and 19*D* as "pumice falls, undivided." In order of increasing SiO_2 content, they are from beneath Aniakchak II ignimbrite in upper Lava Creek (98AC15C) and lower Reindeer Creek (98AC70D) (fig. 4), and above the Aniakchak I deposit but below the Black Nose Pumice at the caldera rim north of The Gates (AC-11f). The last has compositional affinity with Black Nose Pumice, but with the upper, not lower, unit. The other two samples are compositionally distinct from each other and from other analyzed postglacial precaldera eruptive units, yet they must have been produced by significant explosive eruptions. They serve as reminders that our record of the pre-3,400-yr-B.P. eruptive history of Aniakchak is incomplete and that further evidence of explosive eruptions there is waiting to be discovered through study of promising tephra sections.

Aniakchak II Products

The striking contrast in color between rhyodacite and andesite flow units of the Aniakchak II ignimbrite is borne out by chemical compositions of clasts. Discounting a few analyses of banded or possibly mixed clasts, 20 rhyodacites have 69.4–70.4 weight percent SiO_2 while 30 andesites have 57.2–60.4 weight percent SiO_2. The two samples from the pre-ignimbrite Plinian pumice fall (AC37A and 92CNA37a) are indistinguishable from the most silicic rhyodacite clasts from the ignimbrite. The rhyodacite samples, more evolved than any other analyzed Aniakchak products, define trends on variation diagrams that are consistent with crystallization differentiation or minor differences in phenocryst contents (fig. 20). The trends extend those for postcaldera dacites, though FeO*/MgO (fig. 21) ranges to higher values. REE concentrations, Eu/Eu*, and La/Yb (figs. 22*A*, 20, and 21, respectively) are similar to those of other evolved silicic products, notably lower Black Nose Pumice. However, middle REE (MREE) abundances are somewhat lower in Aniakchak II rhyodacite, probably owing to hornblende fractionation. On a multielement diagram (fig. 23*A*), in comparison to other silicic units Aniakchak II rhyodacite has an unremarkable pattern, except that P content is lowest of any sample analyzed.

Andesite of the Aniakchak II eruption is notable among postglacial eruptives in having high TiO_2 content for its silica range (fig. 20). However, it is the exceptionally high P_2O_5 content, emphasized also by Dreher and others (2005), that truly sets Aniakchak II andesite apart from all other analyzed samples (figs. 20 and 21). The REE in Aniakchak II andesite are present at levels similar to in other andesites of comparable silica content, though chondrite-normalized patterns are subtly steeper than in andesites other than those of the Aniakchak I eruption (figs. 21 and 22*A*). The high P of Aniakchak II andesite stands out as a positive anomaly in multielement patterns (fig. 23*A*), which is virtually unique among Aniakchak samples. With the exception of other compatible elements (for example, Sr, Ti, and to some extent MREE), multielement patterns for the andesite are subparallel to those for Aniakchak II rhyodacite.

Subaqueous Domes

Compositions of the four subaqueous domes mainly plot in a smooth array on silica variation diagrams (fig. 20). Pumice Dome is most evolved (two samples at 67.2 and 67.7 weight percent SiO_2), Bolshoi Dome least evolved (64.2 weight percent SiO_2), and chemically indistinguishable Vulcan and West Domes (65.6 and 65.8 weight percent SiO_2, respectively) intermediate. The subaqueous dome dacites are compositionally similar to the more evolved dacites from Vent Mountain and, together, they plot on a trend toward Aniakchak II rhyodacite (figs. 20 and 21). Note that in figure 24 Pumice Dome samples (the two most silicic orange inverted triangles) plot close to northwest flank dacite–rhyodacite lava and to rhyodacite lava exposed in the southeast wall of the 1931 Main Crater (cluster of magenta inverted triangles).

Abundances of REE (fig. 22*B*) are lower than in precaldera dacites, subparallel to and lower than those of Aniakchak I, but comparable to those in some Vent Mountain and Half Cone samples (figs. 18 and 22). On the multielement plot (fig. 22*B*), similarity to Vent Mountain and Half Cone dacites is apparent. The order of increasing differentiation from Bolshoi to Vulcan and from West to Pumice Dome is most clearly seen in Cs–U and P, the most incompatible trace elements and the essential structural constituent of apatite, respectively.

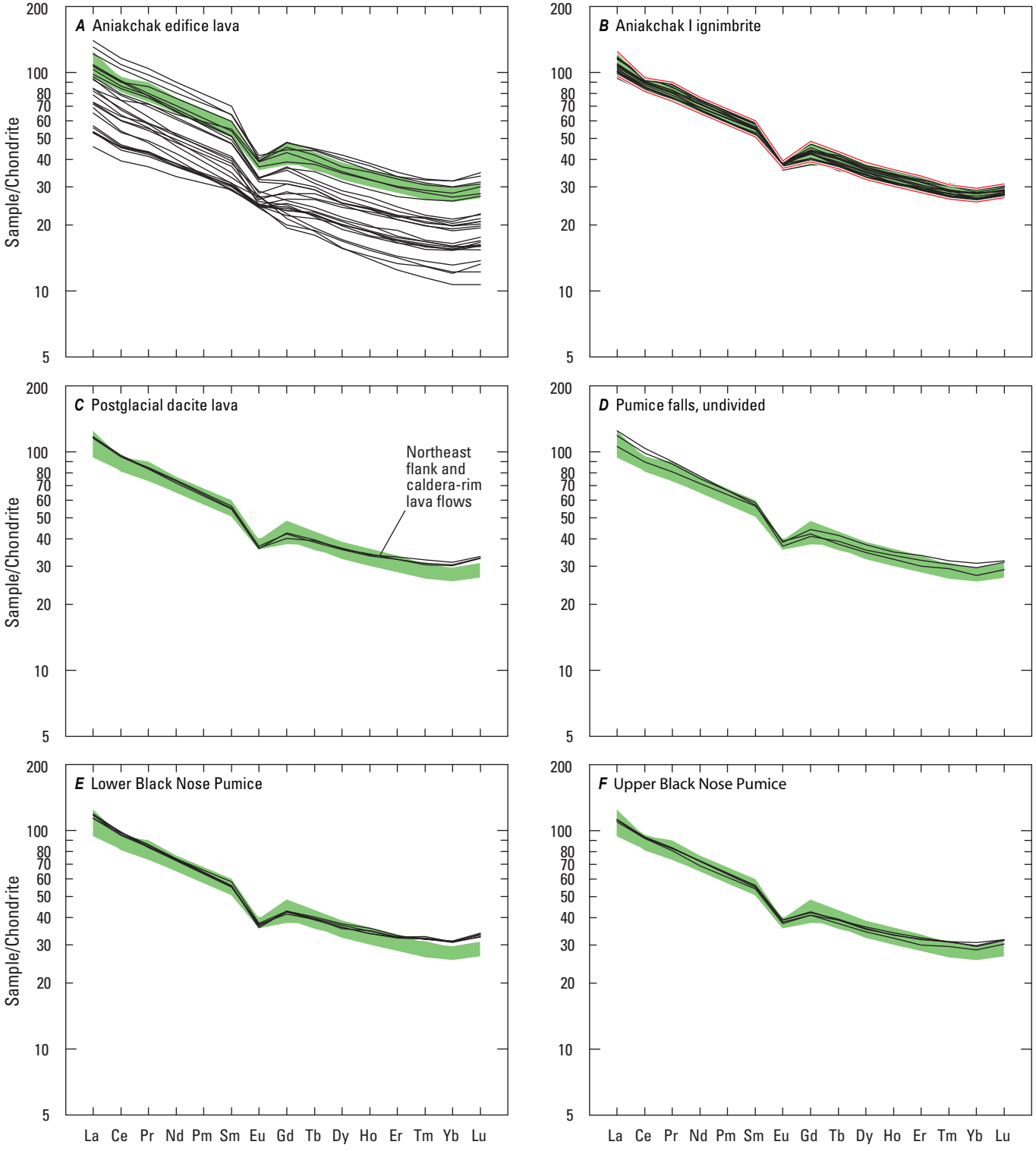

Figure 18. Chondrite-normalized rare-earth-element diagrams (McDonough and Sun, 1995) for pre-3,400-yr.-B.P. Aniakchak products. Green field indicating range of patterns for Aniakchak I ignimbrite serves as index for comparison with other units. Uptick at Lu evidently results from normalization value for Lu relative to other heavy rare earth elements (HREE) in chondrites in comparison with our inductively coupled plasma mass spectrometry (ICPMS) analyses. *A*, Edifice lavas. *B*, Aniakchak I ignimbrite; red lines indicate data for samples with extreme values of most REE. *C*, Postglacial dacite lava. *D*, Pumice falls, undivided. *E*, Lower Black Nose Pumice. *F*, Upper Black Nose Pumice.

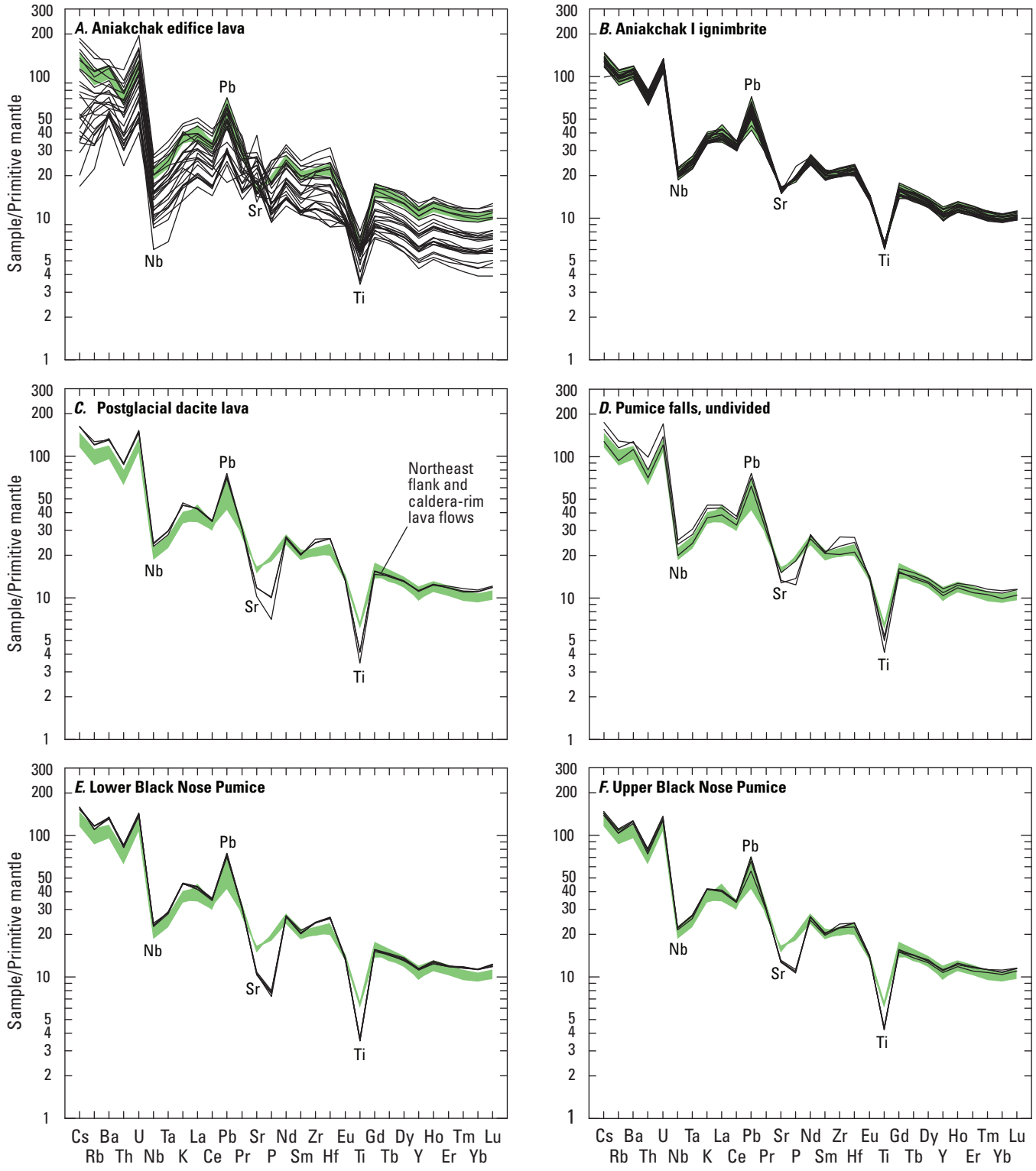

Figure 19. Primitive-mantle-normalized multielement diagrams (McDonough and Sun, 1995) for pre-3,400-yr-B.P. Aniakchak products. Green field indicating range of patterns for Aniakchak I ignimbrite serves as index for comparison with other units. *A*, Edifice lavas. *B*, Aniakchak I ignimbrite. *C*, Postglacial dacite lava. *D*, Pumice falls, undivided. *E*, Lower Black Nose Pumice. *F*, Upper Black Nose Pumice.

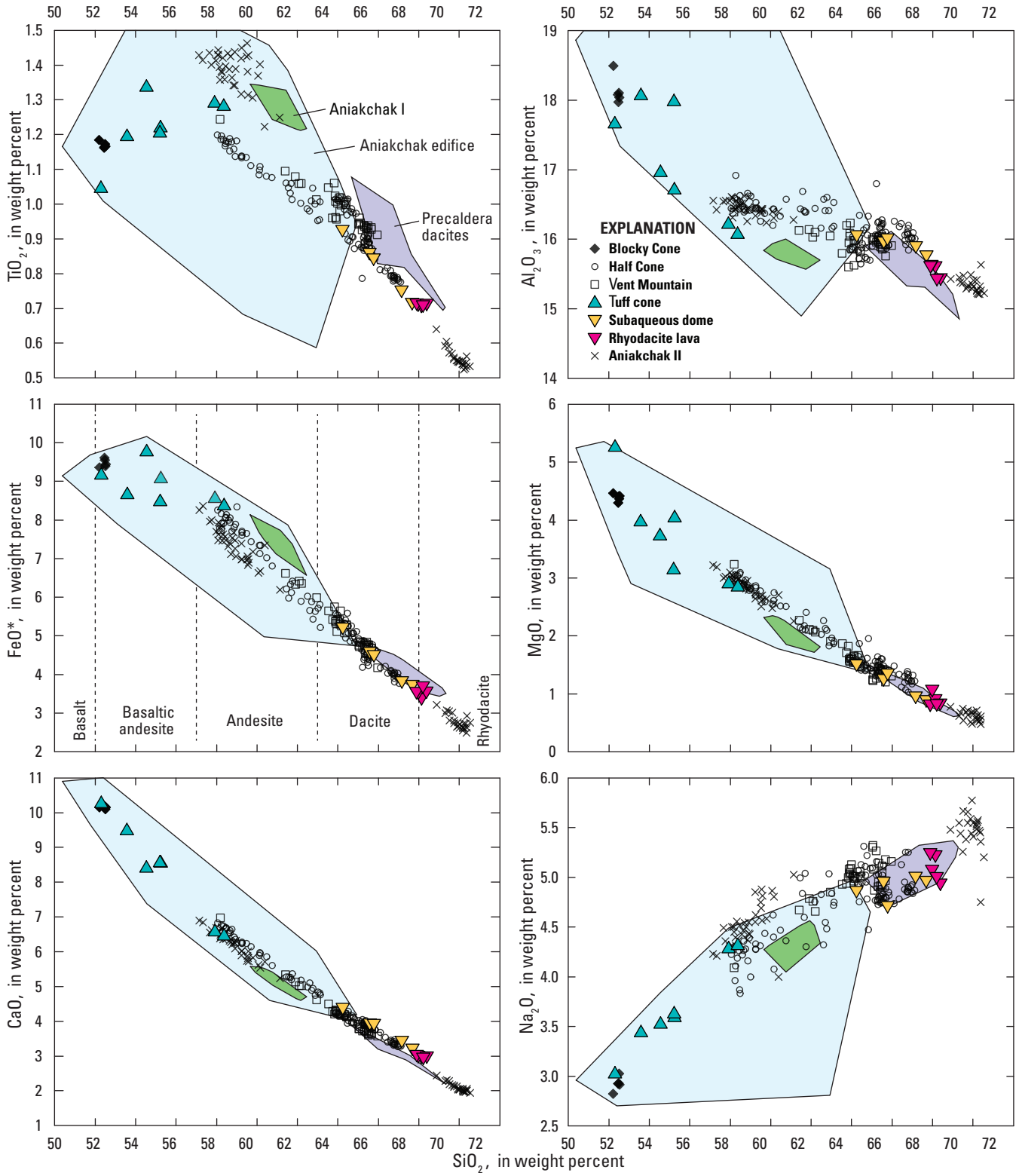

Figure 20. Silica variation diagrams for Aniakchak II and postcaldera, pre-1931 samples. Major element oxides recalculated to sum to 100 weight percent volatile-free. Fields indicate compositional ranges of edifice (blue), Aniakchak I (green), and precaldera dacite (purple) units.

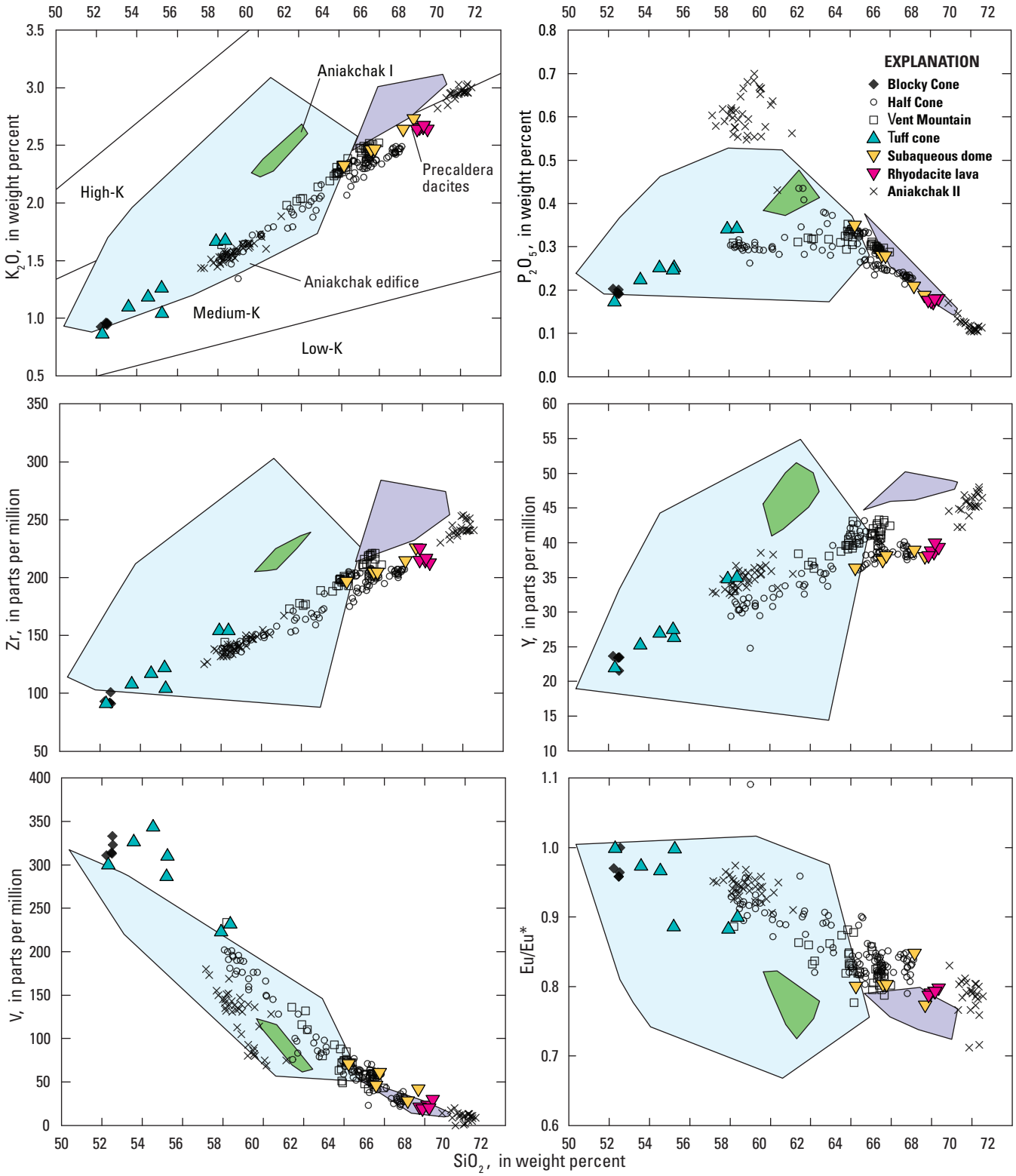

Figure 20.—Continued.

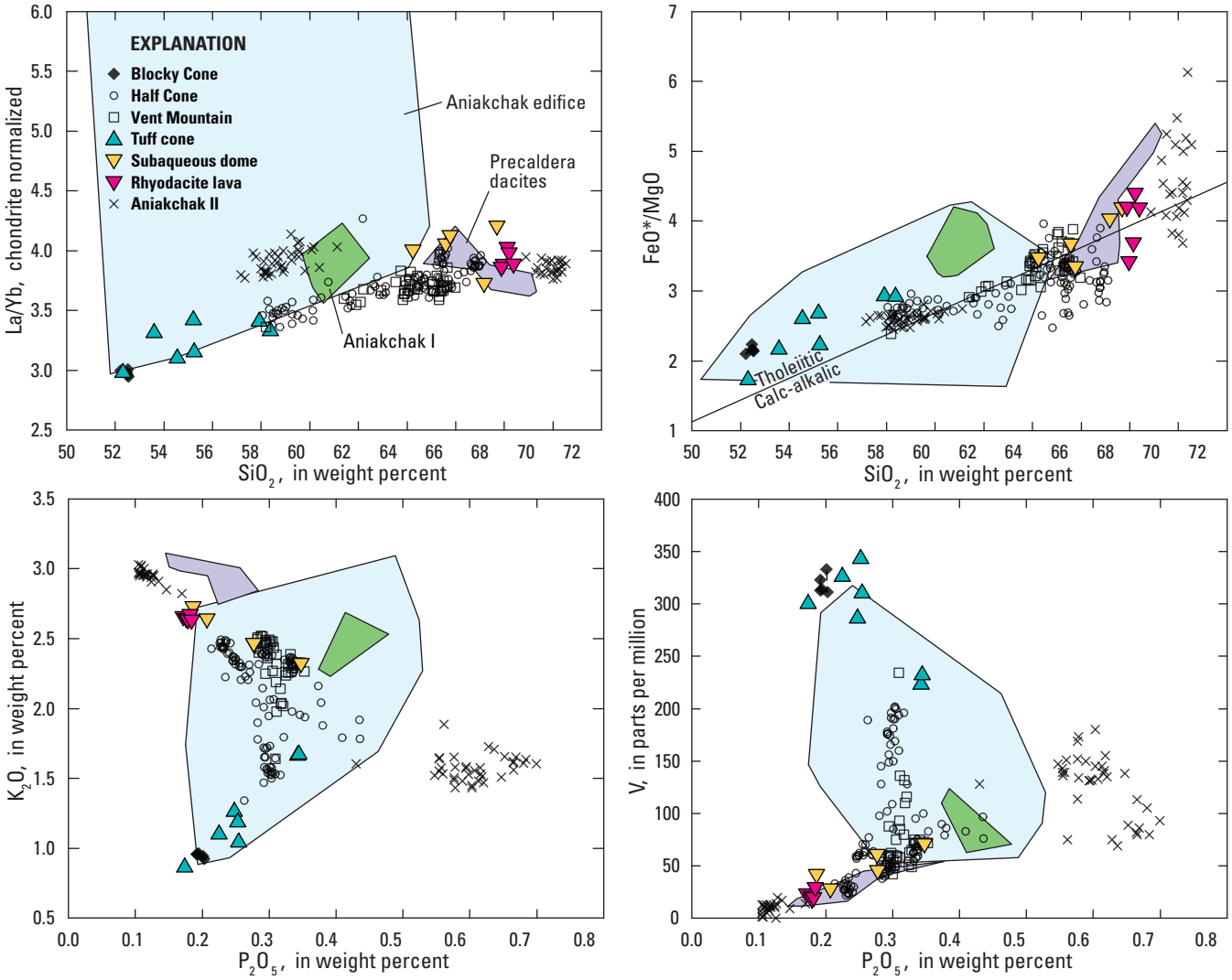

Figure 21. Silica and P_2O_5 variation diagrams for Aniakchak II and postcaldera, pre-1931 samples. Major element oxides recalculated to sum to 100 weight percent volatile-free. La/Yb ratios normalized to values for CI chondritic meteorites (McDonough and Sun, 1995). FeO* is total Fe calculated as FeO. Fields indicate compositional ranges of edifice (blue), Aniakchak I (green), and precaldera dacite units (purple).

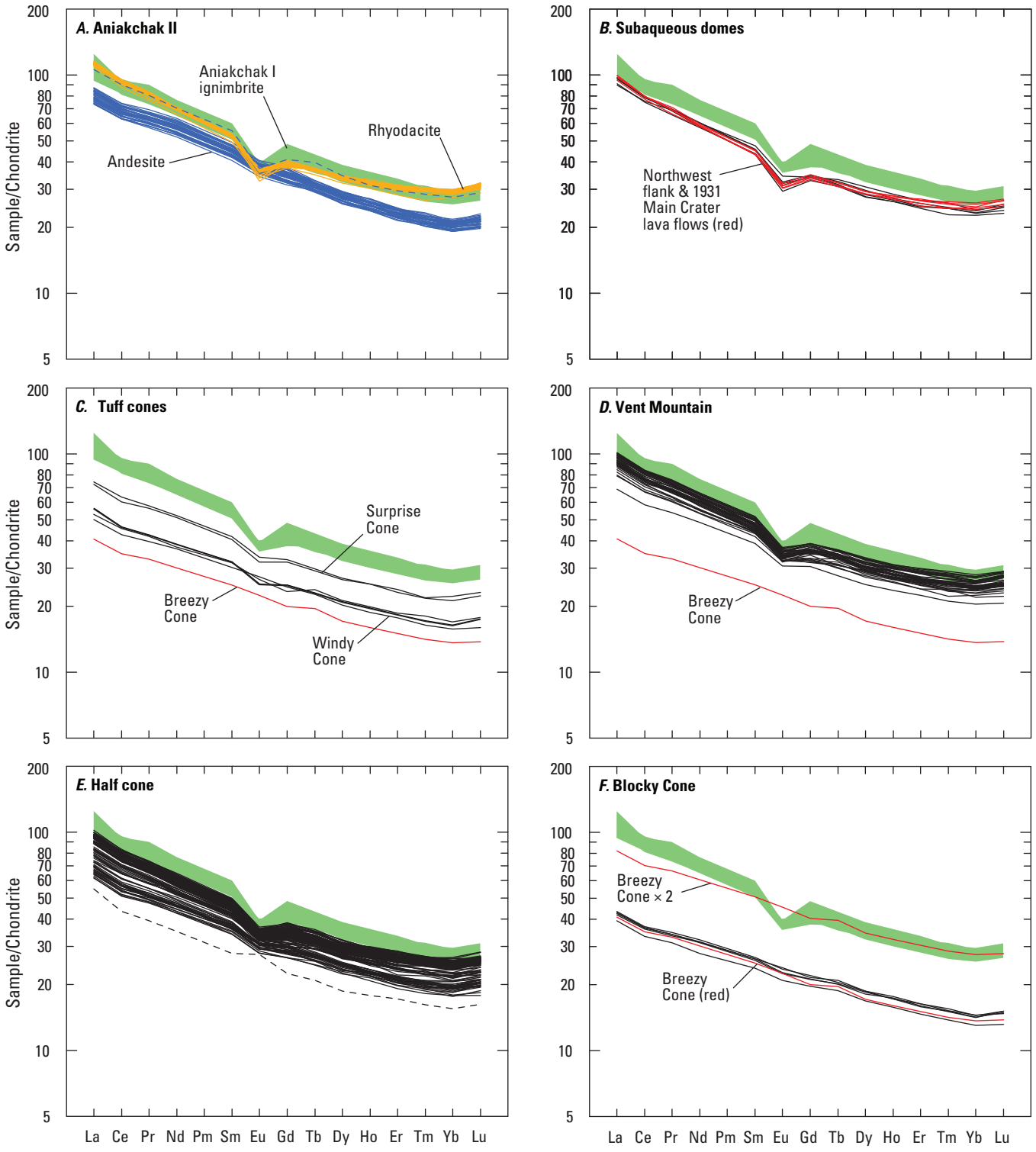

Figure 22. Chondrite-normalized rare-earth-element diagrams (McDonough and Sun, 1995) for Aniakchak II and postcaldera, pre-1931 samples. Green field indicating range of patterns for Aniakchak I ignimbrite serves as index for comparison with other units. Uptick at Lu evidently results from normalization value for Lu relative to other heavy rare earth elements (HREE) in chondrites in comparison with our inductively coupled plasma mass spectrometry (ICPMS) analyses. *A*, Aniakchak II. Dashed pattern is for Plinian fall. *B*, Subaqueous domes. *C*, Tuff cones. *D*, Vent Mountain. *E*, Half Cone. Dashed pattern is for sample ANI-02-10 from agglutinate. *F*, Blocky Cone.

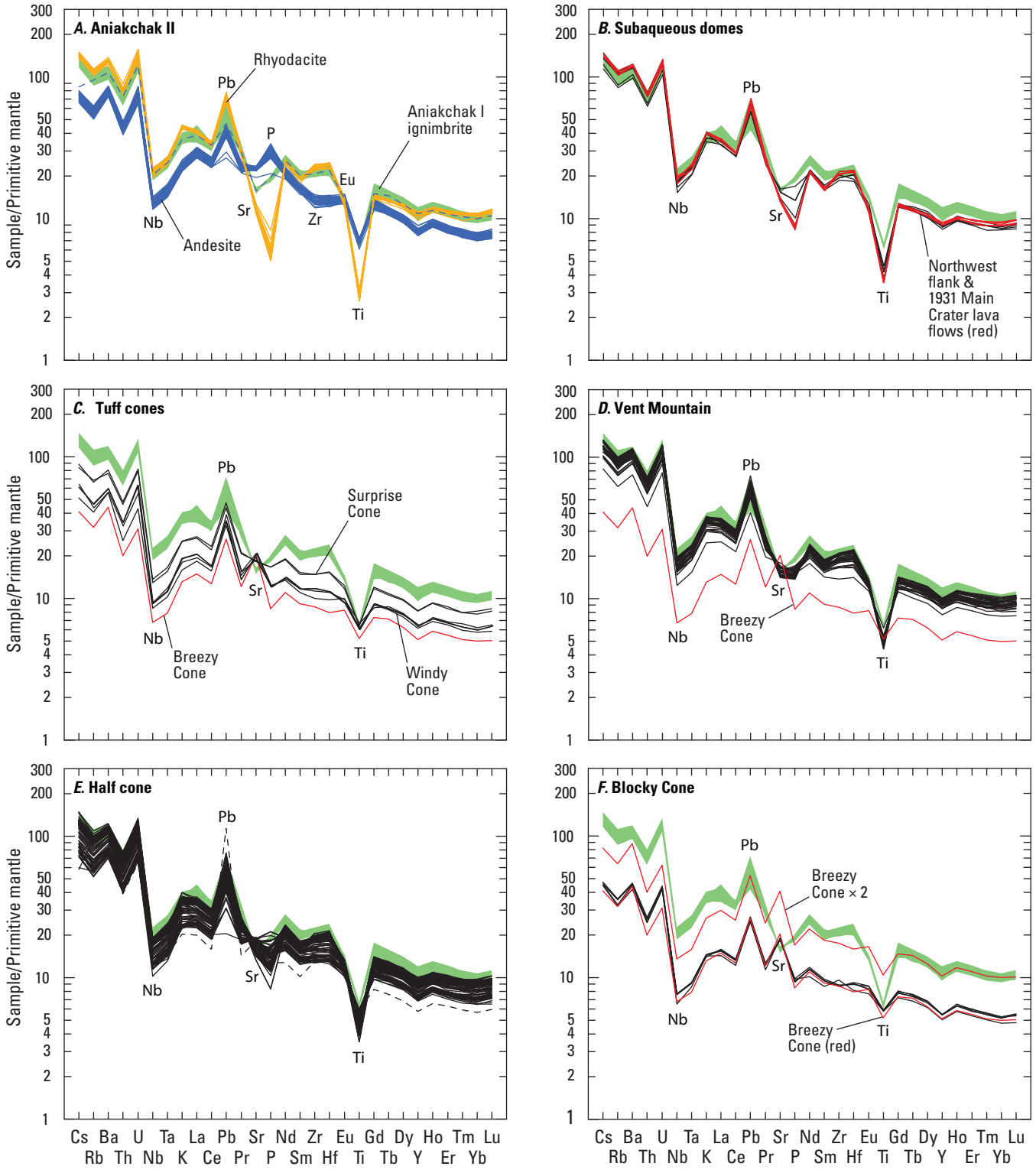

Figure 23. Primitive-mantle-normalized multielement diagrams (McDonough and Sun, 1995) for Aniakchak II and postcaldera, pre-1931 samples. Green field indicating range of patterns for Aniakchak I ignimbrite serves as index for comparison with other units. *A*, Aniakchak II. Dashed pattern is for Plinian fall. *B*, Subaqueous domes. *C*, Tuff cones. *D*, Vent Mountain. *E*, Half Cone. Dashed pattern is for sample ANI-02-10 from agglutinate. *F*, Blocky Cone.

Northwest Flank and Intracaldera Rhyodacite Lava Flows

As already noted, the northwest flank rhyodacite lava flow (67.9–68.4 weight percent SiO_2), which stratigraphic evidence suggests postdates the Aniakchak II caldera-forming eruption, is compositionally indistinguishable from rhyodacite lava exposed in the west wall of the 1931 Main Crater. The geochemical similarity is so complete that we are confident that these two lava flows represent a single magma and, therefore, probably were extruded at about the same time. These rhyodacite lavas are only marginally more evolved than Pumice Dome, so probably are closely related in origin.

Tuff Cones

Scoria from Surprise Cone, the most evolved of the three tuff cones (57.9 and 58.4 weight percent SiO_2), is andesite, (fig. 20). Scoria from Windy Cone (55.3 weight percent SiO_2) is less evolved, but more so than tephra from Breezy Cone (NA93-102, 52.3 weight percent SiO_2). Although tephra from Blocky Cone is compositionally similar, the Breezy Cone sample is the most magnesian (NA93-101, 5.27 weight percent MgO) of any postglacial Aniakchak sample. Windy Cone scoria is compositionally similar to "purple scoria" from above The Gates (NA947), lava (92CNA14) exposed in the wall of the northeast young maar, and lava (NA94-5) from 300 m north of the maar, attributed to Vent Mountain but more mafic than any other materials from that source, which suggests that the latter three samples in fact may have been from Windy Cone or a nearby hidden vent. Surprise Cone scoria is similar to other mafic postcaldera andesites in most geochemical respects, though it is slightly higher in TiO_2, FeO*, and V, as well as in K_2O, P_2O_5, and Zr; Y content and La/Yb (fig. 21) are relatively high, similar to Aniakchak II andesite.

On chondrite-normalized REE plots (fig. 22*C*), patterns for tuff cone samples are approximately parallel, but those for Surprise Cone show modest negative Eu anomalies whereas those for less-differentiated Breezy and Windy Cone typically do not. The same parallelism applies to multielement patterns (fig. 23*C*), except for elements compatible in plagioclase (Sr and Eu).

Vent Mountain

Most lava and tephra samples that are considered to have a Vent Mountain source are silicic andesites and dacites (61.4–66.0 weight percent SiO_2; fig. 20). Lava from west of The Gates (97ANB59), which may have been effused early in the history of Vent Mountain, is markedly less differentiated at 58.2 weight percent SiO_2. The silicic andesites and, especially, dacites of Vent Mountain origin typically have higher K_2O and lower Al_2O_3 and CaO at a given silica concentration than do products of Half Cone. The subtle geochemical difference between magmas from the two vents is perhaps most apparent on the P_2O_5 versus K_2O plot in fig. 21. Compositions of the Vent Mountain silicic andesites and dacites form relatively smooth trends on silica variation diagrams. There does not appear to be a consistent relationship between inferred stratigraphic order and composition, except that the oldest lava thought to have come from Vent Mountain is the least differentiated one.

Rare-earth-element patterns for Vent Mountain silicic andesites and dacites show a restricted concentration range, moderate negative Eu anomalies, and a relatively shallow slope for HREE (fig. 22*D*). The above characteristics also are evident in multielement plots (fig. 23*D*). The mafic andesite sample has REE and multielement (fig. 23*D*) patterns like those for silicic andesites but with lower incompatible element abundances.

Half Cone

The 58.1–68.1 range in silica (figs. 20 and 24) of tephra and lava attributed to Half Cone is greater than that of the Vent Mountain samples and extends to more silicic dacite. There are few gaps in the array of Half Cone data on variation diagrams. However, in the ~64–66 weight percent SiO_2 range, there is a distinct second group of high-Ti dacites (using TiO_2 as a convenient index) with higher TiO_2, K_2O, P_2O_5, and incompatible trace element contents as are more typical of Vent Mountain dacites (figs. 20, 21, and 24). A few silicic andesite lava and tephra samples continue this trend to as low as ~62 weight percent SiO_2. Half Cone andesites cross from the tholeiitic to the calc-alkalic fields on the SiO_2 versus FeO*/MgO diagram at ~61 weight percent SiO_2 (fig. 21), and most of the more silicic Half Cone samples are calc-alkalic.

When eruption order is considered, we find that the highTi dacites are predominantly early tephras and lavas, such as are exposed in the wall of Half Cone (fig. 24). Andesites and the other dacites are mainly from the ca. 400 yr B.P. Brown Pumice fall, Pink Pumice fall, and the Cobweb lava flow. Pink Pumice fall samples cluster between 66 and 67 weight percent SiO_2 and Brown Pumice samples between 58 and 61 weight percent SiO_2, though intermediate compositions are present as well. Partly welded or indurated coarse pyroclastic-flow material exposed at the base of the north wall of the 1931 Main Crater contains andesite bombs (~59 weight percent SiO_2) that are compositionally similar to Brown Pumice fall clasts (fig. 24), which strongly implicates a Half Cone source.

Andesites and dacites from Half Cone have parallel REE patterns (fig. 22*E*), except that Eu anomalies are less negative in andesites (see also fig. 20, Eu/Eu*). Maximum REE concentrations are similar to those in dacites of Vent Mountain. A single pattern, for a sample from Half Cone agglutinate (ANI-02-10), has low REE abundances and a positive Eu anomaly. Multielement patterns (fig. 23*E*) are similar to those for Vent Mountain products, but andesites are heavily

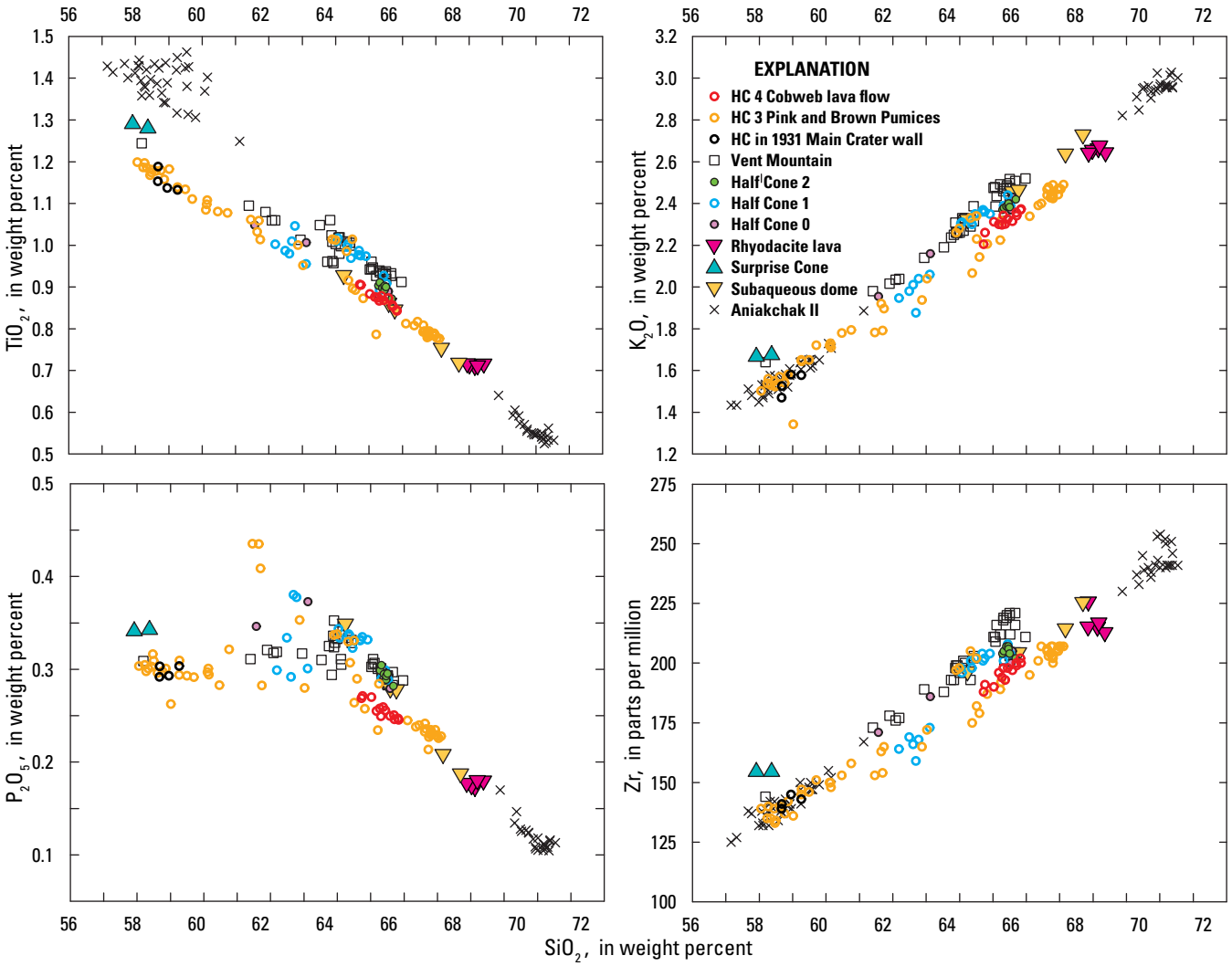

Figure 24. Silica variation diagrams for Aniakchak II and postcaldera, pre-1931 samples with >56 weight percent SiO_2. Major element oxides recalculated to sum to 100 weight percent volatile-free. Symbols for products of Half Cone (HC) indicate order of eruption, progressively warmer colors with decreasing age. "Half Cone 0, 1, 2" refer to informal geologic map units of C.A. Neal (unpublished geologic map, 2014) that refer to order of eruption.

represented by detailed sampling of the Brown Pumice fall. The outlier (ANI-02-10) has low incompatible element abundances but high Pb, consistent with the feldspar accumulation implication of its positive Eu anomaly.

Description of Half Cone geochemistry would not be complete without mention of the white felsite xenoliths that are common in the ca. 400 yr B.P. deposits. The analyzed felsite xenolith (97ANB03; appendix B, table B1; not plotted on figures) has 77.0 weight percent SiO_2 and is therefore high-silica rhyolite. The abundance of such xenoliths implies that they were derived from shallow intrusive rock, possibly related to the Quaternary magmatic system. Regardless, the analyzed quartz + plagioclase-phyric xenolith has high concentrations of elements that are incompatible in feldspar + mafic silicates + Fe–Ti oxides + apatite and low concentrations of elements strongly partitioned into these phases.

Blocky Cone

Blocky Cone is the youngest basaltic vent at Aniakchak volcano. Four analyzed tephra samples from Blocky Cone have 52.2–52.5 weight percent SiO_2. The only other postglacial eruptive material with such low silica content is from Breezy tuff cone, which has somewhat lower TiO_2 and Al_2O_3 and ~1 weight percent higher MgO (fig. 20). Blocky Cone thus is the best known candidate for most primitive recent Aniakchak magma. The Blocky Cone tephra FeO*/MgO ratio plots unequivocally in the tholeiitic field (fig. 21). Few precaldera edifice samples are as mafic.

Blocky Cone tephra REE patterns are parallel, span a narrow range, and lack significant Eu anomalies (figs. 20 and 22*F*). They are similar to the pattern for Breezy Cone, though the latter has a slightly more negative slope. Blocky

Cone and Breezy Cone REE patterns have the shallowest slopes of any postglacial Aniakchak samples (fig. 21). Blocky Cone tephra multielement patterns likewise are similar to that for Breezy Cone, though the latter has slightly lower abundances of several incompatible elements (fig. 23*F*). The subduction-related geochemical signature is strongly displayed by these relatively primitive samples, which makes a strong case for its inheritance from subcrustal processes, though doubtless these magmas experienced considerable crystallization differentiation after they left the mantle.

Products of the 1931 Eruption

The 1931 eruption of Aniakchak vented juvenile magma ranging in composition from basaltic andesite to rhyodacite (56.0–67.3 weight percent SiO_2; late bombs and lava reached 68.9). Among 47 analyzed samples, the compositional variation is nearly continuous, though a discontinuity at approximately 59.5 and a gap at 63–65 weight percent SiO_2 suggest that there are at least three groups: basaltic and mafic andesite, silicic andesite, and dacite–rhyodacite (fig. 25). The most silicic 1931 sample, from the north end of the Slag Heap flow, is compositionally similar to least-evolved Aniakchak II rhyodacite pumice, though the latter has somewhat lower compatible element abundances. At the mafic end of the spectrum, 1931 basaltic andesite has relatively high TiO_2, Na_2O, and P_2O_5 in comparison with earlier postcaldera basaltic andesites. In a manner qualitatively similar to Half Cone eruptives, 1931 andesites cross from tholeiitic to calc-alkalic fields on the SiO_2 versus FeO*/MgO diagram at ~60 weight percent SiO_2 (fig. 26). Dacite–rhyodacite samples have distinctly higher FeO*/MgO than less evolved 1931 products. Most of the 1931 samples define smooth trends on variation diagrams, but there are exceptions. Three andesite bombs and a scoria clast have anomalously low TiO_2, Na_2O, and, especially, P_2O_5 (figs. 25 and 26). It is possible that these four andesite samples, which were collected from Blocky Cone and the Doublet Crater rim, are not juvenile 1931 magma. Dacite–rhyodacite samples fall into two groups, one consisting of four basal tephra samples that plot on the projected trend defined by andesites and a second that comprises lava, bombs, and other tephra and that has higher incompatible element (for example, K_2O, Zr, Y) and lower compatible element (for example, V) concentrations and Eu/Eu*.

Rare earth elements display systematic variation with major element composition of 1931 products. Chondrite-normalized patterns for basaltic andesites and andesites are approximately parallel (fig. 27*A–D*) to each other and to the Aniakchak I reference field. Europium anomalies are lacking in the most mafic samples to slightly negative in andesites (figs. 25 and 27). For comparison, Aniakchak II andesite has roughly similar LREE and MREE, lower HREE, and Eu/Eu* ~1 (fig. 27*A*). Lava from the Main Crater floor, representative of 1931 mafic andesites, has smooth REE patterns that are elevated and slightly steeper relative to the base level suggested by Blocky Cone basaltic andesite tephra (fig. 27*C*). Overall REE abundances are higher in dacite–rhyodacite, Eu anomalies become increasingly negative, and patterns develop a concave-upward shape with increasing differentiation (figs. 27*D–F* and 25), though the most evolved 1931 lava does not attain the REE concentrations present in Aniakchak II rhyodacite (compare with fig. 22*A*).

The primitive-mantle-normalized multielement diagrams in figure 28 illustrate the geochemical characteristics of the 1931 magmas. Basaltic andesites through rhyodacites have subparallel patterns that are in most respects, other than Sr, P, and Ti, simply elevated versions of the Blocky Cone tephra patterns (fig. 28*C*). Incompatible element concentrations systematically increase with differentiation, and compatible element concentrations decrease as plagioclase, titanomagnetite, and, in turn, apatite, join the fractionating assemblage.

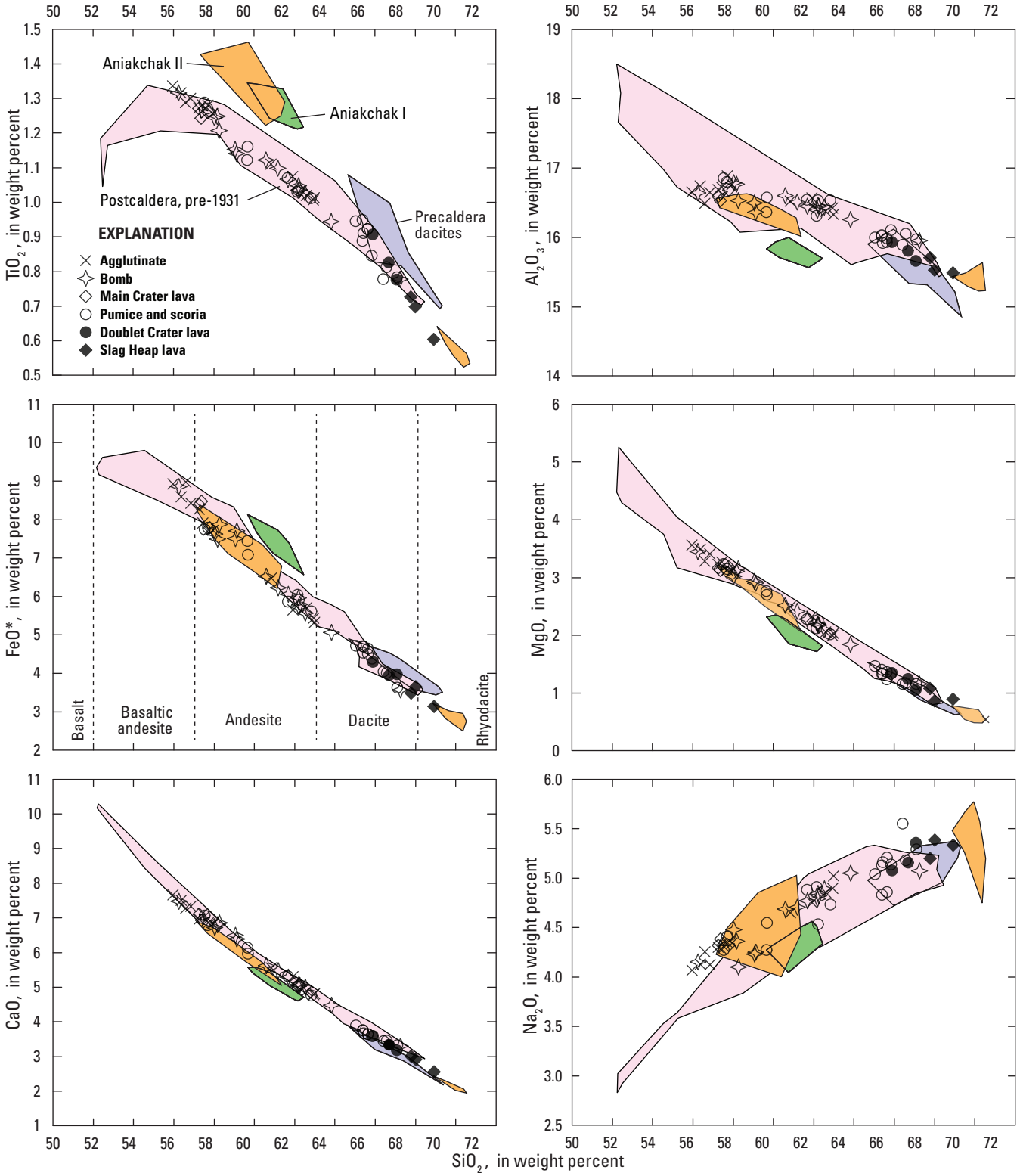

Figure 25. Silica variation diagrams for products of 1931 eruption of Aniakchak volcano. Major element oxides recalculated to sum to 100 weight percent volatile-free. Fields indicate compositional ranges of precaldera dacites (purple), Aniakchak I (green), Aniakchak II (orange), and pre-1931, postcaldera units (pink).

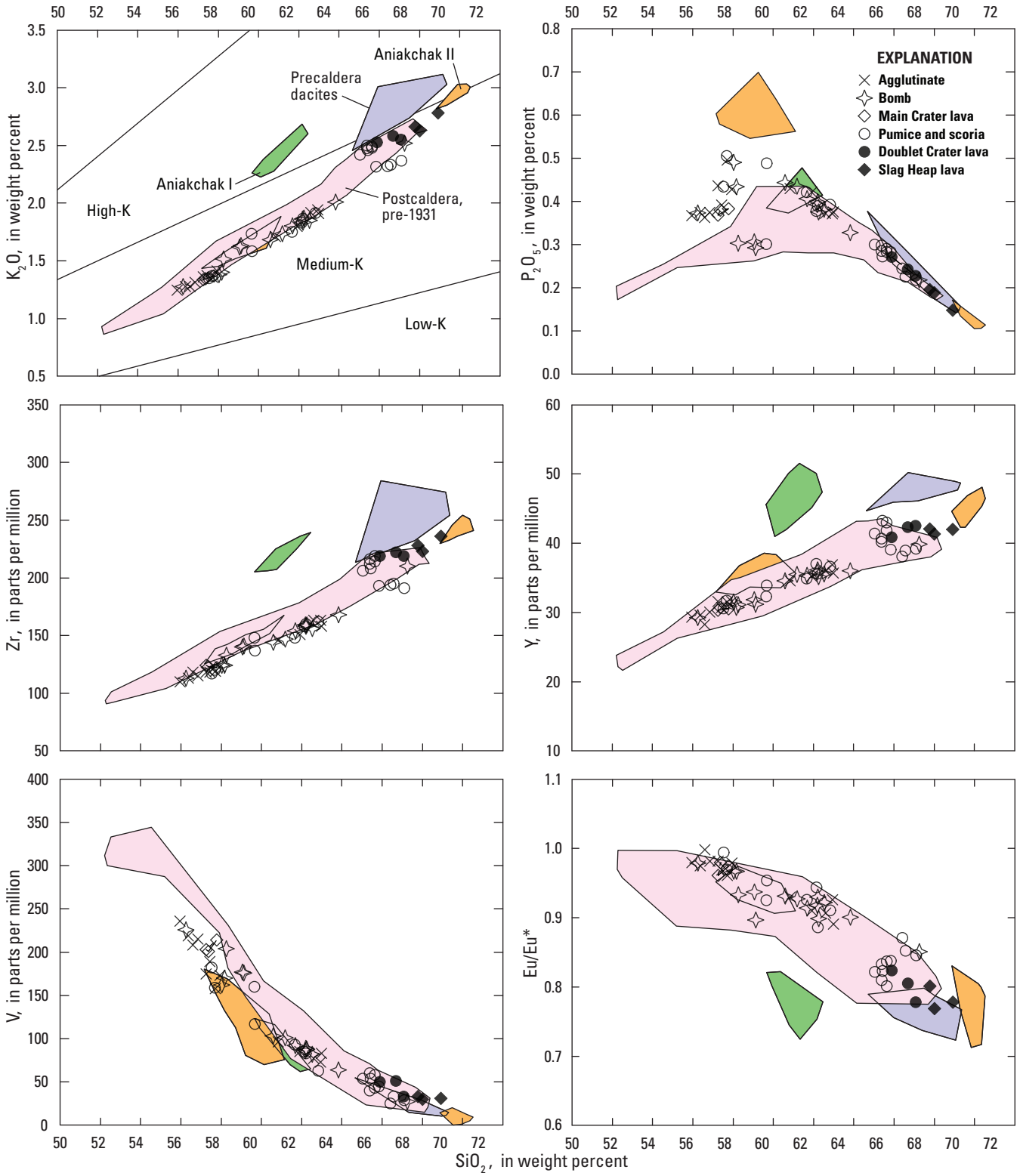

Figure 25.—Continued.

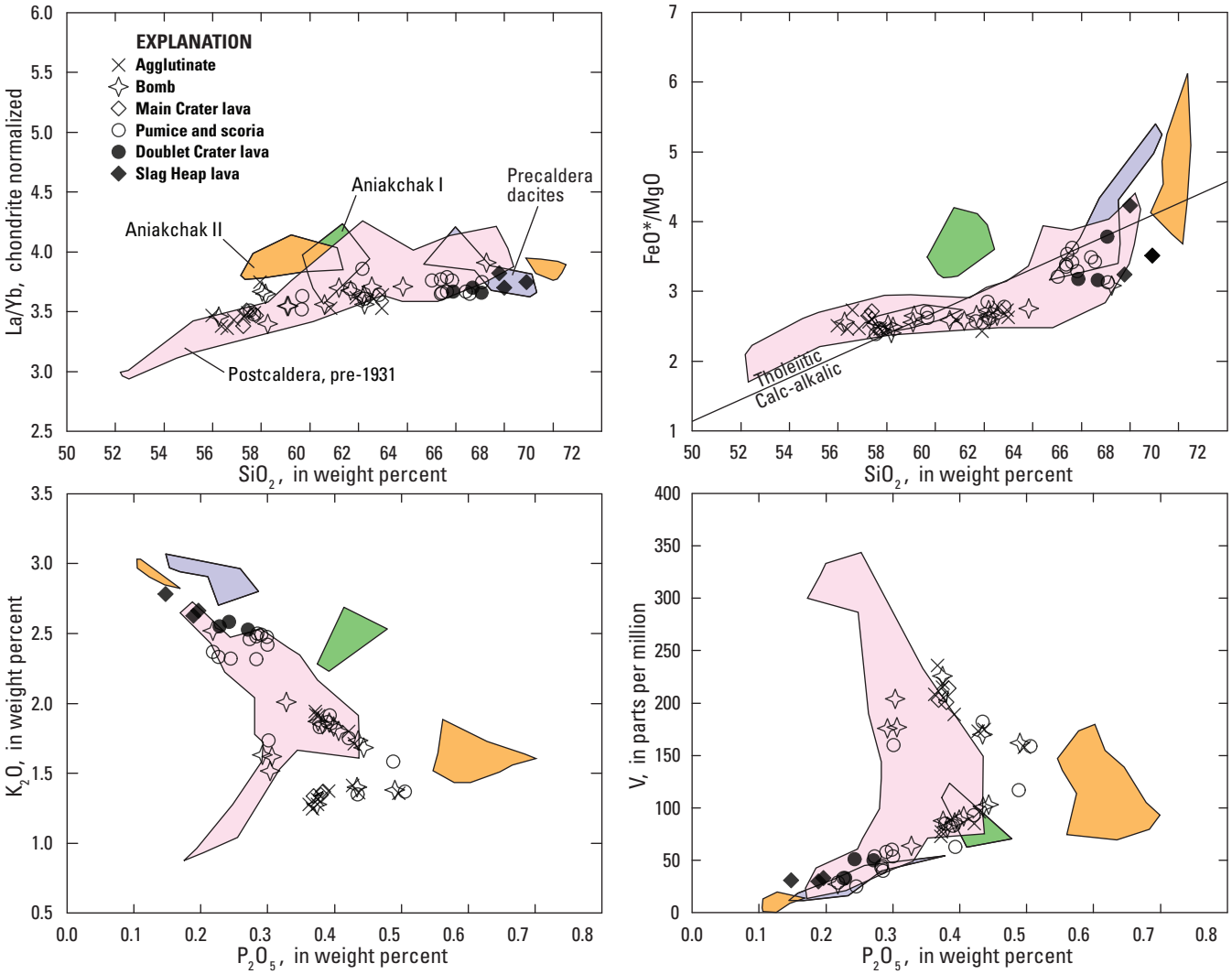

Figure 26. Silica and P_2O_5 variation diagrams for products of 1931 eruption of Aniakchak volcano. Major element oxides recalculated to sum to 100 weight percent volatile-free. La/Yb ratios normalized to values for CI chondritic meteorites (McDonough and Sun, 1995). FeO* is total Fe calculated as FeO. Fields indicate compositional ranges of precaldera dacites (purple), Aniakchak I (green), Aniakchak II (orange), and pre-1931, postcaldera units (pink).

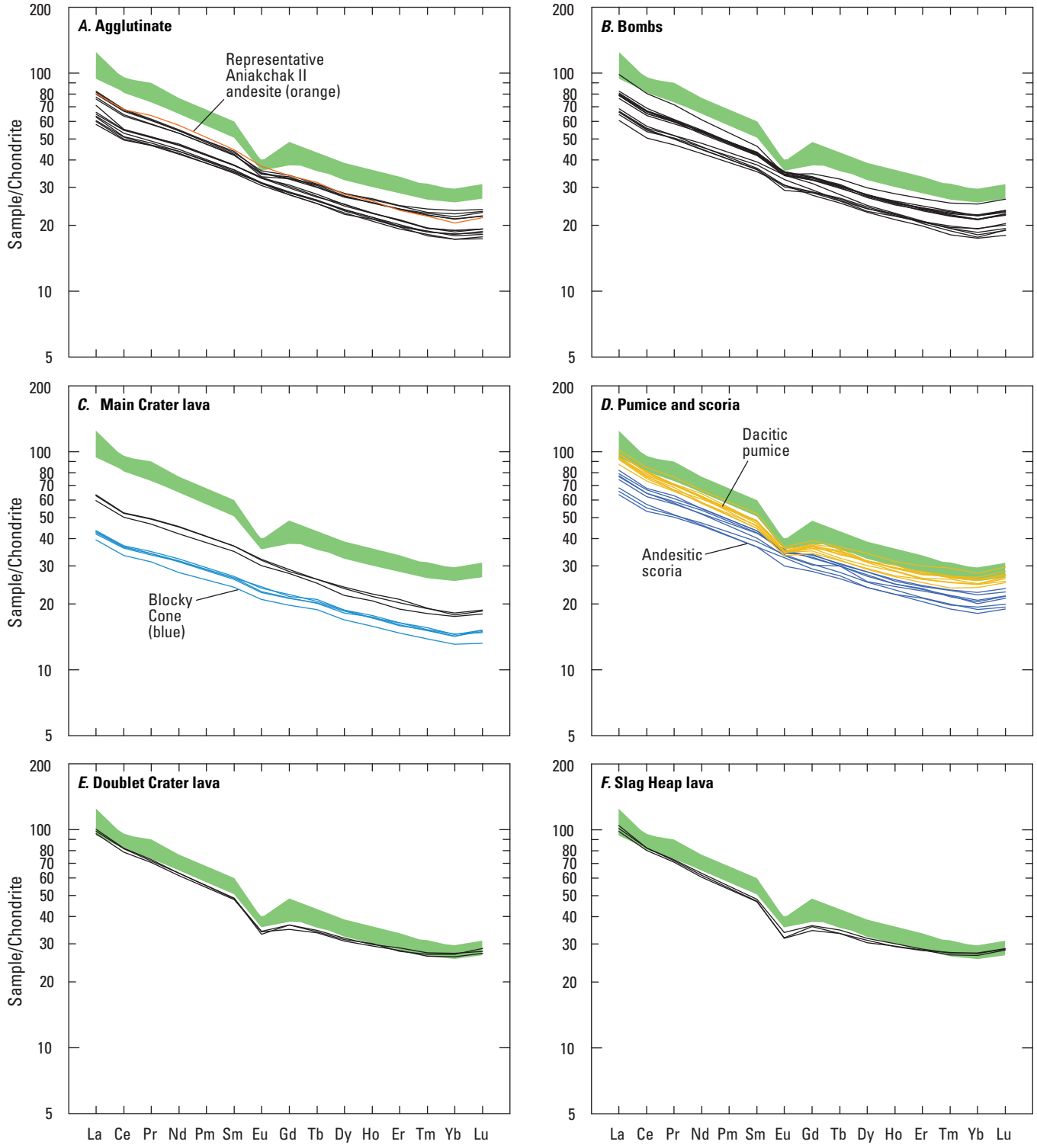

Figure 27. Chondrite-normalized rare earth element diagrams (McDonough and Sun, 1995) for products of 1931 eruption of Aniakchak volcano. Green field indicating range of patterns for Aniakchak I ignimbrite serves as index for comparison with other units. Uptick at Lu evidently results from normalization value for Lu relative to other heavy rare earth elements (HREE) in chondrites in comparison with our inductively coupled plasma mass spectrometry (ICPMS) analyses. *A*, Agglutinate. Orange pattern is for representative Aniakchak II andesite. *B*, Bombs. *C*, Main Crater lava. Blue patterns are for Blocky Cone tephra. *D*, Pumice and scoria; dacite pumice in yellow, andesite scoria in purple. *E*, Doublet Crater lava. *F*, Slag Heap lava.

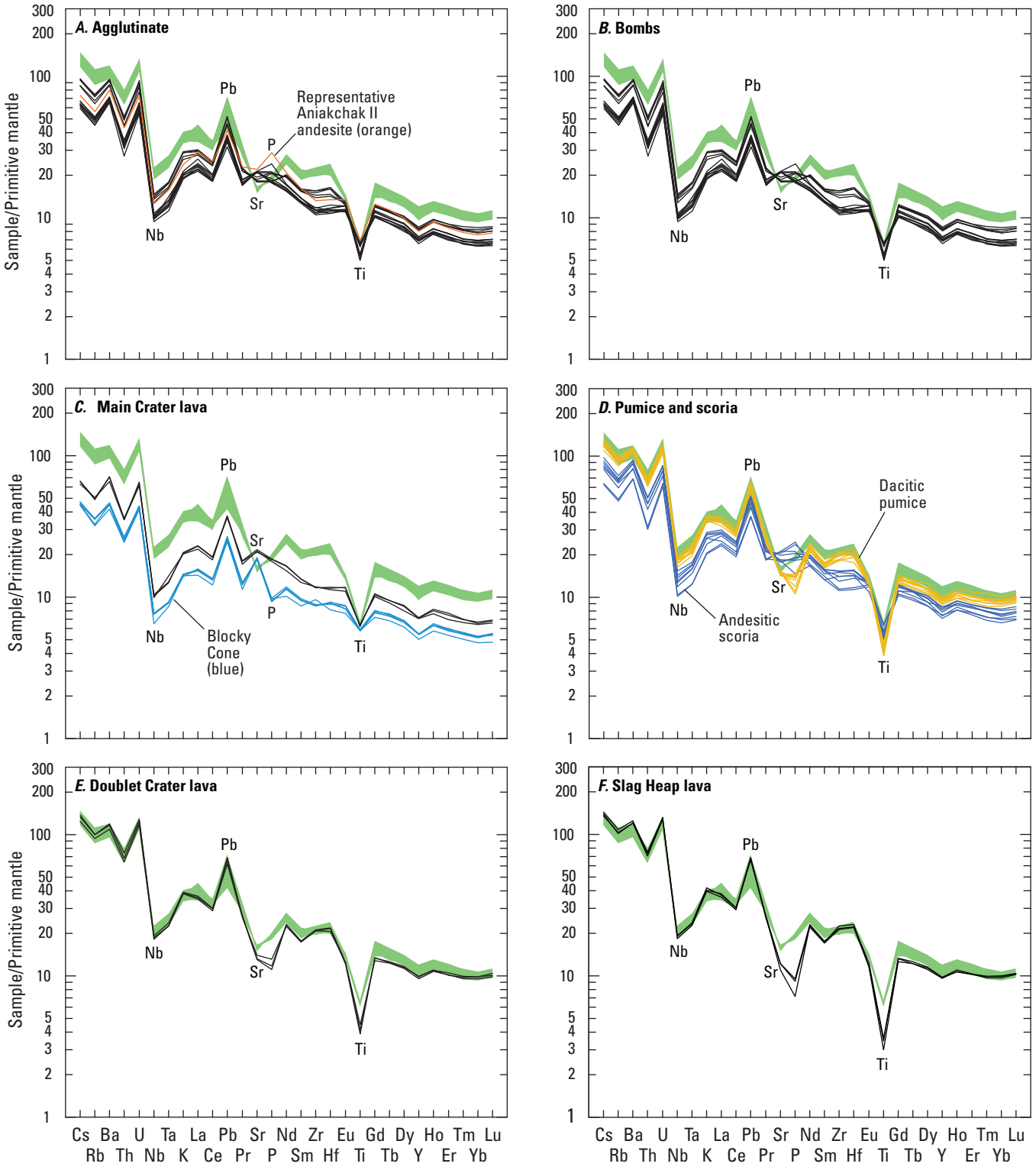

Figure 28. Primitive-mantle-normalized multielement diagrams (McDonough and Sun, 1995) for products of 1931 eruption of Aniakchak volcano. Green field indicating range of patterns for Aniakchak I ignimbrite serves as index for comparison with other units. *A*, Agglutinate. Orange pattern is for representative Aniakchak II andesite. *B*, Bombs. *C*, Main Crater lava. Blue patterns are for Blocky Cone tephra. *D*, Pumice and scoria; dacite pumice in yellow, andesite scoria in purple. *E*, Doublet Crater lava. *F*, Slag Heap lava.

Radiogenic Isotopes

The Sr, Nd, Pb, Th, and U isotopic compositions of 15 samples from postglacial Aniakchak eruptive units were determined by George and others (2004). In addition, Ra isotope data were given for the eight samples of products of the 1931 eruption. The principal focus of the George and others (2004) study was on U-series disequilibria, and these authors did not subdivide data on diagrams beyond separating 1931 from prehistoric eruptions. We present the data of George and others (2004) in figure 29, in which analyses are plotted by eruptive unit as in the other geochemical figures in this paper. One sample ("94CNA11") in table 2 of George and others (2004) has been omitted from figure 29 because its reported major element chemical analysis does not match any in the AVO database and, in that database, 94CNA11 is a Pleistocene basalt. We have plotted sample NA94–7 as being from Windy Cone on the basis of its elemental composition reported by George and others (2004, table 2), though the source vent for this tephra deposit is uncertain. It is not a goal of this paper to exhaustively interpret the limited isotopic data but to present them for the sake of completeness. We revisit implications of the isotopic analyses in the "Discussion" section, where they apply to specific eruptive units.

Radiogenic isotope data for Aniakchak volcanic rocks can be expected to show effects of assimilation of Mesozoic or younger continental crust of the Alaska Peninsula superimposed on some variability in mantle contributions owing to incorporation of subduction-related components into the mantle wedge. In Sr isotope data (fig. 29*A*), the basaltic andesites of Blocky Cone, lava southwest of The Gates (plotted here as a tuff cone product), and Windy Cone have $^{87}Sr/^{86}Sr$ ratios of 0.70325–0.70331. The Aniakchak II andesite sample similarly has the relatively low $^{87}Sr/^{86}Sr$ ratio of 0.70333, whereas Sr in dacite from Vent Mountain is marginally more radiogenic and Aniakchak II rhyodacite is defensibly higher at 0.70340. The 1931 lavas of Doublet Crater and Slag Heap overlap with Aniakchak II rhyodacite, as does one 1931 andesite bomb. However, the rest of the 1931 samples have Sr that is notably more radiogenic, including Main Crater andesite lava, the highest $^{87}Sr/^{86}Sr$ ratio being for basal dacite tephra at 0.70351.

The Sr–Nd diagram (fig. 29*B*) separates Blocky Cone, lava southwest of The Gates, and dacitic Vent Mountain samples from a larger group, forming two arrays that have decreasing $^{143}Nd/^{144}Nd$ with increasing $^{87}Sr/^{86}Sr$. Two 1931 samples plot slightly above the larger group. That both high $^{143}Nd/^{144}Nd$ and low $^{143}Nd/^{144}Nd$ arrays have basaltic andesite samples at their high $^{143}Nd/^{144}Nd$, low $^{87}Sr/^{86}Sr$ ends suggests at least two different parent magmas, or possibly an unreported Nd analytical problem. Assuming that the difference in $^{143}Nd/^{144}Nd$ ratios is real, each of the two arrays is interpreted as a mixing trend. Because $^{87}Sr/^{86}Sr$ increases with SiO_2 (fig. 29*A*), it is reasonable to suggest that the principal influence that raised $^{87}Sr/^{86}Sr$ ratios was incorporation of crustal material. Among the 1931 samples, basal dacite tephra has the highest $^{87}Sr/^{86}Sr$ and lowest $^{143}Nd/^{144}Nd$, consistent with it containing the largest crustal contribution. The $^{87}Sr/^{86}Sr$ and $^{143}Nd/^{144}Nd$ data indicate that Aniakchak II rhyodacite cannot be solely a product of closed-system differentiation of Aniakchak II andesite. Either the rhyodacite includes assimilated crustal rock or melt, or it differentiated from a parent different from Aniakchak II andesite.

The Pb isotope data define a single array of well-correlated Pb isotope ratios. Figure 29*C* plots $^{206}Pb/^{204}Pb$ versus $^{207}Pb/^{204}Pb$. Although not shown, a plot of $^{206}Pb/^{204}Pb$ versus $^{208}Pb/^{204}Pb$ appears similar. The reported $^{206}Pb/^{204}Pb$ for outlier (97ANB-44, Main Crater lava) evidently is incorrect, because this sample lies at the radiogenic end of a linear array on a plot of $^{207}Pb/^{204}Pb$ versus $^{208}Pb/^{204}Pb$. The stated analytical uncertainties are large relative to the range in ratios, but nevertheless the data are consistent with the Sr and Nd results in their indication of mixing between a mantle component that has Pb isotopic composition near the Northern Hemisphere Reference Line (Hart, 1984) and a more radiogenic component. The $^{206}Pb/^{204}Pb$ versus $^{207}Pb/^{204}Pb$ Aniakchak array has the positive correlation that is typical of magmatic arcs and commonly is attributed to addition of Pb to the mantle from subducted sediment. However, for Aniakchak postglacial samples, this trend does not project to the measured composition of marine sediment suggested by George and others (2004) to be represented by Aleutian sediment (Plank and Langmuir, 1998, their table 2). Alternatively, the radiogenic end member at Aniakchak could be close to the composition of Alaska trench sediment given by Plank and Langmuir (1998, their table 2) or of Alaska Peninsula crust.

The U-series diagram (fig. 29*D*) plots activity ratios of long-lived parent isotope ^{238}U to ^{232}Th versus short-lived daughter ^{230}Th (half-life ~76,000 yr) to ^{232}Th. Where a point lies on this plot is sensitive to magmatic processes and to time elapsed since the Th/U ratio of the magma was last modified. Through in-growth of ^{230}Th on the right or decay on the left, points will move counterclockwise back to the equiline after a few half lives. In young rocks, such as postglacial Aniakchak samples, the $^{230}Th/^{232}Th$ ratio also is an isotopic tracer. Here ($^{230}Th/^{232}Th$) ratios for 1931 products are broadly similar but do suggest differences, for instance, between Main Crater andesite and Doublet Crater lava that are consistent with Sr and Nd isotopic compositions. The greatest difference among contemporaneous eruptives, well in excess of analytical uncertainty, is shown by Aniakchak II andesite and rhyodacite.

A useful property of U-series isotopic composition is its implication for processes that contribute to a magma's composition (Gill and Williams, 1990). Points for relatively primitive samples in figure 29*D* that plot with U excess, that is, to the right of the equiline, such as Windy Cone and lava southwest of The Gates, are thought to reflect dominance of U-enrichment relative to Th in the mantle source by subduction-related fluids. On the contrary, points for mafic samples that plot to the left of the equiline, such as Blocky Cone, may have been affected more by interactions with deep crustal rocks than by subduction-related geochemical modification of the mantle source. In addition to source-related

isotopic characteristics, intermediate and silicic volcanics may present evidence of comparatively recent events that modified their Th/U ratios, such as crystallization differentiation or partial melting. That 1931 samples plot on both sides of the equiline (for example, Slag Heap and basal tephra on the left, Doublet on the right) suggests mixing of at least two components with different recent histories, those 1931 samples that straddle the equiline being mixtures (Main Crater lava) that may plot there coincidentally.

George and others (2004) reported ($^{226}Ra/^{230}Th$) ratios for the eight 1931 samples (their table 2; uncertainties are given as ±1.3 percent). Because the half-life of ^{226}Ra is a mere 1,600 years, variation in ($^{226}Ra/^{230}Th$) provides information on the time scale of recently active magmatic processes. The ($^{226}Ra/^{230}Th$) ratios of 1931 samples range from 1.167 for an andesite bomb to 1.005 for Slag Heap lava. The latter value is within uncertainty of secular equilibrium, implying dominance of material in the silicic end member of 1931 products that was either magma stored for several thousand years or remelted rock. Curves calculated for two-component mixing between average 1931 andesite and average 1931 silicic samples approximately reproduce variation of ($^{226}Ra/^{230}Th$) with Th concentration and with Eu/Eu* (figs. 29*E* and 29*F*).

Recent Seismicity

The distribution of earthquakes beneath volcanoes may illuminate the subsurface plumbing system for transport and storage of magma. The AVO seismic network at Aniakchak has detected a substantial number of earthquakes since its installation in 1997. Earthquake hypocenters located by AVO between 1 January 2009, and 3 January 2013, a total of 135 events with a maximum M_L of 2.1, are plotted on a shaded-relief map in figure 30*A*. Earthquakes clearly associated with Aniakchak volcano and with hypocentral depths <10 km are concentrated within the caldera. Deeper events occur in a bow-tie pattern centered northwest of Vent Mountain, broadening northwest of Half Cone and southeast of Vent Mountain.

In order to better visualize the distribution of earthquakes in the third dimension we plot hypocenters projected onto a vertical cross section through Vent Mountain oriented parallel to Pacific–North America Plate convergence (fig. 30*B*). This would be the plane of maximum horizontal tectonic compressive stress that is expected to be the preferred orientation of dikes (Nakamura and others, 1977). On this projection, as well as on the map, the events at >25 km below sea level (bsl) occur to the south of Vent Mountain, there is a laterally extensive region with numerous events at depths of 14–25 km, few events 7–14 km in depth occur beneath the caldera, and the shallowest events are beneath Vent Mountain and the south caldera wall. There is an overall focusing of seismicity upward beneath the southern part of the caldera.

The vast majority of located earthquakes are described as low frequency (long period, LP) events. Power and others (2004) found a similar pattern for the period 1997–2002 and interpreted deep long-period (DLP) events to reflect relatively steady-state magma ascent over a broad area in the lower to middle crust. Aniakchak has one of the highest rates of lower to midcrustal seismicity yet lacks the upper mantle events that are common at most of the other monitored Alaska–Aleutian arc volcanoes (Power and others, 2013; Buurman and others, 2014).

The plot of earthquake hypocentral depths in temporal sequence (fig. 30*C*) reveals that LP events commonly occur in clusters that span a substantial depth range. In several cases, the DLP events are closely followed, or even preceded, by shallow earthquakes.

Discussion

Eruptive Processes Through Time

In the Pleistocene Aniakchak volcano built a composite edifice of lava flows and subordinate fragmental strata. This material presumably issued from a central vent in Vulcanian and Strombolian eruptions, as well as by lava effusion at various times over a period of perhaps several hundred thousand years (Nye and others, 1993). The prominent hill of ~2,800 ft (~850 m) elevation on the volcano's flank ~3 km north-northwest of Half Cone is underlain by edifice lava (fig. 4) that may have vented from a hypothetical lateral dike system that would be approximately parallel to the maximum horizontal compressive stress, here the direction of plate convergence as suggested for Aleutian arc volcanoes by Nakamura and others (1977). Our suggestion of a possible small caldera east of Birthday Pass invites speculation on late Pleistocene explosive eruptions, but deposits from such eruptions, should they be preserved, have not yet been identified.

The earliest postglacial volcanism for which deposits are recognized is the Aniakchak I eruption, which occurred sometime between ~9,500 and ~7,000 yr B.P. This violent explosive andesitic eruption was sufficiently energetic and voluminous to deposit bombs on the slopes of the edifice and feed pyroclastic flows that descended Birthday Creek valley and the northwest flank valleys to elevations at least as low as 500–800 ft (150–240 m). In Birthday Pass, Aniakchak I ignimbrite is partly welded, and elsewhere proximal bomb accumulations may be agglutinated. Some exposures of far-traveled nonwelded ignimbrite in southern valleys may be Aniakchak I deposits. An eruption of this magnitude surely left distal tephra that can be identified by its distinctive geochemistry. Proximal lithic breccia has not been identified, and it is unclear if a caldera formed during this eruption. Judging from the known distribution of Aniakchak I ignimbrite, the vent(s), and possibly small caldera, likely were located just west of present Vent Mountain.

Black Nose Pumice and related lava were vented in a series of closely spaced eruptions, which included a Plinian event that was responsible for the pumice bed near Aniakchak Bay that rests on carbonaceous material dated at ca. 7,000 yr B.P. by VanderHoek and Myron (2004) and VanderHoek (2009). Although other eruptions may have occurred in the interval between Aniakchak I and the Black Nose Pumice events, we lack sufficient information to comment further on these. The vent for the Black Nose Pumice and lava must have been located northeast of the summit of ancestral Aniakchak volcano, west-northwest of what is now The Gates, because the precursory lava flow and the intra-Plinian welded ignimbrite have been found only in a paleotopographic low near the top of the caldera wall north of The Gates. Vent-opening explosive eruptions likely produced dacite pumice, possibly represented by deposits stratigraphically between Aniakchak I scoria and the lower Black Nose Pumice north of The Gates. Degassed dacite lava subsequently flowed a short distance to the east-northeast, much as the Cleetwood lava flow at Crater Lake, Oregon, was effused shortly before the climactic eruption of Mount Mazama (Bacon, 1983). After a pause of unknown length, a Plinian eruption resulted in deposition of the lower Black Nose Pumice. Bedding defined by changes in clast size reflects changing conditions between Plinian eruption and less vigorous explosions or lulls in activity. Changes in wind direction are considered unlikely to have affected deposition so close to the Plinian vent. The intraplinian welded ignimbrite near the top of the lower Black Nose Pumice was deposited by a pyroclastic flow that occurred when the eruption column collapsed, presumably owing to high mass eruption rate. After a brief return to Plinian venting of the lower Black Nose Pumice magma, the eruption paused for an unknown but probably brief period before resuming, this time fed by the upper Black Nose Pumice magma.

The fall deposit of upper Black Nose Pumice is bedded, probably because of changes in eruption parameters, as also inferred for the lower unit. Welding of basal upper Black Nose Pumice probably reflects a combination of high mass-eruption rate and relatively low column height at the onset of eruption that led to heat retention by pyroclasts sufficient for welding. Incipient welding of much of the upper Black Nose Pumice at the caldera rim is a consequence of these factors and possibly the slightly less evolved composition and therefore higher preeruption temperature of the magma. Further investigation of Black Nose Pumice exposures doubtless would result in a refined eruption reconstruction, and the distal tephra record of Aniakchak eruptions between Black Nose Pumice and Aniakchak II time is yet to be studied in detail.

The Aniakchak II caldera-forming eruption began with a Plinian column that was the source of pumice fall deposits locally exposed north of the volcano. The location of this vent on the edifice is unknown. The eruption character apparently transformed rapidly to feed pyroclastic flows, initially of rhyodacite exclusively. The rhyodacite ignimbrite shows little welding and may have been sourced by a comparatively high eruption column that allowed admixing of air and cooling of falling pyroclasts. The subsequent mixed rhyodacite–andesite ignimbrite commonly is partly welded, which suggests it may have been emplaced by pyroclastic flows fed by collapsed eruption column(s) issuing at high mass-eruption rate from vents around an incipiently foundering caldera-floor block. Presence of banded rhyodacite–andesite clasts demonstrates that both magmas vented simultaneously and mingled during the transition from venting of one magma composition to the other. The abundance of lithic fragments in the base of the andesite ignimbrite of the final phase of the eruption reported by Dreher (2002) suggests that caldera collapse was underway when the first andesite ignimbrite was deposited. Welding of andesite agglutinate on the flanks of the edifice implies relatively low eruption columns towards the conclusion of the eruption. A key observation yet to be made and documented would be the composition of any juvenile clasts in the proximal lithic breccia found on and near the caldera rim (Druitt and Bacon, 1986). This could indicate when in the eruption scenario the caldera began to collapse. Regardless, the diameter of Aniakchak caldera and the circumferential distribution of postcaldera vents indicates subsidence of a piston-like caldera-floor block and outward expansion of the caldera by inward landsliding of the oversteepened walls during and following the eruption.

Following caldera collapse, a lake developed within the closed basin. By analogy with other caldera lakes, groundwater draining from the walls and precipitation took at most a few hundred years to fill the caldera to its rim. For example, Crater Lake, Oregon, though differing from Aniakchak in being limited in maximum level by leakage through a permeable layer in the caldera wall, reached a depth of nearly 600 m in a little as ~400 years (Nathenson and others, 2007). The ancestral caldera lake at Aniakchak was at most ~300 m deep. The minimum depth is constrained by the summit elevations of subaqueous dacite domes, West Dome being the highest at 610 m asl, and the maximum depth by low points on the caldera rim. Joint patterns indicate that Pumice, Vulcan, Bolshoi, and West Domes were emplaced under lake water. Pyroclastic deposits that may have been produced before or during dome extrusion have not been recognized. The four domes apparently effused slowly from vents located within a ring-fracture system surrounding the foundered caldera block. Sometime after the Aniakchak II eruption, rhyodacite lava whose composition is closely comparable to that of Pumice Dome, was extruded high on the northwest flank of the edifice and near the west caldera wall.

Breezy, Windy, and Surprise tuff cones vented basaltic to andesite magma following draining of the caldera lake. Although the height-to-width aspect ratios of these U-shaped features could imply the name tuff ring (Wohletz and Sheridan, 1983; Cas and Wright, 1987), historical usage at Aniakchak and the ~100 m height of the partial rings leads us to retain the term tuff cone. The Aniakchak tuff cones appear to be transitional between the extremes of tuff rings and tuff cones, though their forms have been modified by erosion and infilling of craters by pyroclastic and alluvial material.

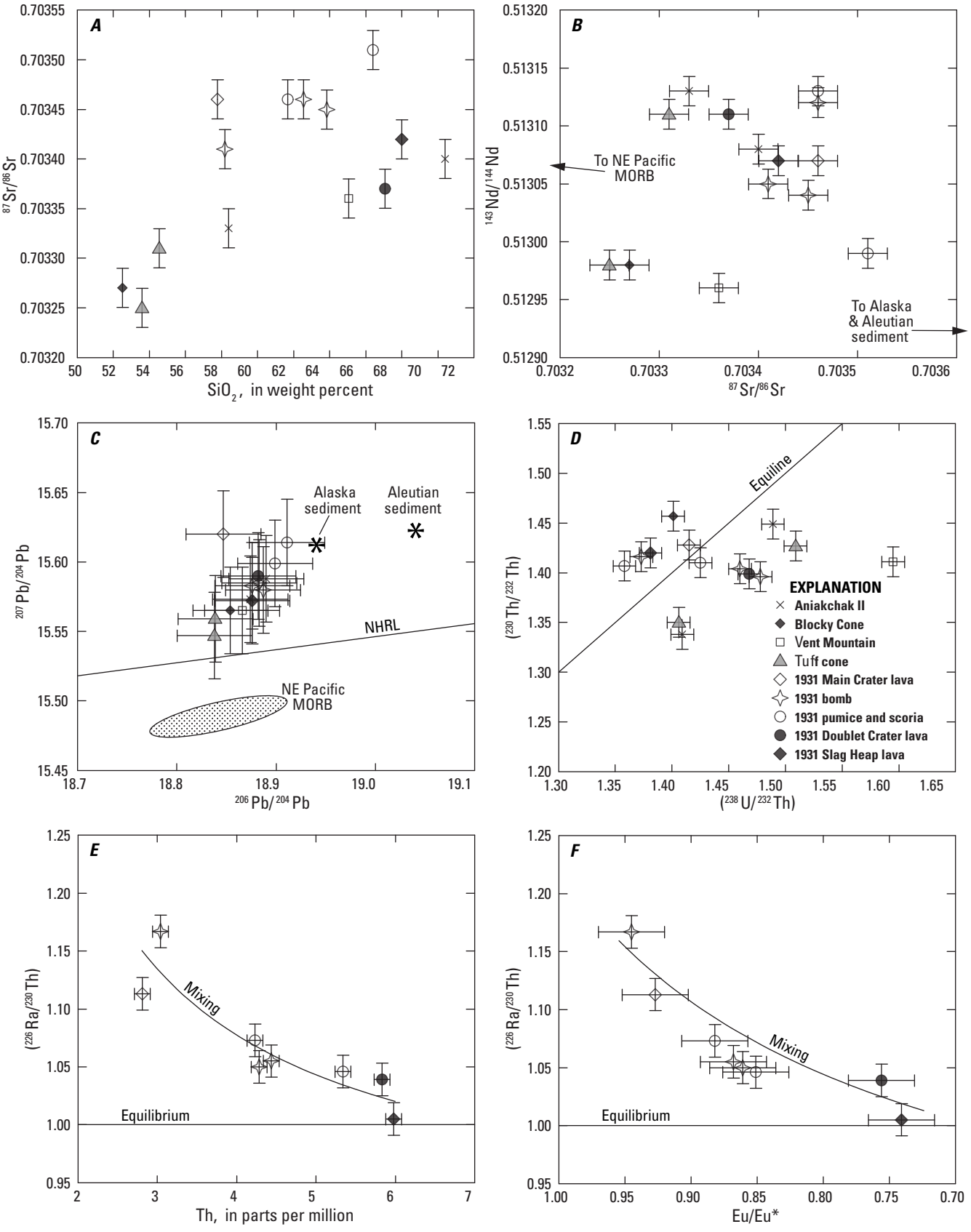
A
$^{87}Sr/^{86}Sr$
SiO_2, in weight percent
B
$^{143}Nd/^{144}Nd$
To NE Pacific MORB
To Alaska & Aleutian sediment
$^{87}Sr/^{86}Sr$
C
$^{207}Pb/^{204}Pb$
Alaska sediment
Aleutian sediment
NHRL
NE Pacific MORB
$^{206}Pb/^{204}Pb$
D
$(^{230}Th/^{232}Th)$
Equiline
EXPLANATION
Aniakchak II
Blocky Cone
Vent Mountain
Tuff cone
1931 Main Crater lava
1931 bomb
1931 pumice and scoria
1931 Doublet Crater lava
1931 Slag Heap lava
$(^{238}U/^{232}Th)$
E
$(^{226}Ra/^{230}Th)$
Mixing
Equilibrium
Th, in parts per million
F
$(^{226}Ra/^{230}Th)$
Mixing
Equilibrium
Eu/Eu*

Figure 29 (facing page). Isotopic data for postglacial products of Aniakchak volcano (George and others, 2004, table 2). Error bars on isotopic ratios are ±2σ; symbols as in earlier figures (see legend in *D*). Where shown in *B* and *C*, following George and others, field of Northeast Pacific mid-ocean ridge basalt (MORB) is from Langmuir and others (1992), and ocean floor sediment averages off the Aleutian and Alaska arc are from Plank and Langmuir (1998). *A*, SiO_2 versus $^{87}Sr/^{86}Sr$. B, $^{87}Sr/^{86}Sr$ versus $^{143}Nd/^{144}Nd$. Arrows indicate vectors to Northeast Pacific MORB and Alaska and Aleutian sediment, off scale at $^{87}Sr/^{86}Sr$ = 0.7026 and ~0.706, respectively. *C*, $^{206}Pb/^{204}Pb$ versus $^{207}Pb/^{204}Pb$. Northern Hemisphere Reference Line (NHRL) is from Hart (1984). Outlier is sample 97ANB44, 1931 Main Crater lava, for which reported $^{206}Pb/^{204}Pb$ is suspect. Alaska and Aleutian trench sediment average compositions from Plank and Langmuir (1998, their table 2). *D*, $(^{238}U/^{232}Th)$ versus $(^{230}Th/^{232}Th)$ activity ratios. Secular equilibrium is represented by the equiline. *E*, Th concentration versus $(^{226}Ra/^{230}Th)$ activity ratio. Horizontal line at $(^{226}Ra/^{230}Th)$ = 1 represents secular equilibrium. Mixing curve (Langmuir and others, 1978) was calculated for simple two-component mixtures of average andesite and average silicic lava. Uncertainty in Th concentration by inductively coupled plasma mass spectrometry (ICPMS) assumed to be ±0.1 ppm, ~2 percent. *F*, Eu/Eu* versus $(^{226}Ra/^{230}Th)$ activity ratio. Line and curve as in *E*. Uncertainty in Eu/Eu* from ICPMS data assumed to be ±0.025, ~3 percent. Uncertainties (±2σ) inferred from George and others (2004) are as follows: $^{87}Sr/^{86}Sr$, 28 ppm (0.000020); $^{143}Nd/^{144}Nd$, 25 ppm (0.000014); Pb isotope ratios, 0.2 percent (0.03–0.08); $(^{230}Th/^{232}Th)$ and $(^{238}U/^{232}Th)$, 1 percent (~0.015) and 0.7 percent (~0.010), respectively; Th concentration by ICPMS, ~2 percent (0.1 ppm); Eu/Eu* from ICPMS data ~3 percent (0.025).

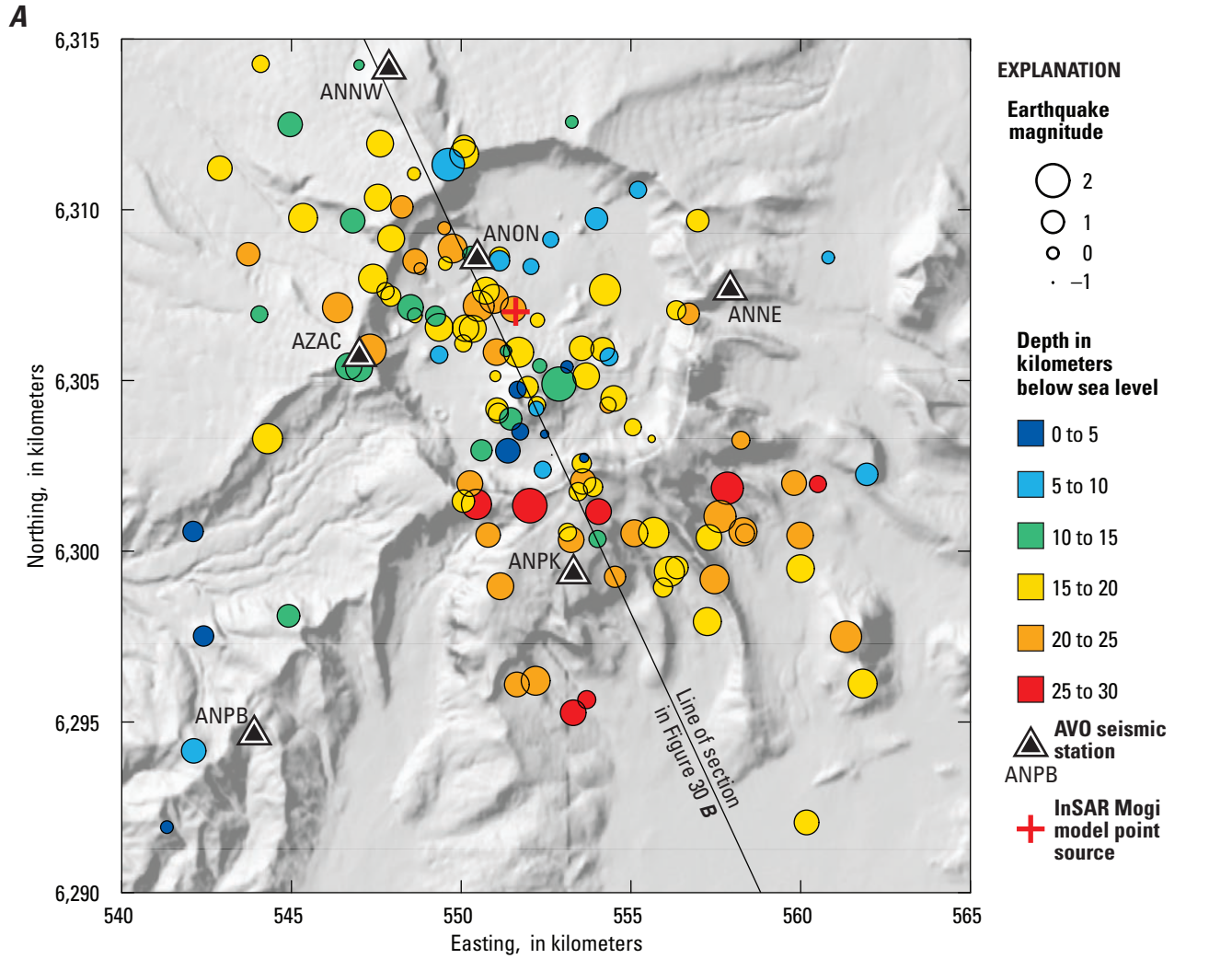

Figure 30. Locations of 135 earthquake hypocenters located by the Alaskan Volcano Observatory (AVO) for the period January 1, 2009, through January 3, 2013 (Dixon and others, 2010, 2011, 2012, 2013). *A*, Map of earthquake locations with magnitude and depth indicated. Northing and Easting in Universal Transverse Mercator (utm) grid in Aniakchak region are rotated ~1 degree clockwise relative to lines of longitude and latitude. Map location for Mogi model point-source for caldera deflation detected by InSAR is from Kwoun and others (2006). Hillshade base from U.S. Geological Survey 30-m digital elevation data. *B*, Hypocenters projected to line of section in *A* plotted as distance north-northwest from arbitrary origin (558.8 km E, 6290.0 km N) versus depth below sea level. Hypocenters ≥8 km from line of section excluded from plot. Line of section is Pacific–North America Plate convergence azimuth (N24°W) from DeMets and others (2010) interpolated from Ryan and others (2012, their figure 3). Minimum magma storage depths below ground surface were calculated from dissolved volatile concentrations in melt inclusions (Bacon, 2002) for vapor-saturated magma and overburden density of 2,200 kg/m^3. *C*, Hypocentral depths through time. Hypocenters ≥8 km from line of section in *A*, excluded from plot.

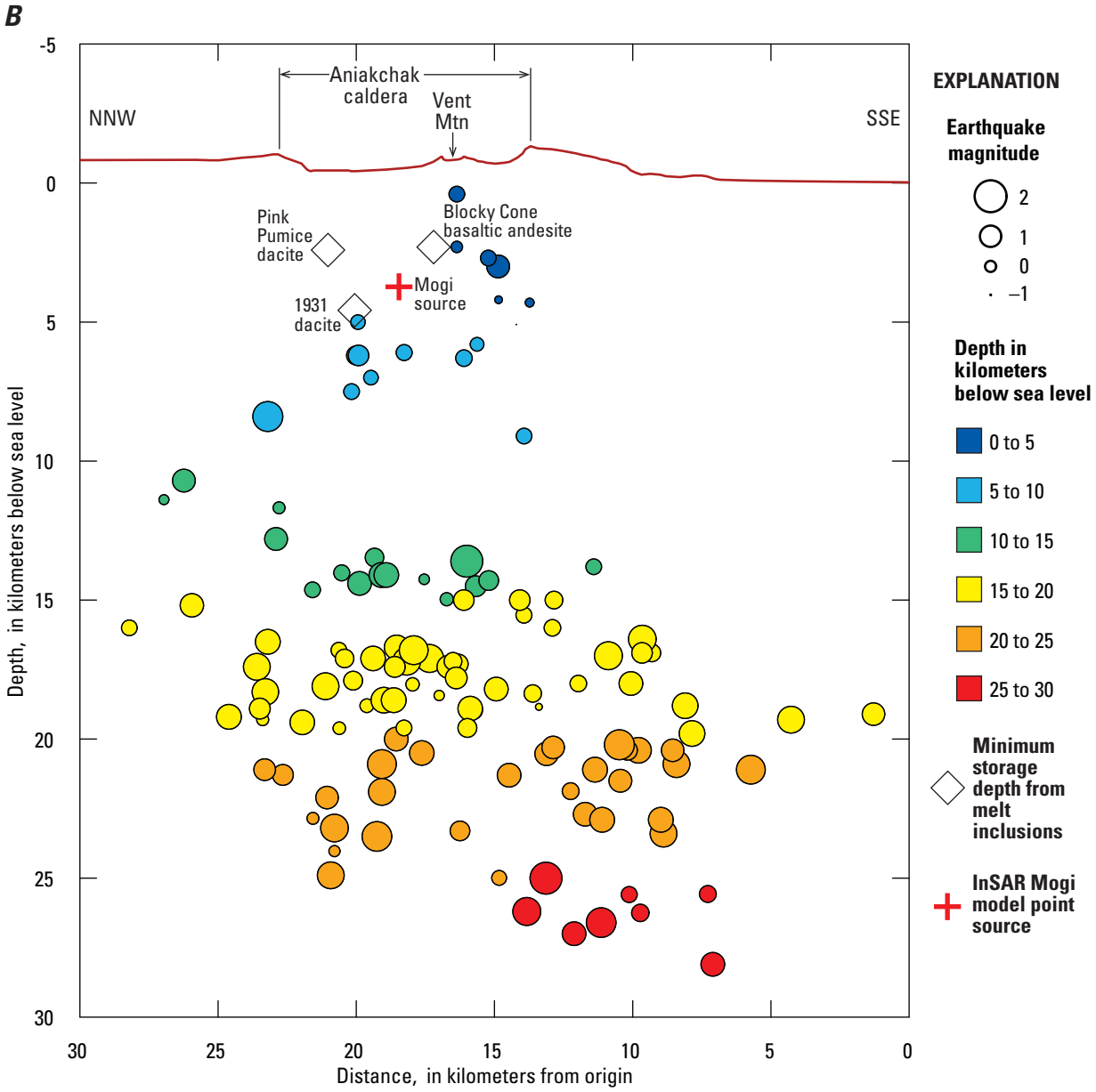

Figure 30.—Continued.

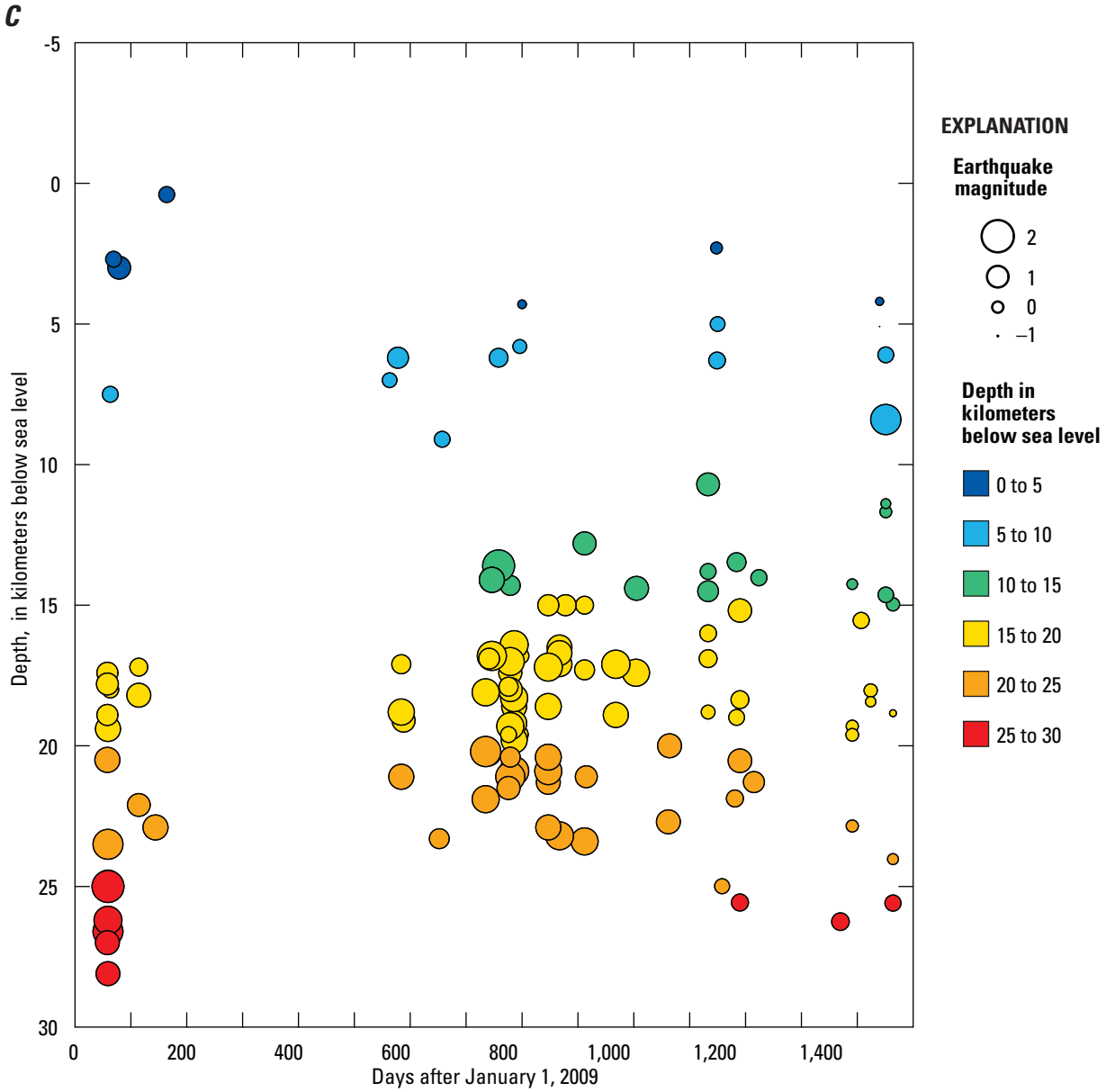

Figure 30.—Continued.

This implies eruption in shallow standing water or saturated ground very near lake level at an elevation of ≤400 m asl, the approximate elevation of their crater floors. This elevation corresponds to the middle terrace, 82 m above modern Surprise Lake, identified by McGimsey and others (1994). The deposits in the cones themselves suggest variation between Surtseyan explosion and hydrovolcanic blasts that resulted in fall and surge deposition, respectively. We speculate that the eruptions of mafic to intermediate magma that built the three tuff cones were triggered by unloading (decompression) of the magmatic system owing to rapid draining of the caldera lake.

Our current understanding of stratigraphic relations between tephra deposits and lava flows indicates that activity of Vent Mountain and Half Cone followed that of the tuff cones and alternated for possibly ~1,000 years between these two andesite–dacite vents situated on the ring-fracture system (fig. 5*C*). Accessible deposits suggest that Half Cone erupted more explosively than Vent Mountain, at least late in their histories. The Vent Mountain cone was built by accumulation of scoria bombs and lapilli from Strombolian to violent Strombolian explosions forming unconsolidated to agglutinated layers. Lava flows issued from the base of the cone and also from fissure eruptions on the southwest flank. New Cone, on the southeast flank of Vent Mountain, was constructed by violent Strombolian eruptions from the same magma plumbing system. Half Cone produced a smaller volume of lava but more voluminous pyroclastic deposits than did Vent Mountain. Early Half Cone explosive eruptions may have been Vulcanian to Plinian, sending pyroclastic flows across the caldera floor to leave partly welded deposits such as are exposed at the base of the north wall of the 1931 Main Crater. These eruptions alternated with effusion of degassed lava as domes and local flows. Towards the end of its life, ca. 400 yr B.P., Plinian eruption of Half Cone resulted in deposition of the widespread pink and brown pumice falls and intracaldera pyroclastic flows and surges. This event was followed by Strombolian or violent Strombolian eruptions that laid down agglutinated spatter on the surface of Half Cone. This activity ended with destruction of the Half Cone edifice and subsequent effusion of the degassed Cobweb lava flow that spread radially about the central conduit, now marked by a ring of tephra.

Blocky Cone is a cinder and scoria cone formed by Strombolian eruption of one of the most primitive of magmas erupted at Aniakchak. Like the majority of postcaldera vents, Blocky Cone is located above the ring-fracture system. Its feeder conduit somehow missed intersecting any resident evolved magma stored beneath the southwestern edge of the caldera at the time of its <400 yr B.P. prehistoric eruption.

In their detailed reconstruction of events of the 1931 eruption, Nicholson and others (2011) concluded that, after initial vent-clearing steam explosions, the principal tephra fall originated from a subplinian column. This phase of the eruption was succeeded by intermittent phreatomagmatic explosions as magma supply diminished and magma interacted with groundwater. While the latter activity was ongoing, effusion of degassed silicic lava began at Doublet Crater and Slag Heap vents. Change to more mafic andesite and basaltic andesite at the Main Crater vent resulted in transition from phreatomagmatic to Strombolian eruption of spatter and effusion of degassed lava on the crater floor. The three 1931 vents are sited on the outer edge of the inferred ring-fracture system. We will return to a conceptual model of the Aniakchak magmatic system after providing interpretation of the geochemistry of erupted magmas.

Magma Evolution

Having described the geochemical characteristics of postglacial eruptive units in earlier sections, we now interpret Aniakchak magma geochemistry in terms of processes likely responsible for the diversity of erupted compositions. This qualitative analysis is intended to highlight notable geochemical features and to guide future research and quantitative modeling of Aniakchak petrogenesis.

Geochemical Features of Arc Magmas at Aniakchak

A framework for understanding magma evolution at Aniakchak is provided by widely accepted common features of magmatism above subduction zones manifested by arc volcanoes. The magma transport and storage systems of arc volcanoes receive input, or parent, magma that originates as basaltic partial melt of the mantle and, with few exceptions, carries with it the geochemical fingerprint of hydrous fluids or melts produced in subduction-related processes. This fingerprint is characterized by high abundances of large-ion lithophile elements (LILE) K, Rb, Cs, Sr, and Ba, as well as Pb, Th, U, and LREE, relative to high field strength elements (HFSE) Nb and Ta (see, for example, fig. 19*F*). En route upward to crustal depths, melts separate from precipitated crystals and some interaction of magma with mantle and deep crustal rocks doubtless occurs, so that parental melts that reach the upper 5–20 km of the crust typically are fractionated relative to primary mantle melts. The most MgO-rich basalts and basaltic andesites at Aniakchak, such as some Pleistocene lavas (fig. 16) and postglacial Breezy and Blocky Cones (fig. 20), we take as representative of the parents of magmas erupted by Aniakchak. Because even these magmas have experienced olivine fractionation, and thus have low contents of olivine-compatible Ni, we plot concentrations of V (figs. 16, 17, 20, 21, 25, and 26) as a moderately compatible trace element that is useful to illustrate fractionation of a plagioclase-dominated, pyroxene- and titanomagnetite-bearing assemblage.

Note that Pleistocene mafic magmas display a range of mantle-incompatible element concentrations (for example, P, K, Y, and Zr in fig. 16) that would be very difficult to explain solely by crystallization differentiation of a single primary magma. It is important to recognize this incompatible-element concentration range because Breezy and Blocky Cones, the most primitive postglacial erupted magmas, may not represent

the entire spectrum of mafic inputs into Aniakchak in postglacial time. Aspects of that spectrum may result from different degrees of partial melting of a uniform source, which would affect all incompatible elements, or from variation in the amount of added subduction component in local domains of the mantle wedge above the Alaska–Aleutian subduction zone, which would affect LILE preferentially. Further variation in certain elemental concentrations in primitive magmas may be attributed to local mantle fertility, the capacity to yield silicate melt at a given temperature and pressure.

Most of the erupted magmas at Aniakchak and the majority of arc volcanoes worldwide show the geochemical effects of processing in the crust. As SiO_2 content increases, concentrations of elements compatible in minerals stable at magmatic temperatures and crustal pressures (olivine, pyroxenes, hornblende, plagioclase, Fe–Ti oxides, apatite, and other accessory minerals) decrease and those of incompatible elements increase. These effects result from crystallization differentiation, that is, separation of melt from crystals, with or without addition of wall rock or partial melts thereof (assimilation–fractional crystallization, or AFC; DePaolo, 1981). Some occurrences of silicic magmas are thought to represent partial melts of crustal rocks with little or no component of mantle-derived magma. Further complications are the possibility of magma mixing (Anderson, 1976) and common admixing of crystal cumulate material from the Quaternary magmatic system (for example, Nakada and others, 1994; Dungan and Davidson, 2004). We use graphical patterns characteristic of these processes to identify those that apparently contributed to produce the compositions of eruptive units at Aniakchak.

Precaldera Magma Geochemistry and Subsurface Processes

The relatively small number of analyses of edifice lavas and the lack of strict temporal control presently limit use of these data to merely providing a measure of the compositional range exhibited at Aniakchak over a relatively long period of time. The range of edifice lava compositions typically encompasses that of all younger analyzed products of Aniakchak volcano, save the most silicic postglacial lavas and pyroclasts. In fact, for a given SiO_2 content, the range in many elemental abundances is far greater among edifice lavas than among later products (figs. 16 and 17).

Aniakchak I ignimbrite data form a coherent trend or grouping on geochemical diagrams. These trends are consistent with crystallization differentiation involving plagioclase and titanomagnetite but not apatite. For example, because of strong preference of plagioclase for Eu^{2+} and of titanomagnetite for Ti and V, Eu/Eu*, TiO_2, and V decrease with increasing SiO_2 (figs. 16 and 17). In contrast, P_2O_5 steadily increases with other incompatible element concentrations and with SiO_2 because Aniakchak I andesite was not crystallizing apatite. The trend for Aniakchak I compositions is not an effect of mixing with silicic magma, because the latter would have a far lower P_2O_5 content that would be inconsistent with Aniakchak I compositional trends (figs. 16 and 17). The narrow range of subparallel patterns in REE (fig. 18*B*) and multielement (fig. 19*B*) diagrams for Aniakchak I also is consistent with crystallization differentiation and is shown as a convenient reference on all other such figures. The parent magma for Aniakchak I ignimbrite had incompatible element concentrations substantially higher than other postglacial eruptives but within the span defined by edifice lavas. These geochemical properties are exemplified by TiO_2, K_2O, Zr, and Y in figure 16. Note that Aniakchak I has a higher FeO*/MgO ratio than other postglacial andesites (fig. 17), which suggests tholeiitic affinity of its parent magma. Aniakchak I andesite also has relatively low Al_2O_3. The AVO database of ~740 analyses of samples from Veniaminof volcano, located ~100 km down the Alaska Peninsula from Aniakchak (fig. 1), contains several low-silica dacite analyses (63.4–64.0 weight percent SiO_2) that are similar to those of Aniakchak I andesites (appendix B, table B2). Relative to Aniakchak I andesite (59.7–62.4 weight percent SiO_2), the Veniaminof dacites have slightly diminished Ti, Fe, Mg, Ca, Sc, V, K, Rb, Cs, Nb, Ta, Th, and U, and slightly elevated Si, Na, and Pb. Overall, however, the similarity of incompatible element abundances in this subset of silicic andesite–low-silica dacite samples from the two volcanoes points to a common process. Because all incompatible elements have high concentrations in these magmas, a credible explanation may be that a relatively low degree of mantle melting was responsible for generating their parent basalts in comparison to parents of the majority of intermediate-composition magmas at each volcano.

Postglacial, precaldera rhyodacites and dacites share diagnostic geochemical features with Aniakchak I andesites. In comparison with other postglacial silicic products, these have low Al_2O_3 and high concentrations of mantle-incompatible elements, such as K, Zr, Y, and Ti. Eruption of the precaldera rhyodacites and dacites shortly after Aniakchak I andesite, coupled with their geochemistry, lead us to conclude that these silicic magmas were generated dominantly by crystallization differentiation of Aniakchak I andesite parent magma and not by partial melting of crustal rocks. The differentiation processes involved separation of residual melt from a plagioclase + pyroxenes + titanomagnetite + apatite assemblage, probably in the mid to upper crust, in which apatite began to crystallize when the residual liquid reached a SiO_2 concentration of ~64 weight percent (fig. 16). Light and heavy REE contents in precaldera rhyodacites and dacites are similar to those of the most REE-rich, evolved Aniakchak I samples, but middle REEs Gd, Tb, and Dy are less elevated (fig. 18). Apatite/melt partition coefficients of REEs are large—substantially greater for trivalent MREE than for LREE or HREE—and their magnitude increases (to ~100) with melt evolution and decreasing temperature (Watson and Green, 1981; Fujimaki, 1986). Similarly, clinopyroxene favors MREE, and all trivalent REE save possibly La are compatible in this phase in the most silicic magmas (Sisson, 1991). The combination of trivalent REE incompatibility in plagioclase and strong

partitioning of MREE into apatite, plus MREE partitioning into modally more abundant clinopyroxene, appears to explain REE behavior in the postglacial, precaldera magmas. The increased effects of fractionation, particularly of plagioclase (Sr), titanomagnetite (Ti), and apatite (P), from Aniakchak I andesite through undivided pumice falls and upper Black Nose Pumice to lower Black Nose Pumice also are evident in the multielement diagrams in figure 19.

Geochemical Implications of Aniakchak II Magma Compositions

The compositionally zoned Aniakchak II eruption raises questions of how the andesite and rhyodacite magmas were formed and how they may have been related to one another. The andesite is unusual for an Aniakchak magma of its silica content in having low V and high Na_2O, Y, TiO_2, and, especially, P_2O_5 (fig. 20). In addition, the andesite Eu/Eu* and La/Yb_N ratios are relatively high (figs. 20 and 21), as are concentrations of Sr and REE La–Tm (appendix B, table B1). Dreher and others (2005) reported many of these observations and called upon addition of ~1 weight percent apatite to account for the anomalous P_2O_5 and MREE in Aniakchak II andesite versus other analyzed andesites. They pointed out, however, that apatite alone would not account for the Sr content of Aniakchak II andesite. Moreover, massive amounts of unusual apatite-rich material (~350 million metric tons) would have to have been assimilated in order to affect the entire 13 km^3 (DRE) of andesite reported by Dreher and others (2005) to have been erupted.

In addition to the high P_2O_5 content, the elevated Na_2O and TiO_2 coupled with low V concentrations are particularly significant to understanding the origin of Aniakchak II andesite. Vanadium in magmas is strongly partitioned into titanomagnetite. Addition of titanomagnetite is not responsible for the high TiO_2 in Aniakchak II andesite samples, because V concentrations in them are low relative to most other Aniakchak andesites. Search of the AVO database of ~740 analyses of samples from Veniaminof volcano returned two andesites whose compositions are similar to the Aniakchak II andesites (appendix B, table B2). Relative to Aniakchak II andesites, the Veniaminof samples have similar geochemistry but slightly less Mg, Ca, Sr, V, Sc, Rb, Cs, Nb, Ta, Th, and U. The observation that Alaska–Aleutian arc volcanoes can produce andesite magmas of similar but rather extreme compositions at different locations argues strongly against assimilation of local crustal material that is exceptionally rich in apatite or other accessory minerals. We suggest that the high P_2O_5, Na_2O, and TiO_2 contents of Aniakchak II andesite are inherited from the mantle source of the andesites' parental basalt. The high P_2O_5, Na_2O, and TiO_2 could reflect partial melting of a relatively fertile mantle domain, that is, one comparatively rich in fusible material. Because incompatible trace elements are not exceptionally concentrated in Aniakchak II andesites, we attribute the high P_2O_5, Na_2O, and TiO_2 contents to source bulk composition rather than enhancement by a low degree of partial melting of an otherwise uniform mantle wedge. The crystal-poor andesite contains plagioclase, augite, hyperthene, and magnetite (Larsen, 2006). It is not lacking in evidence for mantle and crustal contributions, because Dreher and others (2005) also reported traces of olivine, ilmenite, and quartz among a total of ~8 volume percent crystals. The single Aniakchak II andesite sample analyzed by George and others (2004) has Sr, Nd, Pb, and Th isotopic compositions rather similar to their basaltic andesite sample thought to have been vented at Windy Cone (figs. 29*A–D*), which suggests that geochemical effects of upper crustal assimilation in the andesite are minor.

The Aniakchak II rhyodacite (69.4–70.4 weight percent SiO_2) is the most evolved magma known to have erupted from Aniakchak volcano. In figures 20, 21, 25, and 26, the observation that the rhyodacite analyses plot more closely on a trend with postcaldera eruptives than with precaldera silicic rocks suggests that the rhyodacite is not simply a more evolved version of, for instance, lower Black Nose Pumice magma. Moreover, as pointed out earlier, REE patterns for Aniakchak II rhyodacite show depletion in MREE relative to other Aniakchak silicic magmas that would be expected to result from hornblende fractionation (Sisson, 1994). Indeed, hornblende is a common but not abundant phenocryst in the rhyodacite, in which Larsen (2006) reported ~9 volume percent total phenocrysts of plagioclase, hypersthene, magnetite, ilmenite, amphibole, and rare augite. Dreher and others (2005, p. 1,763) suggested that the rhyodacite represents the interstitial liquid in a mafic crystal mush, in other words, the product of crystallization differentiation. The same authors noted the different Sr isotopic compositions (George and others, 2004) of Aniakchak II andesite and rhyodacite (fig. 29*A*) and inferred that the rhyodacite was not derived by crystallization of the coerupted andesite. This inference is supported by differences in Nd–Sr and U–Th isotopic systematics between the two magmas (figs. 29*B* and 29*D*). The Sr and Nd isotopic ratios for the rhyodacite sample would be consistent either with derivation from a parent different from Aniakchak II andesite and or with assimilation of crustal material. The U–Th isotopic results indicate that the rhyodacite magma was not dominated by pre-late-Pleistocene crust; else the analysis would plot near the equiline (fig. 29*D*). The ≥14 km^3 (DRE) of rhyodacite magma vented (Dreher and others, 2005) in the caldera-forming eruption must have separated from the crystal mush and accumulated into a contiguous body, carrying with it or crystallizing in situ its phenocrysts, before the eruption began. Dreher and others (2005) suggested that the rhyodacite magma formed at greater depth and intruded stored andesite magma, triggering the caldera-forming eruption. However, Larsen (2006) concluded that both rhyodacite and andesite magmas resided at similar depth before eruption. The preponderance of evidence indicates that the two magmas were not genetically related and that either Aniakchak II andesite invaded the rhyodacite magma and instigated the eruption or, alternatively, the andesite was drawn up during the evacuation of the

rhyodacite from its holding reservoir. Syn-eruptive mixing and mingling of the two magmas produced hybrid compositions and "banded" (layered) pumice.

Rhyodacite Lava Flows and Subaqueous Domes

The northwest flank rhyodacite, compositionally similar lava exposed high in the 1931 Main Crater west wall, and the subaqueous domes on the caldera floor are the earliest recognized postcaldera eruptive products. Compositions of the four small domes foreshadow dacite magmas of more voluminous eruptions from Vent Mountain and Half Cone (figs. 20–23). At similar SiO_2 contents, the domes have K_2O and P_2O_5 contents like Vent Mountain products but CaO, TiO_2, and Y contents and LREE/HREE more like Half Cone samples. In detail, however, dome compositions are not strictly identical to Vent Mountain or Half Cone dacites. The Bolshoi Dome analysis has no close match, but Vulcan and West Dome analyses are comparable to some Half Cone and, especially for Vulcan, also Vent Mountain and late-erupted 1931 pumice data, the two domes having slightly lower HREE and higher Rb contents. Analyses of the two Pumice Dome samples are much like those of the northwest flank lava and the early lava in the 1931 Main Crater southeast wall. Although dome and rhyodacite lava compositions trend towards Aniakchak II rhyodacite in most silica variation diagrams (excepting CaO, Al_2O_3, and Y; figs. 20 and 21), the most silicic is significantly less evolved and does not appear to be remnant Aniakchak II magma backmixed with andesite. We interpret the subaqueous dome lavas to be differentiates of new andesite magma that was emplaced in the upper crust, or evolved there from basaltic andesite, and partially crystallized in the mushy zone beneath the caldera during the ~2,000 years subsequent to caldera collapse.

Basaltic Andesites of Breezy and Blocky Cones

The basaltic andesites of Breezy and Blocky Cones are the most mafic postglacial Aniakchak eruptives known. They are far from primitive, however, because at 52.2–52.5 weight percent SiO_2 they have only 4.3–5.3 weight percent MgO, 15–17 ppm Ni, and Mg' ≤0.51 (molar Mg/(Mg+Fe)). Fractionation of magnesian olivine readily extracts Ni from silicate melt and lowers Mg'. It is unclear at what depth olivine separation occurs and therefore whether more primitive magmas enter the mid to upper crustal magma storage zone beneath Aniakchak. Regardless, melts at least as primitive as the Breezy and Blocky Cone ejecta definitely get through or around the upper mush column and, therefore, we consider them as representative of input or replenishment magma least modified since it left the mantle. Of the Aniakchak samples analyzed for their isotopic compositions by George and others (2004), the one from Blocky Cone has nearly the least radiogenic Sr and Pb (fig. 29).

Basaltic Andesites of Windy Cone

The four basaltic andesite samples with 53.6–55.3 weight percent SiO_2 plotted in figures 20 and 21 are attributed here to Windy Cone or a nearby hidden vent for similar lava. Two of these had been considered early Vent Mountain lava (NA94-5 and 92CNA14). One (NA94-7) is scoria from above The Gates that had been thought to have had a Vent Mountain source, and one (NA93-102) is scoria from Windy Cone itself. Lacking direct ties in the field to Vent Mountain, the compositions of the isolated scoria deposit and the two lava outcrops, along with their proximity to Windy Cone, argue for grouping them with unequivocal Windy Cone scoria (figs. 22*C* and 23*C*). Like the Blocky Cone sample, the two of these samples analyzed by George and others (2004) have Sr and Pb isotope ratios that are among the least radiogenic. However, reported $^{143}Nd/^{144}Nd$ ratios are similar to that for Blocky Cone for one but higher for the other. In keeping with their higher SiO_2 contents, the geochemistry of the Windy Cone samples indicates that they are more differentiated than Blocky or Breezy Cone ejecta. The observation that REE and multielement patterns (figs. 22*C* and 23*C*) are parallel to those for Breezy and Blocky Cones, but elevated, is consistent with the interpretation that the four Windy Cone samples are simply more differentiated versions of the same general basaltic andesite magma type. If the reported difference in $^{143}Nd/^{144}Nd$ ratios between the two Windy Cone samples plotted in figure 29 is real, it would reflect a difference in mantle source because assimilation of crustal material, or addition of a subduction component, should also raise $^{87}Sr/^{86}Sr$ and $^{207}Pb/^{204}Pb$.

Andesite of Surprise Cone

Closest of known vents to the caldera center, Surprise Cone ejected the earliest post-Aniakchak II andesite yet recognized. The two scoria clasts analyzed have compositions that are unremarkable, but nonetheless subtle differences make them unique in the database (figs. 20 and 21). The most similar material is andesite lava from west of The Gates (97ANB59), which is thought to have a Vent Mountain source. We interpret andesite of Surprise Cone to be the product of differentiation of magma similar to basaltic andesite of Windy Cone.

Vent Mountain and Half Cone

Activity at Vent Mountain and at Half Cone overlapped in time and in composition of their products. Compositional variation appears more continuous for Half Cone, whose interior is exposed and which produced the zoned Pink and Brown Pumice, whereas for Vent Mountain only surface lava and some tephras are available for sampling. For example, the only andesite with <61 weight percent SiO_2 from Vent Mountain is the lava flow southwest of The Gates, but Half Cone Brown Pumice compositions fill in the gap between 59 and 61 weight

percent (figs. 20 and 21). Modest geochemical differences described earlier separate some Half Cone and Vent Mountain ejecta with similar SiO_2 contents. However, the data appear to be consistent with crystallization differentiation of andesite magma in the magma storage and stagnation zone beneath the caldera being the dominant process responsible for the andesite-to-dacite range from Vent Mountain and Half Cone. The one Vent Mountain dacite analyzed by George and others (2004) has low $^{143}Nd/^{144}Nd$ similar to Blocky and Windy Cone basaltic andesites but moderately higher $^{87}Sr/^{86}Sr$ (figs. 29*A* and 29*B*), which suggests that additional crustal material was assimilated during its differentiation. The same dacite has notably high ($^{238}U/^{232}Th$) relative to ($^{230}Th/^{232}Th$), so that it plots the farthest to the right of the equiline of any analyzed sample (fig. 29*D*), which suggests that recent differentiation was dominant over assimilation of older material, though the time scale of differentiation is not constrained by these data.

A small number of Half Cone silicic andesites have anomalously high P_2O_5 contents at ~62–63 weight percent SiO_2. On the P_2O_5 versus K_2O and V plots in figure 21 these samples trend toward the field of Aniakchak II andesite, whereas Vent Mountain and other Half Cone samples form vertical arrays that evolve into decreasing P_2O_5 with increasing differentiation owing to apatite fractionation. These relations suggest admixing of andesite magma that had at least some of the geochemical characteristics of Aniakchak II andesite.

Early Half Cone and most Vent Mountain dacites define a group with relatively high TiO_2, K_2O, P_2O_5, and incompatible trace element contents on silica variation diagrams (figs. 20, 21, and 24), as noted earlier. Using TiO_2 as a convenient index, this highTi trend projects back toward Aniakchak II andesites as potential parent magmas. Overall, the more silicic of these products were erupted later ("Half Cone 2" in fig. 24). The final Half Cone products, the Pink and Brown Pumices and the Cobweb flow, as well as a few earlier Half Cone and Vent Mountain samples, present a fairly continuous array back to ~58 weight percent SiO_2 at lower incompatible element concentrations than the highTi magmas. The Pink Pumice represents the most evolved magma to be definitively attributed to Half Cone. Dacite of the Cobweb flow, last erupted and rich in crystals and crystal clusters with disequilibrium textures, appears to be a mixture of dacite of the Pink Pumice, lesser amounts of coeval andesite of the Brown Pumice, and crystal mush.

Products of the 1931 Eruption

Grouping of data points on the silica variation diagrams in figure 25 indicates that the 1931 eruption tapped several magmas that had histories more complex than can be explained solely by two-component mixing or a single liquid line of descent. The Sr, Nd, and Pb isotopic data of George and others (2004) indicate that analyzed 1931 eruptives contain either more subduction component than Blocky and tuff cone basaltic andesites or, more likely, more crustal material (fig. 29). The four andesite bombs and scoria clasts that have anomalously low TiO_2, Na_2O, and P_2O_5 must have tapped an isolated pocket of magma in the storage system or have been recycled from earlier activity; they evidently do not represent a significant volume of erupted material, cannot be simple mixtures of other erupted 1931 magmas (fig. 26, P_2O_5 versus K_2O and V), and will not be discussed further.

Basaltic andesite and mafic andesite erupted in 1931 (56.0–58.2 weight percent SiO_2), which represent the small-volume late-erupted unit T3, Main Crater lava, and spatter agglutinate of Nicolson and others (2011), differ from other postcaldera eruptives with ≤58 weight percent SiO_2 by their higher TiO_2, Na_2O, and, especially, P_2O_5, as well as low V, contents that are a feature of their parent magma (fig. 25). As in some Half Cone samples, these characteristics are reminiscent of Aniakchak II andesite, though TiO_2 and P_2O_5 concentrations do not attain the levels found in the latter. Compositional variation among the basaltic andesites and mafic andesites appears to be consistent with crystallization differentiation of melts that were not apatite saturated (figs. 25 and 26). Significant $^{226}Ra/^{230}Th$ disequilibrium (fig. 29) in the mafic andesite bomb and Main Crater lava analyzed by George and others (2004) indicates that crystallization differentiation took place in the recent past, though determining the absolute time scale depends on the initial $^{226}Ra/^{230}Th$ ratio assumed for the parent magma.

Dacite and rhyodacite (~65–69 weight percent SiO_2) vented in 1931 form two trends or clusters of points on variation diagrams. The trends could be consistent with crystallization differentiation, in this case involving apatite in addition to plagioclase, pyroxenes, and titanomagnetite, or with mixing of silicic and intermediate-composition end member magmas. We note that four analyzed dacite pumice samples from the base of the 1931 tephra section, the basal part of unit T1 of Nicholson and others (2011), that have relatively low K_2O, Zr, and Y and high compatible element concentrations plot apart from other 1931 silicic samples in figures 25 and 26 (for example, fig. 25, K_2O and Zr versus SiO_2) and more in line with data for andesites. The volume of magma erupted as dacite pumice in unit T1 amounts to at least two orders of magnitude more than that extruded as lava (Nicholson and others, 2011, their figures 4 and 5 and table 4). Dacite–rhyodacite of the Slag Heap lava, the most evolved 1931 product, does not have a counterpart among analyzed 1931 pumices. A dense bomb from the rim of Blocky Cone nearly matches Slag Heap lava chemistry, and that bomb likely was sourced by a part of the Slag Heap feeder system. The less evolved Slag Heap samples are close in composition to the northwest flank rhyodacite flow and lava in the 1931 Main Crater wall. Doublet Crater lava compositions overlap those of the most evolved 1931 pumices. Slag Heap lava has ($^{226}Ra/^{230}Th$) in secular equilibrium, Doublet lava and other dacites and silicic andesites nearly so (fig. 29). The ($^{226}Ra/^{230}Th$) data imply one or more silicic end member components in 1931 magmas that either (1) differentiated several thousand years ago and survived the Aniakchak II caldera-forming eruption or (2) contain a dominant fraction of middle Holocene or older material. Residual Aniakchak II

rhyodacite may be a candidate that meets most criteria but has some characteristics, such as elevated LREE and HREE contents and lower ($^{230}Th/^{232}Th$), that are not a perfect match for the evolved 1931 magmas.

Analyses of bombs, pumice, and scoria with ~59.5–64 weight percent SiO_2 ejected in 1931, including unit T2 of Nicholson and others (2011), form smooth trends on variation diagrams that project towards the group of four basal dacite pumice samples. At the low-silica end of this andesite trend, however, is a discontinuity in some elemental concentrations when compared with more mafic andesites (for example, V in fig. 25). This demands a cryptic mafic andesite magma either as the parent for crystallization differentiation or the end member for mixing with silicic magma. The mafic end member was apatite saturated, as evidenced by decreasing P_2O_5 with increasing SiO_2 (fig. 25) and K_2O and decreasing V (fig. 26). Isotopic variability among 1931 andesites (figs. 29*B* and 29*D*) suggests more complexity than simple crystallization differentiation or two-component mixing.

In summary, the 1931 eruption tapped a variety of magmas. In the order and units presented by Nicholson and others (2011, their figures 4 and 5 and table 4), these were: (1) silicic dacite tephra (T1) from magma derived by crystallization differentiation of andesite and containing a substantial component derived from precaldera materials; (2) relatively voluminous andesite tephra and bombs of a series of differentiated melts, or hybrid mixtures with T1 dacite, of a cryptic mafic andesite; (3) a tiny volume of resident or remelted dacite–rhyodacite magma of Doublet Crater and Slag Heap, possibly related to nonerupted Aniakchak II rhyodacite; and (4) also a relatively small volume of mafic andesite to borderline basaltic andesite of unit T3, spatter agglutinate, and the Main Crater lava flow that form a differentiation series in their own right, likely evolved recently from a basaltic andesite parent with some characteristics in common with Aniakchak II andesite. Significantly, the geologic record that will remain accessible for perhaps some millennia will consist of the voluminous and widespread tephra units T1 and T2 whose magmas clearly are related to one another, whereas the extreme mafic and silicic eruptives may not be detectable.

Aniakchak Magmatic System

By postglacial time, Aniakchak volcano had a well-established feeder system that brought magma from the mantle wedge into and through the crust along repeatedly used pathways. A portion of this magma erupted, but much of it likely crystallized at depth. Magma was drawn from a region of the mantle broader than the footprint of the Aniakchak edifice and focused, probably in the deep crust, into the magma conduit and storage system beneath the volcano (fig. 31*A*). Heating of wall rocks through time conditioned the mid to upper crust for magma storage and differentiation. The eruptive history and magma geochemistry of postglacial Aniakchak, along with other studies of active and extinct arc volcanoes (for example, Mangan and others, 2009), provide a basis for our conceptual model of what took place in the upper ~15 km beneath Aniakchak and what might be anticipated for the future.

The distinctive incompatible element abundance pattern of the crystal-poor andesite magma of the voluminous Aniakchak I eruption implies that this differentiation product of atypical parent magma had accumulated in an anomalously large crustal reservoir (fig. 31*B*). There, or earlier at a deeper level, crystallization differentiation produced andesite melt that separated from accumulating crystals. Explosive eruption vented the andesite melt, but enough must have been left behind to impart aspects of its geochemical fingerprint to subsequently erupted precaldera dacites (for example, Black Nose Pumice). The precaldera dacite magmas are thought to have formed by crystallization differentiation of andesite melt left behind in the magma storage region for the Aniakchak I eruption, perhaps as intergranular melt in crystal mush or as a crystal-poor melt lens. Magma that produced the Upper Black Nose Pumice likely came from a region or layer in the storage system that was somewhat hotter and possibly deeper than that of the more-evolved lower Black Nose Pumice magma; both erupted from a vent that may have been northeast of the Aniakchak I feeder (fig. 31*B*). Because precise geochronological control is lacking for the deposits and hybrid or physically mingled andesite–dacite ejecta, it remains unknown whether the dacite magma was stored in a region not tapped by the Aniakchak I eruption or whether the dacite evolved subsequent to that event. Our new electron microprobe analyses and those reported by Dreher (2002) indicate preeruptive temperatures of ~940–950 °C for lower Black Nose Pumice from Fe–Ti oxide thermometry, notably higher than those reported by Larsen (2006) for the more evolved, hornblende phyric Aniakchak II rhyodacite. The northeast flank dacite flow probably also was fed from the general vicinity of Black Nose magma storage. The association of Aniakchak I and the precaldera dacite eruptions indicates that a mature storage and differentiation system had been established by Black Nose Pumice time and the mid to upper crust had been thermally conditioned to provide a nursery for accumulation of silicic magma. By this time, if not before, a composite pluton had begun to grow in the upper crust beneath Aniakchak. The relative proportions of crystal mush with intergranular melt and solidified intrusions cycled as thermal conditions fluctuated owing to the interplay of magmatic input, eruption, and hydrothermal cooling.

A
WSW
ENE
Ice
Pleistocene intrusive complex
Dikes
Mush column with solidified intrusions
DCHZ
Moho
Depth, in kilometers below sea level
Distance, in kilometers from origin
B
Northeast lava flow
Black Nose Pumice
Aniakchak I
Crystal mush & solidified intrusions
Pleistocene intrusive complex
C
Aniakchak II rhyodacite
Aniakchak II andesite
Crystal mush & solidified intrusions
Pleistocene intrusive complex
D
Northwest lava flow
West Dome
Dacite lava
Lake
Caldera fill
Vulcan Dome
Bolshoi Dome
Pumice Dome
Crystal mush & solidified intrusions
Pleistocene intrusive complex
E
Surprise Cone
Breezy Cone
Windy Cone
Maar
Crystal mush & solidified intrusions
Pleistocene intrusive complex
F
Blocky Cone
Half Cone
Vent Mtn
Basaltic andesite
Dacite
Andesite
Crystal mush & solidified intrusions
Pleistocene intrusive complex
G
Main Crater
Dacite
Basaltic andesite
Andesite
Crystal mush & solidified intrusions
Pleistocene intrusive complex
Depth, in kilometers below sea level
Distance, in kilometers from origin

Figure 31. (facing page) Schematic west-southwest–east-northeast cross-sections of the Aniakchak magmatic system through time. Surface features projected to N78°E line with arbitrary origin at 541.8 km E, 6,304.8 km N; some features translated slightly or exaggerated for clarity. Thicknesses of dikes and sills and sizes of some magma bodies enhanced for clarity. Dikes shown as cutting intrusive rock and crystal mush with low fraction of intergranular melt, but not mush with high melt fraction. No attempt has been made to depict variable crystallinity within mass of crystal mush and solidified intrusions. *A*, Late Pleistocene. Crustal thickness inferred after Fliedner and Klemperer (2000); seismic Moho may represent transition to ultramafic cumulates rather than to mantle peridotite (Calvert and McGeary, 2013). Deep crustal hot zone (DCHZ) modified after Annen and others (2006) and Solano and others (2012). DCHZ is equivalent to zone of melting, assimilation, storage, and homogenization (MASH) of Hildreth and Moorbath (1988). Patterns within DCHZ indicate sills of varying age and composition. Aniakchak volcano edifice reconstructed without allowing for glacial erosion. Several hundred meters of ice were present during glacial intervals. Pleistocene intrusive complex patterns indicate range of magmas released from mush column and frozen in stagnation region beneath edifice. *B*, Precaldera postglacial system depicting Aniakchak I and Black Nose magma bodies. Pleistocene intrusive complex in *B*–*G* generalized from *A*; some features, such as magma reservoirs and intracaldera volcanoes, not included in successive diagrams for simplicity. Black Nose Pumice magma shown as developed after Aniakchak I eruption and crystallization of remaining Aniakchak I magma. Note common source of Black Nose Pumice and northeast dacite lava flow. *C*, Aniakchak II reservoirs before the caldera-forming eruption. *D*, Dacite volcanism within the caldera lake. Caldera fill consists of juvenile pyroclastic material (lighter shading) and landslide megabreccia (darker shading). Note common sources of Pumice Dome and northwest lava flow, and of West and Vulcan Domes. Appearance of crossing conduits is an artifact of projection to cross section. *E*, After draining of the caldera lake. Surprise, Breezy, and Windy tuff cones vented where andesite–basaltic andesite dikes could penetrate mush east of active core zone. Source depth of andesite of Surprise Cone may have been shallower than implied by feeder dike. Although the large maar crater is shown here, it may be younger. *F*, Ca. 400 yr B.P. For simplicity, Half Cone and Vent Mountain are shown as supplied by a common reservoir, though geochemistry indicates subtle differences between erupted magmas. Basaltic andesite of Blocky Cone avoided mush near its southwestern edge and erupted from within the ring-fracture zone. *G*, 1931 C.E., showing Main Crater and principal reservoir only. Sources of minute volumes of evolved dacite–rhyodacite erupted at Doublet Crater and Slag Heap are thought to have been stagnant residual melt pockets within mush. See Nicholson and others (2011, their figure 9) for a more detailed series of cross sections that depict the plumbing system for the 1931 eruptions. Modern seismicity (see fig. 30) suggests that the Vent Mountain plumbing system, not shown in G, remains active.

Andesite and rhyodacite of the Aniakchak II caldera-forming eruption have geochemical characteristics suggesting that these magmas represent fresh recharge and a new cycle of storage and differentiation. The two magma types do not appear to be genetically related, despite comingling during the eruption. Instead, a body of crystal-poor rhyodacite magma segregated from crystal mush to be stored at a minimum pressure between 95 to 150 MPa, as constrained by phase equilibria for H_2O-saturated magma (Larsen, 2006). Assuming an average upper crustal density of 2,620 kg/m^3 from measurements on Naknek Formation in the Katmai area (Kienle, 1970), this corresponds to a depth range of 3.7 to 5.8 km (though the Jurassic–Cretaceous sedimentary section near Aniakchak is perhaps no thicker than ~2 km according to Detterman and others, 1981a, and it is uncertain what lies beneath it). Taking into account a lower density of the volcanic edifice above Naknek rocks leads to a depth range of perhaps 3.9 to 6.0 km. Note that this is depth below the ground surface, which of course depends on the precaldera height of the volcanic edifice, perhaps as much as 2,300 m above sea level. Minimum depth of the stored rhyodacite magma then would have been 1.6–3.7 km below sea level. Ring-fracture-controlled collapse of Aniakchak caldera suggests that the rhyodacite melt lens underlay approximately the area of the foundered cauldron block. Presence of andesite and mixed ignimbrite on all sides of the edifice implies that, at the time of eruption, the andesite magma either underlay the rhyodacite in a sheet or was drawn into the feeder vents from deeper in the system as a consequence of eruption of the rhyodacite (fig. 31*C*). The distribution of postcaldera vents suggests the maximum dimensions of the cauldron block are 5.8 km northwest–southeast by 7.7 km northeast–southwest, outlining an area of 35 km^2. If this constrains the lateral dimensions of rhyodacite and andesite magma reservoirs, erupted volumes require that each was equivalent to an elliptical disk at least ~400 m thick. Rapid evisceration of part or all of the liquid-rich portion of the magmatic system, foundering of the cauldron block along with infall of pyroclasts and landslide megabreccia, and subsequent filling of the caldera lake must have affected physical conditions in the upper crustal magmatic system. However, the disturbance was not so profound or lasting as to stifle production of evolved magmas.

By the time the subaqueous domes were emplaced, ongoing recharge with basaltic to andesitic magma had led to renewed segregation of silicic magma within the intrusive complex beneath Aniakchak volcano and its caldera lake (fig. 31*D*). These dacites and rhyodacites do not appear to be remnant Aniakchak II magma. Vulcan and West Domes consist of identical magma, distinct from the less evolved Bolshoi Dome and more evolved Pumice Dome, yet Vulcan was effused in the cluster that includes Bolshoi and Pumice Domes and West Dome vented 5.5 km to the southwest, on the opposite side of the inferred cauldron block. The Vulcan and West Dome compositional uniformity implies either a laterally extensive dacite melt lens or, considered more plausible, lateral transport of magma from a smaller reservoir in dikes subparallel to the arc axis. Relatively low-density evolved magma within the intrusive complex, and possibly the added load imposed by the lake, inhibited throughgoing transport of mafic magma, which instead lodged within or beneath the complex.

The dacite–rhyodacite lava of the northwest flank lava flow and the compositionally similar lava high in the 1931 Main Crater west wall apparently were emplaced sometime before the Half Cone vent became active. These lavas are virtually identical chemically to Pumice Dome, though slightly more evolved. Conceivably, Pumice Dome bears a similar relationship to the northwestern flank–1931 Main Crater wall dacite–rhyodacites as Vulcan Dome does to West Dome, that is, likely fed by lateral dikes emanating from a more centrally located reservoir rather than from different pockets of evolved magma located directly beneath the vents. A conundrum remains as to why a vent on the northwest flank at ~1,800 ft (550 m) would produce relatively voluminous lava identical to a flow that apparently emanated from a vent at lower elevation nearby within the caldera and similar to Pumice Dome. The mechanical difficulty of venting lava on the northwest flank in preference to within the caldera would be decreased but not eliminated by the load imposed by a deep caldera lake.

Catastrophic draining of the caldera lake and the resulting unloading of the magmatic system is thought to have immediately preceded eruption of the three tuff cones. We speculate that eruption of basaltic andesite at Breezy and Windy Cones on the ring-fracture system and andesite magma within the cauldron block at Surprise Cone was enabled by decompression of the magmatic system consequent on draining of the lake. Decompression could have caused degassing-induced crystallization of locally resident dacite magma, which would have allowed mafic–intermediate magma to fracture through the intrusive complex, and (or) transient decompression-melting boosted recharge with mafic magma that fed the eruptions (fig. 31*E*).

The only postcaldera vents that have persisted long enough to build composite edifices are Half Cone and Vent Mountain, both located on the ring-fracture system. From that time forward, magmatic eruptions have been confined to the western half of the caldera (fig. 10). Even accounting for Half Cone's ca. 400 yr B.P. Pink and Brown Pumice eruption, Vent Mountain appears to have erupted a larger volume of magma (ejecta volumes of $\leq$1.0 km^3 versus $\geq$1.5 km^3, respectively). Activity at the two volcanoes has overlapped in time and produced similar silicic andesite and dacite, though Half Cone may have ejected a greater amount of mafic andesite. Both have erupted dacite of the highTi group, but only Half Cone is known to have also produced highTi andesite (fig. 24). Still, most Half Cone andesite belongs to the lowTi group. The highTi andesite and dacite magmas are thought to have evolved by crystallization differentiation from andesite magma with Aniakchak II geochemical characteristics, whether stored within the mush column from that time or newly arrived. The lowTi andesite and dacite, including the Pink Pumice, evolved by a similar process within the mush column but from a more typical Aniakchak basalt or basaltic andesite parent. The ca. 400 yr B.P. eruption was sufficiently intense that andesite of the Brown Pumice was drawn into the

conduit and vented, along with hybrid mixtures of Pink and Brown Pumice magmas, or, alternatively, recharge with Brown Pumice magma triggered eruption of the Pink Pumice magma. The Cobweb flow, erupted last from Half Cone, is a mixture of these end member magmas. Preeruption magmatic temperatures from Fe–Ti oxide thermometry (Bacon and others, 1997) and measurement of dissolved volatiles in melt inclusions in phenocrysts in Pink Pumice dacite (Bacon, 2000, 2002) indicate storage at shallow depth (fig. 31*F*). Dacite magma partially degassed, losing any CO_2 and some sulfur but retaining ~3 weight percent H_2O, before erupting. Assuming vapor saturation, as implied by evidence for passive degassing, the H_2O concentration implies a confining pressure of 60 MPa. Depending on choice of roof rock density, this corresponds to a depth of 2.3 km (ρ=2,620 kg/m^3; Naknek Formation, Kienle, 1970) to 2.8 km (ρ=2,200 kg/m^3; minimum estimate for heterogeneous caldera fill) below the modern caldera floor. The zoned ca. 400 yr B.P. Half Cone eruption, along with compositional similarity of Half Cone and Vent Mountain products, provides compelling evidence for the existence of a range of magma compositions in the intrusive complex beneath Aniakchak and for repeated crystallization differentiation of recharge magma. This view is supported by the one U-series isotopic analysis of Vent Mountain lava presented by George and others (2004), the U excess of which (fig. 29) is consistent with recent differentiation.

Prehistoric eruption of Blocky Cone sometime after the ca. 400 yr B.P. Half Cone eruption demonstrates that basaltic andesite, among the most primitive of postglacial erupted magmas, was supplied to the subcaldera intrusive complex recently. Additionally, Blocky Cone shows that recharge magma was not trapped by lower density magma or mush beneath its feeder conduit at the southwest edge of the ring-fracture system (fig. 31*F*). Dissolved volatile concentrations in melt inclusions suggest that olivine phenocrysts crystallized in basaltic andesite of Blocky Cone at a pressure of at least 60 MPa, meaning at about the same depth as preeruption storage of Pink Pumice dacite of the ca. 400 yr B.P. Half Cone eruption (Bacon, 2002). The basaltic andesite magma had passively degassed any CO_2 before melt was trapped in growing olivine.

Detailed knowledge of the eruption products and chronology presented by Nicholson and others (2011), supplemented by isotopic data from George and others (2004) and chemical analyses (appendix B, table B1), provides the basis for a conceptual model of the magmatic system during Aniakchak's latest eruption in 1931 (fig. 31*G*). Schematic cross sections that illustrate the series of events in 1931 are shown by Nicholson and others (2011, their figure 9). Dissolved volatile concentrations in melt inclusions from basal dacite tephra indicate passive degassing during preeruptive storage at a pressure of 110 MPa (Bacon, 2000), or a depth of 4.3 to 5.1 km using the same range of densities of overburden as employed above for the dacite of Half Cone. The voluminous dacite and andesite tephra, units T1 and T2 of Nicholson and others (2011), represent genetically related magmas that had evolved by crystallization differentiation of cryptic basaltic andesite combined with assimilation of older material near the western margin of the subcaldera intrusive complex. The two magmas mixed to form intermediate andesite hybrids during the transition from eruption of dacite to andesite. Pressurization and (or) changes in the local stress field during the Plinian eruption caused miniscule volumes of resident, largely degassed dacite–rhyodacite magma to extrude at Doublet Crater and Slag Heap, perhaps thawed at depth by heat given off by accumulating T1–T2 magma. Sufficient magma was vented as units T1 and T2 that recharge basaltic andesite–mafic andesite subsequently erupted as the small-volume unit T3. Unrelated to the more voluminous andesite of unit T2, the recharge magma was derived by recent crystallization differentiation of magma with geochemical characteristics similar to the parent for Aniakchak II andesite.

Magma Transport and Storage Suggested by Earthquakes, Deformation, and Degassing

With the 1931 eruption as a reminder of upper crustal storage of evolved magma and recharge with basaltic andesite magma from greater depth, what is the current state of the magmatic system beneath Aniakchak volcano? Clues are provided by seismic, geodetic, and gas-emission monitoring. Earthquake hypocenters plotted in figure 30 give an indication of the magmatic plumbing system beneath Aniakchak volcano that can be compared with petrologic and geodetic inferences. The bow-tie distribution of hypocenters in figure 30*A* presumably reflects movement of magma, particularly in the mid to deep crust, in dikes oriented parallel to the maximum horizontal compressive stress, here tending to be parallel to plate convergence (Nakamura and others, 1977). Magma is drawn from a substantial region at depth and focused on the established conduit system and mush column beneath the volcano. Also shown in figure 30*B*, in addition to hypocenters, are (1) the Mogi point source from a model by Kwoun and others (2006) for caldera floor subsidence documented by InSAR and (2) minimum storage depths from melt inclusion data for vapor-saturated dacite magma of the Pink Pumice and 1931 eruptions and basaltic andesite of Blocky Cone (Bacon, 2002). Implied storage depths below sea level for these magmas are in the same range as determined by Larsen (2006) for Aniakchak II rhyodacite (accounting for the load of the precaldera edifice). The principal body of long-lived crystal-rich mush could be within the seismically quiet zone roughly 7–14 km bsl beneath the caldera, from which evolved magma escapes upward to be stored ephemerally within as little as ~3 km of the surface. It is important to note that Blocky Cone is 2.6 km west of the cross section, near the caldera margin, where basaltic andesite magma clearly found its way to the surface without being trapped in the mush or by more buoyant evolved magma. The deep long-period (DLP) events, ~14–28 km bsl, may result from input of basalt to basaltic andesite magma, or other fluid flow, in the cumulate, largely solid part of the mush column and in its surroundings where fractures can be created and sustained long enough to produce LP signals. Presence of evolved melt, probably as a small fraction within crystal mush, in the seismically quiet depth range (~7–14 km bsl) may limit fracturing and instead promote intergranular percolation and accumulation of magma.

The LP event clusters (fig. 30*C*) may reflect pulses of intrusion of magma from greater depth that produce DLP events and transient pressure increases within the mush column. Pressure increases in mush could induce fluid pressure pulses within the overlying brittle upper crust, resulting in fracture propagation or slip on faults implied by the shallow earthquakes. The shallowest earthquakes likely are associated with the magma and (or) hydrothermal plumbing system beneath Vent Mountain and the caldera ring-fracture system to its south.

An interferometric synthetic aperture radar (InSAR) geodetic study of Aniakchak for 1992–2002 netted a bull's-eye pattern of subsidence within the caldera with maximum mean annual subsidence rate of ~13 mm/yr (Kwoun and others, 2006). No substantial surface deformation was detected outside of the caldera within a 40-km radius of the caldera center. The InSAR results are fit well by the simple Mogi model of a point source at 4.2±0.8 km depth and volume change of –0.0012±0.000375 km^3/yr. Kwoun and others (2006) suggest that the cause of the subsidence is related to (1) cooling, crystallization, and (or) degassing of residual magma from recent eruptions or magma intruded since 1931 and (or) (2) reduction of pore-fluid pressure within a hydrothermal system. Alternatively, perhaps as a corollary to (2), we suggest that subsidence also might result from ongoing compaction of Aniakchak II intracaldera tuff, which could be most readily compacted in the center of the caldera because relatively incompressible megabreccia would be concentrated near the caldera margins (Lipman, 1997).

The sole gas analysis reported from Aniakchak is for CO_2-rich gas bubbling through shallow water in what is described as a soda spring (25 °C) at the southwestern shore of Surprise Lake (Symonds and others, 2003a). This gas sample has a $^3He/^4He$ ratio ($R/R_A \approx 8$) and $\delta^{13}C$ (–6.1 per mil) value that indicate shallow degassing of magma. The anhydrous gas composition is consistent with dominance of mantle-derived magmatic gas. Understandably, this gas sample has been affected by contact with air-saturated water. It is interpreted as high-temperature magmatic gas that has been scrubbed in the upper crustal hydrothermal system at low gas/water ratio with simultaneous water-rock reaction (Symonds and others, 2003b). Regardless of caveats, the composition of the Surprise Lake gas sample provides compelling evidence for ongoing degassing of subsurface magma.

Hazards

The data and analysis presented here augment the existing volcano hazard assessment for Aniakchak (Neal and others, 2001) by providing a more detailed, geochemically informed conceptual framework for the magmatic system and the nature of its likely future activity. Aniakchak will erupt again and could do so on short notice at any time. Because of the locations of recent vents, eruption would be more likely in the southwestern half of the caldera than in the northeastern half, and eruption is very unlikely outside of the caldera. Eruptions could be explosive, either because of interaction with groundwater or because they involved gas-rich magma. Apparent quiescence of Half Cone and possibly Vent Mountain since ca. 400 yr B.P. and the venting of recently differentiated andesite followed by a different basaltic andesite in 1931 suggest that future eruptions will feature new batches of magma. Seismicity, the $^3He/^4He$ ratio of gas, presence of weak thermal areas, and deformation revealed by InSAR all suggest that the magmatic system—the mush column—is active. Because Half Cone and Vent Mountain have been quiet for a century or more and the 1931 eruption apparently exhausted its own stored dacite magma, a future silicic eruption likely would involve newly differentiated magma or resident magma rejuvenated by mafic-to-intermediate recharge. An event comparable to that of 1931 would not be a surprise, nor would a Strombolian to Vulcanian eruption of basaltic andesite to mafic andesite from a ring-fracture vent, such as occurred at Blocky Cone. An explosive hydrovolcanic eruption could eject lithic debris, with or without juvenile magma, virtually anywhere within the caldera if a propagating dike ascended close to the surface. Eruption of partially degassed andesite to dacite magma, such as occurred at Vent Mountain, is possible, especially if encouraged by mafic recharge. Another caldera-forming eruption of dacite–rhyodacite magma is highly unlikely because of the varied geochemical nature and small volume of 400-yr-B.P. and 1931 dacites and the fact that they were followed by andesite. However, should a large volume of volatile-rich andesite magma accumulate in the mush, a voluminous explosive eruption, such as enlarged or formed the caldera at Veniaminof volcano (Miller and Smith, 1987; Bacon and others, 2007), might be possible. The subsidence documented by InSAR appears inconsistent with this possibility for present-day Aniakchak. Determining the probabilities of specific types of eruption awaits more detailed chronology of postcaldera eruptions through application of direct methods for dating features within the caldera and through further study of tephra from Aniakchak.

Conclusions

Pleistocene Aniakchak was a composite volcano that grew over a period of several hundred thousand years atop Jurassic–Tertiary sedimentary rocks by effusion of basaltic andesite to dacite lava. The Aniakchak edifice was smaller than those of other volcanoes with ~10 km diameter calderas in the eastern Aleutian arc, and it was repeatedly sculpted by ice during glacial intervals so that deep valleys were present at the end of the last glaciation. Basaltic magmas, with a range of incompatible element concentrations characteristic of arcs, were drawn from the mantle wedge into the deep crust beneath Aniakchak, where they were modified through crystallization differentiation and interaction with their surroundings in a deep crustal hot zone. Fractionated magmas that escaped upward further differentiated and partially to completely solidified to gradually build an intrusive complex, or mush column, in the mid to upper crust that was well developed by the end of the last glaciation. Postglacial Aniakchak magmas have traversed or been extracted from the mush column, and

all show some degree of fractionation in comparison with primary melts of the mantle.

The earliest recognized products of postglacial Aniakchak are andesite ignimbrite, Aniakchak I, present near the modern caldera rim and beneath younger deposits in peripheral valleys. Aniakchak I andesite has distinctly high concentrations of incompatible elements, notably Zr, and differentiated from a parent that originated as a low-degree partial melt of the mantle. This ignimbrite may be sufficiently voluminous that a small caldera could have formed during the eruption ca. 9,500–7,000 yr B.P., when glacial ice evidently reached as low as 560 m elevation in Birthday Creek valley. The dacitic Black Nose Pumice, which followed Aniakchak I, comprises extensive Plinian fall deposits and minor lava flows and welded ignimbrite that are present along the eastern half of the modern caldera rim. Correlation with a distal pumice bed that lies on carbonaceous material indicates an age of ca. 7,000 yr B.P. for the Plinian eruption. The dacite probably was derived by crystallization differentiation of Aniakchak I andesite magma lodged within the upper mush column.

The 3,590–3,588±11 cal yr B.P. Aniakchak II catastrophic eruption of rhyodacite followed by andesite left rhyodacite Plinian fall deposits dispersed along a northerly axis and compositionally zoned ignimbrite in valleys surrounding the edifice. The modern caldera collapsed during the ignimbrite-producing phase of this eruption. Aniakchak II rhyodacite accumulated in the upper reaches of the mush column and evolved by crystallization differentiation, but not from the co-erupted andesite or the precaldera Black Nose Pumice dacite. The distinctive composition of Aniakchak II andesite, such as its exceptionally high P_2O_5 content, suggests that it evolved from a parent derived from relatively fertile mantle. Both Aniakchak I and II andesites have close analogs at Veniaminof volcano 100 km down the Alaska Peninsula. Aniakchak II rhyodacite and andesite indicate a vigorous new cycle of recharge, storage, and differentiation in a mush column that had become well established through thermal conditioning owing to subsurface crystallization of magma during the prior history of the volcano.

Subsequent to the Aniakchak II eruption, a lake accumulated in the caldera and four dacite–rhyodacite domes were extruded on its floor above the ring-fracture system. Apparently during the same period, dacite–rhyodacite lava issued from vents near the base of the west caldera wall and immediately beyond the caldera rim, the latter feeding a 3-km-long flank flow. Similarity of dome and lava compositions on opposite sides of the caldera suggests lateral transport of magma approximately parallel to the arc axis. The dacites–rhyodacites reflect differentiation of post-Aniakchak II recharge magma.

After the lake drained catastrophically ca. 1,860 yr B.P., cutting The Gates through the caldera wall, the character of volcanism changed to hydromagmatic eruptions that built three tuff cones of basaltic andesite and andesite on the east caldera floor, including at Breezy Cone the least differentiated of any postglacial magma. This escape of basaltic andesite along the ring fracture system and of andesite inboard is thought to be linked to sudden unloading of the magmatic system by ~200 m lowering of the lake level.

After the eruption of the tuff cones, Half Cone on the northwest and Vent Mountain on the south ring-fracture system erupted broadly similar andesite–dacite, alternating their activity. Minor geochemical differences distinguish products of the two volcanoes, though there also is compositional overlap. Crystallization differentiation yielded nearby or contiguous andesite–dacite reservoirs in the mush column, as shallow as 1.9–2.4 km bsl (2.3–2.8 km below the caldera floor). In the ca. 400 yr B.P. Plinian eruption from Half Cone, evolved Pink Pumice dacite was followed by Brown Pumice andesite in a recent prehistoric example of a zoned eruption. The final Half Cone eruptive, the Cobweb flow, is a mixture of those magmas and crystal mush. Younger than Half Cone and most Vent Mountain lava, late-prehistoric Blocky Cone vented basaltic andesite nearly as primitive as that of Breezy Cone. Blocky Cone magma skirted the mush by ascending at the southwest edge of the ring-fracture system, though partially degassing and crystallizing olivine at ~2 km bsl.

The May–June 1931 subplinian eruption, like 400 yr B.P. Half Cone, produced dacite and andesite tephra whose compositions can be related by crystallization differentiation. Mafic andesite and basaltic andesite ejected and effused later in the sequence are related to each other, but not to the principal volume of zoned tephra. Magma of the initial dacite tephra was stored at a minimum depth of 3.8–4.6 km bsl. Uranium-series isotopic data suggest that the small volumes of dacite and rhyodacite lava effused from Doublet crater and at Slag Heap are older material remobilized in 1931. These isotopic data also suggest that basaltic andesite–mafic andesite differentiation was recent and that dacite magma contains a substantial component that may be precaldera in age. Postcaldera silicic magmas, except possibly Slag Heap, evidently did not include large fractions of nonerupted Aniakchak II rhyodacite. In contrast, some mafic–intermediate magmas, such as late-erupted 1931 basaltic andesite, have elemental relative-concentration patterns that suggest derivation from parents similar to that for Aniakchak II andesite.

The Aniakchak magmatic system continues to be active, as evidenced by escaping magmatic gas, caldera subsidence revealed by InSAR, and episodic bursts of low-frequency earthquakes. Seismicity is consistent with the concept of a deep crustal hot zone of basaltic magma injection that focuses upward as melt-bearing and solidified intrusions—the mush column—beneath the caldera. Events at 14–28 km bsl may result from injection of magma into the cumulate, largely solid part of the mush column and its surroundings. A seismically quiet zone at 7–14 km bsl may correspond to a region in which a fraction of melt limits fracturing and promotes percolation and accumulation of magma in long-lived crystal–liquid mush, from which magma batches escape upward to be stored ephemerally at depths as shallow as ~2 km bsl. These observations indicate that Aniakchak is likely to erupt again, most likely within the caldera and after a period of unrest of uncertain duration. Small explosive or effusive eruptions and hydrovolcanic explosions, to subplinian or Plinian eruptions like the 1931 and 400 yr B.P. events are possible, whereas another caldera-forming eruption is considered highly unlikely.

Acknowledgments

The information and data synthesized in this paper were collected by many scientists, technical experts, and students associated with the Alaska Volcano Observatory (AVO) and supported by the Volcano Hazards Program of the U.S. Geological Survey. We particularly appreciate the theses and publications that resulted from graduate research at the University of Alaska Fairbanks by Scott Dreher, Robert Nicholson, and Brandon Browne. The commitment of the GeoAnalytical Laboratory at Washington State University to delivering precise, accurate chemical analyses of rocks over many years of service to AVO enabled the geochemical correlations and process inferences that we have made. Kristi Wallace, Chad Hults, and Rich VanderHoek provided samples, and Leslie Hayden performed electron microprobe analyses, for correlation of Black Nose Pumice with distal tephra. We thank Wes Hildreth and Michelle Coombs for technical reviews that led to clearer presentation of data and interpretations. Our work at Aniakchak started with the reconnaissance of the Alaska Peninsula volcanoes funded by the Geothermal Research Program of the U.S. Geological Survey and conducted by Thomas P. Miller and Robert L. Smith in the 1970s. We are particularly indebted to Smith for guidance therein and for emphasizing the geologic significance and natural heritage of Aniakchak.

References Cited

Allen, S.R., and McPhie, J., 2000, Water-settling and resedimentation of submarine rhyolitic pumice at Yali, eastern Aegean, Greece: Journal of Volcanology and Geothermal Research, v. 95, p. 285–307.

Anderson, A.T., 1976, Magma mixing—Petrological process and volcanological tool: Journal of Volcanology and Geothermal Research, v. 1, p. 3–33.

Annen, C., Blundy, J.D., and Sparks, R.S.J., 2006, The genesis of intermediate and silicic magmas in deep crustal hot zones: Journal of Petrology, v. 47, p. 505–539.

Bacon, C.R., 1983, Eruptive history of Mount Mazama and Crater Lake caldera, Cascade Range, U.S.A.: Journal of Volcanology and Geothermal Research, v. 18, p. 57–115.

Bacon, C.R., 2000, Preeruptive volatiles in the most recent eruptions of Aniakchak volcano, Alaska [abs.]: Eos (American Geophysical Union Transactions), v. 81, no. 48, p. 1376–1377.

Bacon, C.R., 2002, Depths of magma reservoirs inferred from preeruptive dissolved volatiles in the most recent postcaldera eruptions of Aniakchak volcano, Alaska [abs.]: Eos (American Geophysical Union Transactions), v. 83, no. 19, p. S378.

Bacon, C.R., and Hirschmann, M.M., 1988, Mg/Mn partitioning as a test for equilibrium between coexisting Fe-Ti oxides: American Mineralogist, v. 73, p. 57–61.

Bacon, C.R., Neal, C.A., Nye, C.J., and McGimsey, R.G., 1997, Pre-eruptive temperatures for postcaldera magmas of Aniakchak Volcano, Alaska [abs.]: Eos (American Geophysical Union Transactions), v. 78, no. 46, p. 792–793.

Bacon, C.R., Sisson, T.W., and Mazdab, F.K., 2007, Young cumulate complex beneath Veniaminof caldera, Aleutian arc, dated by zircon in erupted cumulate blocks: Geology, v. 35, p. 491–494.

Begét, J., Mason, O., and Anderson, P., 1992, Age, extent, and climatic significance of the ca. 3400 BP Aniakchak tephra, western Alaska, U.S.A.: The Holocene, v. 2, no. 1, p. 51–56.

Browne, B., 2006, Investigating magma withdrawal dynamics during plinian eruptions through mineral and eruptive stratigraphies; Examples from the chemically zoned 400 yr BP eruption of Half Cone volcano, Aniakchak National Park, Alaska [abs]: Eos (American Geophysical Union Transactions), v. 87, no. 52, Fall Meeting Supplement, Abstract V53E-05.

Buurman, H., Nye, C.J., West, M.E., and Cameron, C., 2014, Regional controls on volcano seismicity along the Aleutian arc: Geochemistry, Geophysics, Geosystems, v. 15, p. 1147–1163.

Calvert, A.J., and McGeary, S.E., 2013, Seismic reflection imaging of ultradeep roots beneath the eastern Aleutian island arc: Geology, v. 41, p. 203–206.

Cas, R.A.F., and Wright, J.V., 1987, Volcanic successions: London, Allen and Unwin, 528 p.

Coulter, S.E., Pilcher, J.R., Plunkett, G., Baillie, M., Hall, V.A., Steffensen, J.P., Vinther, B.M., Clausen, H.B., and Johnson, S.J., 2012, Holocene tephras highlight complexity of volcanic signals in Greenland ice cores: Journal of Geophysical Research, v. 117, doi:10.1029/2012JD017698.

DeMets, C., Gordon, R.G., and Argus, D.F., 2010, Geologically current plate motions: Geophysical Journal International, v. 181, p. 1–80.

Denton, J.S., and Pearce, N.J., 2006, Confirming the 1645±4 BC date for the 2nd millennium BC caldera forming eruption of Aniakchak [abs.]: Eos (American Geophysical Union Transactions), v. 87, no. 52, Abstract V33B-0669.

DePaolo, D.J., 1981, Trace element and isotopic effects of combined wallrock assimilation and fractional crystallization: Earth and Planetary Science Letters, v. 53, p. 189–202.

Detterman, R.L., Miller, T.P., Yount, M.E., and Wilson, F.H., 1981a, Geologic map of the Chignik and Sutwik Island Quadrangles, Alaska: U.S. Geological Survey Miscellaneous Investigations Series Map I-1229, scale 1:250,000.

Detterman, R.L., Miller, T.P., Yount, M.E., and Wilson, F.H., 1981b, Quaternary geologic map of the Chignik and Sutwik Island Quadrangles, Alaska: U.S. Geological Survey Miscellaneous Investigations Series Map I-1292, scale 1:250,000.

Dixon, J.P., Stihler, S.D., Power, J.A., and Searcy, C.K., 2010, Catalog of earthquake hypocenters at Alaskan volcanoes—January 1 through December 31, 2009: U.S. Geological Survey Data Series 531, 84 p., available at http://pubs.usgs.gov/ds/531/.

Dixon, J.P., Stihler, S.D., Power, J.A., and Searcy, C.K., 2011, Catalog of earthquake hypocenters at Alaskan volcanoes—January 1 through December 31, 2010: U.S. Geological Survey Data Series 645, 82 p., available at http://pubs.usgs.gov/ds/645/.

Dixon, J.P., Stihler, S.D., Power, J.A., and Searcy, C.K., 2012, Catalog of earthquake hypocenters at Alaskan volcanoes—January 1 through December 31, 2011: U.S. Geological Survey Data Series 730, 82 p., available at http://pubs.usgs.gov/ds/730/.

Dixon, J.P., Stihler, S.D, Power, J.A., Haney, M., Parker, T., Searcy, C.K., and Prejean, S., 2013, Catalog of earthquake hypocenters at Alaskan volcanoes—January 1 through December 31, 2012: U.S. Geological Survey Data Series 789, 84 p., available at http://pubs.usgs.gov/ds/789/.

Dreher, S.T., 2002, The physical volcanology and petrology of the 3400 yBP caldera-forming eruption of Aniakchak volcano, Alaska: Fairbanks, University of Alaska Fairbanks, Ph.D. dissertation, 174 p.

Dreher, S.T., Eichelberger, J.C., and Larsen, J.F., 2005, The petrology and geochemistry of the Aniakchak caldera-forming ignimbrite, Aleutian arc, Alaska: Journal of Petrology, v. 46, p. 1747–1768.

Druitt, T.H., and Bacon, C.R., 1986, Lithic breccia and ignimbrite erupted during the collapse of Crater Lake caldera, Oregon: Journal of Volcanology and Geothermal Research, v. 29, p. 1–32.

Dungan, M.A., and Davidson, J., 2004, Partial assimilative recycling of the mafic plutonic roots of arc volcanoes—An example from the Chilean Andes: Geology, v. 32, p. 773–776.

Fliedner, M.M., and Klemperer, S.L., 2000, Crustal structure transition from oceanic arc to continental arc, eastern Aleutian Islands and Alaska Peninsula: Earth and Planetary Science Letters, v. 179, p. 567–579.

Fujimaki, H., 1986, Partition coefficients of Hf, Zr, and REE between zircon, apatite, and liquid: Contributions to Mineralogy and Petrology, v. 94, p. 42–45.

George, R., Turner, S., Hawkesworth, C., Bacon, C.R., Nye, C., Stelling, P., and Dreher, S., 2004, Chemical versus temporal controls on the evolution of tholeiitic and calc-alkaline magmas at two volcanoes in the Alaska—Aleutian arc: Journal of Petrology, v. 45, p. 203–219.

Ghiorso, M.S., and Evans, B.W., 2008, Thermodynamics of rhombohedral oxide solid solutions and a revision of the Fe-Ti two-oxide geothermometer and oxygen-barometer: American Journal of Science, v. 308, p. 957–1039.

Gill, J.B., 1981, Orogenic andesites and plate tectonics: Berlin, Springer-Verlag, 390 p.

Gill, J.B., and Williams, R.W., 1990, Th isotope and U-series studies of subduction-related volcanic rocks: Geochimica et Cosmochimica Acta, v. 54, p. 1427–1442.

Goto, Y., and McPhie, J., 1998, Endogenous growth of a Miocene submarine dacite cryptodome, Rebun Island, Hokkaido, Japan: Journal of Volcanology and Geothermal Research, v. 84, p. 273–286.

Hart, S.R., 1984, A large-scale isotope anomaly in the Southern Hemisphere mantle: Nature, v. 309, p. 753–757.

Hildreth, W., and Moorbath, S., 1988, Crustal contributions to arc magmatism in the Andes of central Chile: Contributions to Mineralogy and Petrology, v. 98, p. 455–489.

Hubbard, B.R., 1932, Mush, you malemutes!: New York, America Press, 179 p.

Kamata, H., Suzuki-Kamata, K., and Bacon, C.R., 1993, Deformation of the Wineglass Welded Tuff and the timing of caldera collapse at Crater Lake, Oregon: Journal of Volcanology and Geothermal Research, v. 56, p. 253–265.

Kaufmann, D., and Hopkins, D., 1985, Late Cenozoic radiometric dates, Seward and Baldwin Peninsulas, and adjacent continental shelf, Alaska: U.S. Geological Survey Open-File Report 85–374, 27 p.

Kienle, J., 1970, Gravity traverses in the Valley of Ten Thousand Smokes, Katmai National Monument, Alaska: Journal of Geophysical Research, v. 75, p. 6641–6649.

Kwoun, O.-I., Lu, Z., Neal, C., and Wicks, C., Jr., 2006, Quiescent deformation of the Aniakchak Caldera, Alaska, mapped by InSAR: Geology, v. 34, p. 5–8.

Langmuir, C.H., Vocke, R.D., Jr., Hanson, G.N., and Hart, S.R., 1978, A general mixing equation with applications to Icelandic basalts: Earth and Planetary Science Letters, v. 37, p. 380–392.

Langmuir, C.H., Klein, E.M., and Plank, T., 1992, Petrological systematics of mid-ocean ridge basalts; constraints on melt generation beneath ocean ridges, *in* Phipps Morgan, J., Blackman, D.K., and Sinton, J.M., eds., Mantle flow and melt generation at mid-ocean ridges: American Geophysical Union Geophysical Monograph 71, p. 183-280.

Larsen, J.F., 2006, Rhyodacite magma storage conditions prior to the 3430 yBP caldera-forming eruption of Aniakchak volcano, Alaska: Contributions to Mineralogy and Petrology, v. 152, p. 523–540.

Lescinsky, D.T., and Fink, J.H., 2000, Lava and ice interaction at stratovolcanoes—Use of characteristic features to determine past glacial extents and future volcanic hazards: Journal of Geophysical Research, v. 105, p. 23711–23726.

Lipman, P.W., 1997, Subsidence of ash-flow calderas—Relation to caldera size and magma-chamber geometry: Bulletin of Volcanology, v. 59, p. 198–218.

Mangan, M., Miller, T., Waythomas, C., Trusdell, F., Calvert, A., and Layer, P., 2009, Diverse lavas from closely spaced volcanoes drawing from a common parent—Emmons Lake volcanic center, Eastern Aleutian arc: Earth and Planetary Science Letters, v. 287, p. 363–372.

McDonough, W.F., and Sun, S.-s., 1995, The composition of the Earth: Chemical Geology, v. 120, p. 223–253.

McGimsey, R.G., Waythomas, C.F., and Neal, C.A., 1994, High stand and catastrophic draining of intracaldera Surprise Lake, Aniakchak Volcano, Alaska, *in* Till, A.B., and Moore, T.E., eds., Geologic studies in Alaska by the U.S. Geological Survey, 1993: U.S. Geological Survey Bulletin 2107, p. 59–71.

McGimsey, R.G., Neal, C.A., Adleman, J.N., Larsen, J.F., and Ramsey, M.S., 2003, Black Peak caldera, Alaska—Preliminary investigations of the ~4600 BP caldera-forming eruption and subsequent post-caldera activity [abs.]: Eos (American Geophysical Union Transactions), v. 84, no. 46, Fall Meeting Supplement, Abstract V42B-0342.

Mellors, R.A., and Sparks, R.S.J., 1991, Spatter-rich pyroclastic flow deposits on Santorini, Greece: Bulletin of Volcanology, v. 53, p. 327–342.

Miller, T.P., and Smith, R.L., 1977, Spectacular mobility of ash flows around Aniakchak and Fisher calderas, Alaska: Geology, v. 5, p. 173–178.

Miller, T.P., and Smith, R.L., 1987, Late Quaternary caldera-forming eruptions in the eastern Aleutian arc, Alaska: Geology, v. 15, p. 434–438.

Miyashiro, A., 1974, Volcanic rock series in island arcs and active continental margins: American Journal of Science, v. 274, p. 321–355.

Nakada, S., Bacon, C.R., and Gartner, A.E., 1994, Origin of phenocrysts and compositional diversity in pre-Mazama rhyodacite lavas, Crater Lake, Oregon: Journal of Petrology, v. 35, p. 127–162.

Nakamura, K., Jacob, K.H., and Davies, J.N., 1977, Volcanoes as possible indicators of tectonic stress orientation—Aleutians and Alaska: Pure and Applied Geophysics, v. 115, p. 87–112.

Nathenson, M., Bacon, C.R., and Ramsey, D.W., 2007, Subaqueous geology and a filling model for Crater Lake, Oregon: Hydrobiologia, v. 574, p. 12–27.

Neal, C.A., McGimsey, R.G., Miller, T.P., Riehle, J.R., and Waythomas, C.F., 2001, Preliminary volcano-hazard assessment for Aniakchak volcano, Alaska: U.S. Geological Survey Open-File Report 00-519, 35 p.

Nicholson, R.S., Gardner, J.E., and Neal, C.A., 2011, Variations in eruption style during the 1931 A.D. eruption of Aniakchak volcano, Alaska: Journal of Volcanology and Geothermal Research, v. 207, p. 69–82.

Nye, C.J., Neal, C.A., and McGimsey, R.G., 1993, Extreme and abrupt transition from tholeiitic to calcalkaline volcanism at Aniakchak volcano, eastern Aleutian arc [abs.]: Eos (American Geophysical Union Transactions), v. 74, no. 43, p. 674.

Pearce, N.J.G., Westgate, J.A., Preece, S.J., Eastwood, W.J., and Perkins, W.T., 2004, Identification of Aniakchak (Alaska) tephra in Greenland ice core challenges the 1645 BC date for Minoan eruption of Santorini: Geochemistry, Geophysics, Geosystems, v. 5, no. 3, doi:10.1029/2003GC000672.

Plank, T., and Langmuir, C.H., 1998, The chemical composition of subducting sediment and its consequences for the crust and mantle: Chemical Geology, v. 145, p. 325–394.

Power, J.A., Stihler, S.D., White, R.A., and Moran, S.C., 2004, Observations of deep long-period (DLP) seismic events beneath Aleutian arc volcanoes; 1989–2002: Journal of Volcanology and Geothermal Research, v. 138, p. 243–266.

Power, J.A., Stihler, S.D., Ketner, D.M., Haney, M.M., Prejean, S.G., and Parker, T.J., 2013, Lower-crustal and upper-mantle seismicity beneath Aleutian arc volcanoes—A temporal link for magmatic processes between the lower-crust and the surface [abs.]: Abstract V13B-2615 presented at 2013 Fall Meeting, American Geophysical Union, San Francisco, California, 9–13 December.

Reimer, P.J., Bard, E., Bayliss, A., and 27 others, 2013, IntCall13 and Marine13 radiocarbon age calibration curves 0–50000 years cal BP: Radiocarbon, v. 55, no. 4, p. 1869–1887.

Riehle, J.R., Meyer, C.E., Ager, T.A., Kaufman, D.S., and Ackerman, R.E., 1987, The Aniakchak tephra deposit, a late Holocene marker horizon in western Alaska, *in* Hamilton, T.D., and Galloway, J.P., eds., Geologic studies in Alaska by the U.S. Geological Survey during 1986: U.S. Geological Survey Circular 998, p. 19–22.

Riehle, J.R., Meyer, C.E., and Miyoka, R.T., 1999, Data on Holocene tephra (volcanic ash) deposits in the Alaska Peninsula and Lower Cook inlet of the Aleutian volcanic arc, Alaska: U.S. Geological Survey Open-File Report 99–135, unpaginated.

Ryan, H.F., von Huene, R., Wells, R.E., Scholl, D.W., Kirby, S., and Draut, A.E., 2012, History of earthquakes and tsunamis along the eastern Aleutian-Alaska megathrust, with implications for tsunami hazards in the California Continental Borderland, *in* Dumoulin, J.A., and Dusel-Bacon, C., eds., Studies by the U.S. Geological Survey in Alaska, 2011: U.S. Geological Survey Professional Paper 1795–A, 31 p., http://pubs.usgs.gov/pp/1795/a.

Sisson, T.W., 1991, Pyroxene-high silica rhyolite trace element partition coefficients measured by ion microprobe: Geochimica et Cosmochimica Acta, v. 55, p. 1575–1585.

Sisson, T.W., 1994, Hornblende-melt trace element partition coefficients measured by ion-microprobe: Chemical Geology, v. 117, p. 331–344.

Solano, J.M.S., Jackson, M.D., Sparks, R.S.J., Blundy, J.D., and Annen, C., 2012, Melt segregation in deep crustal hot zones—A mechanism for chemical differentiation, crustal assimilation and the formation of evolved magmas: Journal of Petrology, v. 53, p. 1999–2026.

Spörli, K.B., and Rowland, J.V., 2006, 'Column on column' structures as indicators of lava/ice interaction, Ruapehu andesite volcano, New Zealand: Journal of Volcanology and Geothermal Research, v. 157, p. 294–310.

Stormer, J.C., Jr., 1983, The effects of recalculation on estimates of temperature and oxygen fugacity from analyses of multicomponent iron-titanium oxides: American Mineralogist, v. 68, p. 586–594.

Stuiver, M., and Reimer, P.J., 1993, Extended ^{14}C data base and revised CALIB 3.0 ^{14}C age calibration program: Radiocarbon, v. 35, p. 215–230.

Symonds, R.B., Poreda, R.J., Evans, W.C., Janik, C.J., and Ritchie, B.E., 2003a, Mantle and crustal sources of carbon, nitrogen, and noble gases in Cascade-Range and Aleutian-Arc volcanic gases: U.S. Geological Survey Open-File Report 03-436, 26 p.

Symonds, R.B., Janik, C.J., Evans, W.C., Ritchie, B.E., Counce, D., Poreda, R.J., and Iven, M., 2003b, Scrubbing masks magmatic degassing during repose at Cascade-Range and Aleutian-Arc volcanoes: U.S. Geological Survey Open-File Report 03-435, 22 p.

U.S. Geological Survey, 1963, Chignik (D–1), Alaska: U.S. Geological Survey topographic map, scale 1:63,360.

VanderHoek, R., 2009, The role of ecological barriers in the development of cultural boundaries during the later Holocene of the central Alaska Peninsula: Urbana, Illinois, University of Illinois at Urbana-Champaign, Ph.D. dissertation, 413 p.

VanderHoek, R., and Myron, R., 2004, An archaeological overview and assessment of Aniakchak National Monument and Preserve: U.S. National Park Service Research/Resources Management Report AR/CRR-2004-47.

Watson, E.B., and Green, T.H., 1981, Apatite/liquid partition coefficients for the rare earth elements and strontium: Earth and Planetary Science Letters, v. 56, p. 405–421.

Waythomas, C.F., Walder, J.S., McGimsey, R.G., and Neal, C.A., 1996, A catastrophic flood caused by drainage of a caldera lake at Aniakchak Volcano, Alaska, and implications for volcanic hazards assessment: Geological Society of America Bulletin, v. 108, p. 861–871.

Wohletz, K.H., and Sheridan, M.F., 1983, Hydrovolcanic explosions II—Evolution of basaltic tuff rings and tuff cones: American Journal of Science, v. 283, p. 385–413.

Appendix A. Electron Microprobe Analyses

This appendix consists of two Excel tables available at http://pubs.usgs.gov/pp/1810.

Table A1. Electron microprobe analyses of glass from lower Black Nose Pumice and from tephra at Cabin Bluff.
Table A2. Electron microprobe analyses of iron-titanium oxide crystals from lower Black Nose Pumice and from tephra at Cabin Bluff.

Appendix B. Whole-Rock Chemical Analyses

This appendix consists of two Excel tables available at http://pubs.usgs.gov/pp/1810.

Table B1. Chemical analyses of rock specimens from Aniakchak volcano and vicinity.
Table B2. Chemical analyses of rock specimens from Aniakchak and Veniaminof volcanoes.

Menlo Park, California, and Raleigh, North Carolina,
Publishing Service Centers
Manuscript approved for publication November 29, 2014
Edited by Peter H. Stauffer
Layout and design by James E. Banton

ISSN 1044-9612 (print)
ISSN 2330-7102 (online)
http://dx.doi.org/10.3133/pp1810